Physics – Nonlinear Optics

Gad Mansour Ahmed Gad

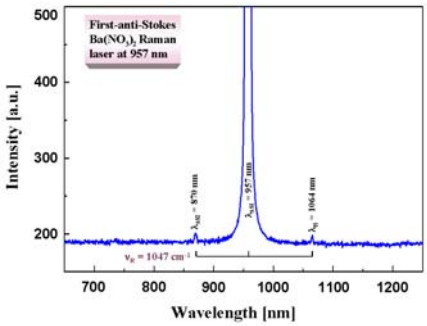

Stimulated scattering in solids and new Raman lasers in near-infrared and visible regions

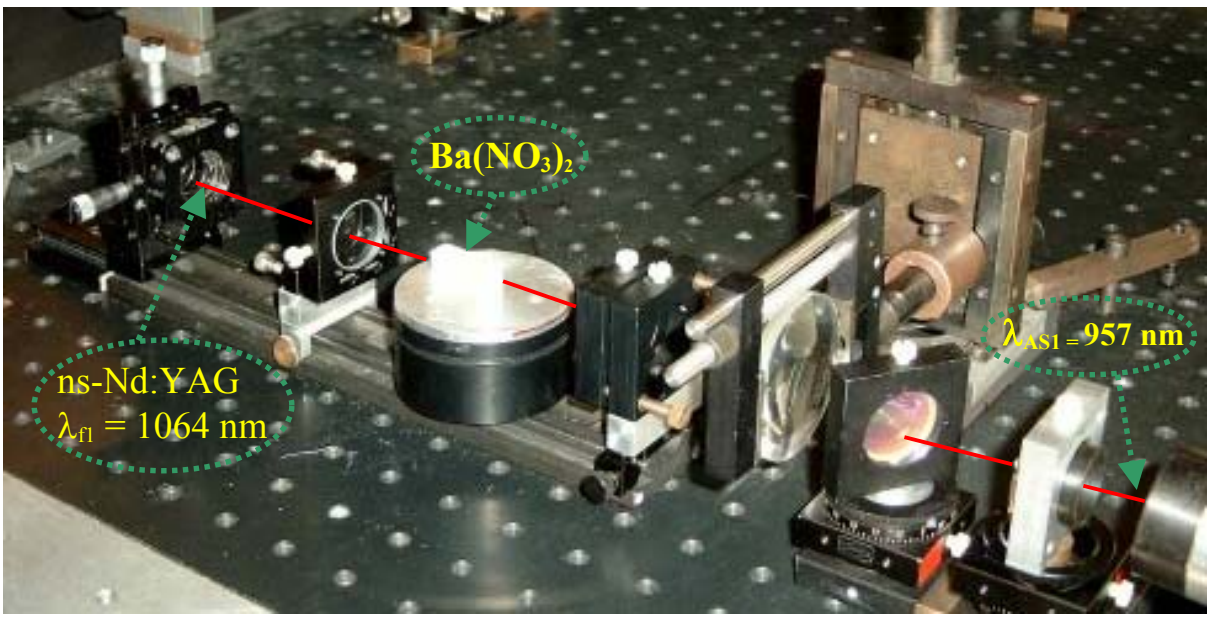

First-anti-Stokes Barium nitrate Raman laser

Stimulated scattering in solids and new Raman lasers in near-infrared and visible regions

Von

MSc., Dipl.-Phys. Gad Mansour Ahmed Gad

aus Ägypten

Von der Fakultät II-Mathematik und Naturwissenschaften
der Technischen Universität Berlin
zur Erlangung des akademischen Grades
Doktor der Naturwissenschaften
Dr. rer. nat.
genehmigte Dissertation

Promotionsausschuss:

Vorsitzender: Prof. Dr. J. Sahm
Berichter/Gutachter: Prof. Dr. H.-J. Eichler
Berichter/Gutachter: Prof. Dr. H.-G. Weber
Tag der wissenschaftlichen Aussprache: 25. Juli 2003

Berlin 2003
D 83

To
my family and my dear wife

(Mohamed, Omar, Karim, Mona)

Abstract

The frequency shifts based on stimulated Raman scattering SRS in Raman-active materials are experimentally investigated. A mode-locked Nd:YAG ps-single-pulse laser is used to study the Stokes and anti-Stokes shifting under single pass and resonant conditions. This leads to generation of new solid-state Raman lasers.

First part of this work is the generation of SRS in inorganic, organic crystals and glassy materials. The laser radiation shifts to Stokes lines with frequency smaller than the laser frequency and anti-Stokes lines with frequency higher than the laser frequency.

BiB_3O_6, $Bi_4Ge_3O_{12}$, $Bi_4Si_3O_{12}$, AANP, $C_{13}H_{10}O$, GuZN-III and 4′-Nitrobenzylidene-3-Acetamino-4-Methoxyaniline crystals are investigated as a new efficient shifter crystals. They combine SRS and second harmonic generation SHG nonlinear frequency conversion in the same crystal and allow to efficiently shift the Nd:YAG laser emission to discrete lines in the visible.

Self-SHG is observed in a $C_{16}H_{15}N_3O_4$ crystal, SHG of the first (λ_{S1} = 1280.4 nm) and second (λ_{S2} = 1606.9 nm) Stokes lines generate λ_{SHG} = 640.2 nm and λ_{SHG} = 803.4 nm, respectively. This is the first observation of the self-SHG effect in organic single crystals.

Second part of this work is the investigation of Raman lasers to reach new near-IR wavelengths and conversion to the visible. Resonant SRS to the second-Stokes line and subsequent SHG with a doubler crystal extends the Nd:YAG wavelengths to the red spectral region. Second-Stokes Raman-lasers with $PbWO_4$ and $Ba(NO_3)_2$ crystals at wavelengths 1316.6 nm and 1369 nm, respectively are available. Raman Stokes lines in IR at 1316.6 and 1369 nm are converted to the visible spectral region at 658 nm and 685 nm wavelengths with KD*P frequency doubling conserving the good Stokes beam quality.

Finally, Solid-state Raman laser with wavelength shorter than the pump beam is available. First-anti-Stokes $Ba(NO_3)_2$ Raman laser at wavelength 957 nm is demonstrated for the first time. For generation first-anti-Stokes Raman laser nanosecond Nd:YAG laser at 1064 nm wavelength with pulse duration 8-9 ns was used.

Contents

1 Introduction

Raman light scattering is a third order nonlinear optical process that has been observed in many types of materials. Initially, the investigations of **Raman scattering** centered on trying to understand the fundamental physics associated with the process. Once the physics of the process was understood, Raman scattering become useful as a spectroscopic tool to study the vibrational, structural, and chemical properties of molecules and solids and a common method for chemical analysis [1-1]. **Stimulated Raman scattering (SRS)** was first observed by *Woodbury and Ng* [1-2] with ruby lasers in 1962. SRS has been then demonstrated in various gas, liquid and solid state media [1-3, 1-4], but most practical applications involve the use of a gas cell. Fig. 1.1.a shows a single pass SRS experiment, with the Raman active material between two convex lenses. The first lens focuses the pump beam into the Raman medium and the second lens collects the scattered beam into the spectrometer. SRS can be used to shift the emission frequency of lasers to different spectral region. **Solid-state Raman active crystals** are attractive media for SRS, offering high gain and better thermal characteristics than more-widely used, gaseous media. A great variety of crystals have been investigated for Raman scattering and these provide Raman frequency shifts from 10 cm^{-1} to 3000 cm^{-1} in the spectral range from the ultraviolet to infrared [1-1]. However, few crystals have been identified that possess the narrow, isolated, and intense **Raman active modes** necessary for efficient scattering [1-5]. In solids there are intense modes that can be attributed to internal symmetrical vibrations within covalent ion

complexes, such as $(CO_3)^{1-}$, $(NO_3)^{1-}$ and $(WO_4)^{2-}$. It has been suggested by *Eckhardt* [1-5] that molecular crystals containing these complexes should exhibit strong SRS. The first experiments on SRS in solids were made in **diamond**, **calcite** and **α-sulfur single crystals** [1-6]. Natural calcite has been investigated as SRS crystal due to its comparatively large size and easy availability. It has an isolated molecular vibronic mode with a large phonon energy of 1086 cm^{-1}.

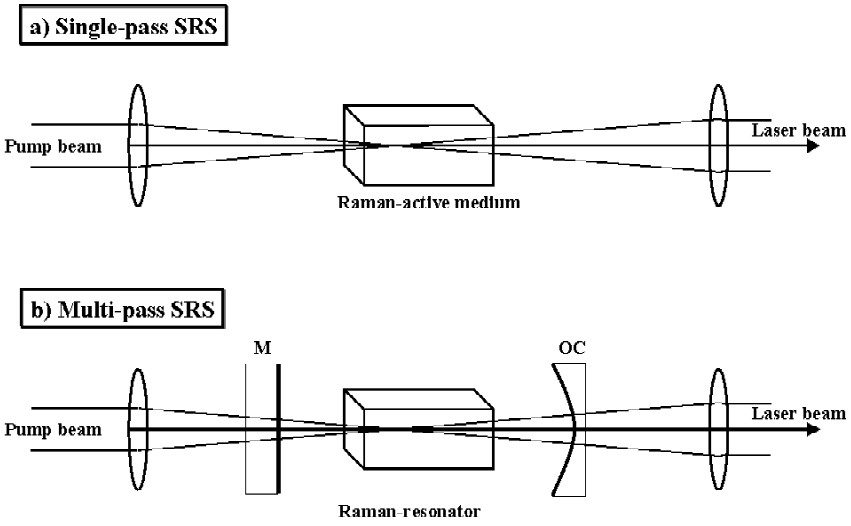

Fig. 1.1: *Experimental set-up to observe SRS a) the investigated material was positioned between two lenses for single-pass SRS.*
b) the crystal is equipped with two mirrors M and OC to form Raman-resonator or Raman-laser.

The SRS efficiency can be quite high and further improvement is possible by arranging the **Raman crystals** between two mirrors forming an **optical resonator**. Such **Raman lasers** convert up to 80% of the pump power into the **first Stokes** power. Fig. 1.1.b shows a plano-concave linear resonator for Raman lasers. The Raman active material was positioned between the plane mirror *M* and the output coupler *OC*. At present, the **SRS-active media** most commonly used in Raman lasers are the cubic **$Ba(NO_3)_2$**, monoclinic **$KGd(WO_4)_2$–(KGW)** and tetragonal **$PbWO_4$** crystals. The Raman laser crystals which have been investigated intensively during the last few years are listed in Table 1.1. A Raman laser in the visible region based on $Ba(NO_3)_2$ crystal was investigated [1-7, 1-8]. Furthermore, infrared $Ba(NO_3)_2$ Raman laser in the eye-safe region have been demonstrated [1-9, 1-10]. Compact, solid state and multi-wavelength Raman laser action based on Nd^{3+}:KGW crystal for IR and visible spectral regions was demonstrated [1-11]-[1-12]. Recently, a laser diode-pumped compact, passively Q-switched, self-stimulating Nd:PWO/Cr:YAG Raman laser was achieved [1-13].

Table 1.1: *Optical transparency, Raman shift (ν_R), Raman gain (g_R), Raman line width ($\Delta\nu$) and relaxation time (T_R) of selected Raman active crystals which are suitable for Raman lasers.*

Crystal	Optical transparency (μm)	ν_R (cm^{-1})	g_R [cm/GW]	$\Delta\nu$ [cm^{-1}]	T_R [ps]
$Ba(NO_3)_2$	≈ 0.4 - ≈ 1.8	1047	10-11	0,42	25
$CaWO_4$	≈ 0.24 – ≈ 6	908	3 ± 0.8	7	≈ 1.5
$KGd(WO_4)_2$	≈ 0.34 – ≈ 5.5	901	≈ 3.3	≈ 5.7	1.9
		768	≈ 4.4	≈ 6.7	1.6
KH_2PO_4(KDP)	≈ 0.18 – ≈ 1.45	915	≈ 0.2	≈ 0.59	≈ 18
$KY(WO_4)_2$	≈ 0.34 – ≈ 5.5	905	≈ 3.6	5,9	1,4
		765	≈ 3.6	7,8	1,2
$NaClO_3$	≈ 0.24 – ≈ 4.8	936	3.1 ± 0.8	0.44	≈ 24
$PbWO_4$	≈ 0.33 – ≈ 5.5	901	3.1 ± 0.8	4,3	2.5
		323		7.5	≈ 1.42

The use of SRS in solids to shift the wavelength of laser emission is becoming more widespread [1-14]. During the last decade, this growth in activity has been made possible by the discovery and development of several SRS-active insulating crystals. Their successful application in the creation of **nanosecond** and **picosecond** Raman lasers emitting at specific and otherwise hard to reach wavelengths in the **visible** and **near-IR**, including the **eye-safe** range (from 563 nm to 1598 nm). Among other technological applications of new Raman lasers, remote sensing of the atmosphere is of great interest, which typically requires high peak-power laser pulses at wavelengths that are difficult to produce by other all-solid-state laser system. Furthermore, solid state lasers using SRS conversion processes are attractive for medical treatments [1-15] and for laser guide star experiments [1-16]. In addition, Raman amplifiers are becoming very important for fiber telecommunications. Such fiber amplifiers have been extensively studied as a key device for wavelength division multiplexing (WDM) optical communication systems pumped by laser diodes [1-17]-[1-19]. Small diameter, few or single mode silica fibers are used for SRS amplification [1-20]. They can be very long up to 1000 m and have a diameter of less than 5 μm. Therefore, it is possible to arrange a long interaction length between pump and scattering beams at a very high radiation intensity. Fused silica fibers have a broad Raman spectrum spread from 50 to 650 cm^{-1}. Optimal fiber lengths and germanium concentration, where the first Stokes power

reaches maximum, were calculated at various pump power levels for application in Raman amplifiers.

Narrow-band SRS amplification is possible with crystal and crystal fiber, which is very important for the construction of narrow-band SRS converter. Raman shifting in different materials such as **inorganic** and **organic crystals** and **glasses** is a promising technique which can address these needs. SRS on different crystalline and glassy Raman active media, **tungstates** [1-21]-[1-23], **molybdates** [1-24, 1-25], **borates** [1-26, 1-27], **silicates** [1-28, 1-29], **iodates** [1-30, 1-31], **niobates** and **tantalates**[1-28, 1-32], **nitrates** [1-33]-[1-35], **chlorides** and **bromides** [1-36]-[1-38], **aluminates** [1-39], **germanates** [1-40] and **sulfates** [1-32] have been observed. The most efficient and reliable solid state lasers emit in the near infrared, e.g. the Nd:YAG-laser has the main wavelength at **1064 nm** and frequency doubling generates **532 nm**. The number of available wavelengths can be largely increased by SRS covering the visible, near and mid infrared and near ultra violet spectral regions.

Goals of our work

New materials and SRS-experiments

We investigate new inorganic and organic crystals and glasses materials as they became available to use. These materials exhibit covalent bonds and a large polarizibility, which are prerequisites for efficient SRS. The materials pump with a **picosecond Nd:YAG laser** at 1064 nm or its **second harmonic (SHG)** at 532 nm wavelength. We study their **phonon spectrum**, **SRS thresholds** and **SRS gain factors**. We generate higher order **Stokes** and **anti Stokes** frequencies generation. We observe the generation of SRS signals of different phonons and simultaneous generation of several SRS lines of the investigated materials.

Raman lasers

We will use nonlinear frequency conversion in order to generate new coherent light sources over a wide discrete tuning range covering the **visible** and **near IR** spectral range for various potential applications in laser engineering. We will investigate second-Stokes Raman laser to generate coherent beam with wavelength longer than the pump. Furthermore, we generate the frequency doubling of the investigated Raman Laser. We will investigate anti-Stokes Raman laser in crystal for the first time.

In this work high-order Stokes and anti-Stokes are observed in inorganic, organic and glasses materials. Raman shifts ranging from 91 to 3070 cm^{-1} have been observed. The smallest Raman shift of 91 cm^{-1} was identified in cubic $Bi_4Ge_3O_{12}$ and $Bi_4Si_3O_{12}$ inorganic crystals while, the largest Raman shift of 3070 cm^{-1} was determined in orthorhombic Benzophenone ($C_{13}H_{10}O$) organic crystals. Most of the investigated inorganic crystals and BiB_3O_6 and $Bi_4Ge_3O_{12}$ organic crystals are acentric crystals and showing also high quadratic nonlinear susceptibilities (χ_2). Therefore, these crystals generate SRS as well as second harmonic generation (SHG). In addition, **sum frequency mixing (SFM)** was observed in $Bi_4Ge_3O_{12}$ and (MNBA) $C_{16}H_{15}N_3O_4$ crystals. The mean condition for the steady-state pumping condition is the pump pulse duration τ_p is much longer than the vibronic Raman mode **dephasing (relaxation) time T_R ($\tau_f >> T_R$)**. We use a laser with pump pulse duration of $\approx$ 120 ps and the observed relaxation time range from 0.44 to 7 ps in our investigated materials. Furthermore, **Raman gain coefficient (g_R)** for most of the investigated materials, under our experimental conditions was estimated. Finally, second-Stokes $PbWO_4$ Raman laser at λ_{S2} = 1316 nm wavelength with Raman shift ν_R = 901 cm^{-1} has been demonstrated. Second harmonic generation of the second-Stokes line at λ = 658 nm was obtained.

2 Nonlinear frequency conversion in crystals

Lasers generate coherent radiation at many wavelengths ranging from the far infrared region to the soft X-ray spectral region. Nonlinear frequency conversion processes in crystals use to provide new coherent light sources and extend the number of emission wavelengths of currently available solid state lasers. The very wide spectral range and efficiency of nonlinear interactions assures that they will become increasingly important as coherent sources. In this chapter, second and third-order nonlinear processes are described briefly. Second harmonic generation (SHG), stimulated Raman scattering (SRS) and Raman four wave mixing (RFWM) are practically significant applications of these processes. Finally, characteristics of Raman scattering are discussed.

2.1 Nonlinear phenomena

When a medium is subjected to an electric field the atoms and molecules in the medium are polarized [2-1]. The polarization ***P*** is defined as the dipole moment per unit volume that is

induced in a material in response to an electric field applied to the material. For a weak electric fields the polarization $\boldsymbol{P}$ is linearly proportional to the applied electric field $\boldsymbol{E}$

$$\boldsymbol{P} = \varepsilon_0 \chi_1 \boldsymbol{E} \qquad (2.1.1)$$

Where χ_1 is the linear optical susceptibility and $\varepsilon_0 = 8.85 \times 10^{-12}$ *F/m* in mks units, is the permittivity of free space. The linear susceptibility is related to the medium index of refraction n by $\chi_1 = n^2 - 1$.

When the electric field is increased significantly, nonlinear interactions begin to occur within the material. Equation *(2.1.1)* must therefore be generalized to express the polarization $\boldsymbol{P}$ as a power series in the field $\boldsymbol{E}$ as follows

$$\boldsymbol{P} = \varepsilon_0 [\chi_1 E + \chi_2 E^2 + \chi_3 E^3 + \cdots\cdots] \qquad (2.1.2)$$
$$P_{(lin)} + \quad P_2 + \quad P_3 + \cdots\cdots$$

where χ_2 is the second-order nonlinear susceptibility and χ_3 is the third-order nonlinear susceptibility. In addition, the second-and third-order susceptibilities are of the order of $\chi_2 = 2\text{x}10^{-11}$ m/V and of $\chi_3 = 4\text{x}10^{-23}$ m/V respectively. A number of interesting optical phenomena arise from the second and third-order-susceptibilities. For example, χ_2 gives rise second harmonic generation [2-2], parametric oscillation [2-3], and three-frequency processes such as mixing [2-4] and sum generation. The nonlinear susceptibility χ_2 vanishes in crystals that have a center of symmetry. In these crystals second-harmonic generation is not possible. The third-order susceptibility is responsible for third harmonic generation [2-5], and Raman [2-6], Brillouin [2-7], and Rayleigh [2-8] scattering.

2.2 χ_2 -frequency doubling

Probably the simplest second-order process is that of second harmonic generation. In this process, an intense laser beam of angular frequency $\omega_p = 2\pi\nu_p$ is passed through a crystal having a nonzero value of χ_2. The emerging beam from the crystal contains the angular frequency ω of the input beam and also $\omega = 2\omega_p$, twice the frequency of the input beam. Assuming an oscillating electromagnetic field of frequency ω_p incident upon the material, this field can be described by the equation [2-9]

$$E = E_0 e^{-i\omega_p t} + E_0^* e^{+i\omega_p t} \qquad (2.2.1)$$

where the second term on the right is the complex conjugate of the first term. The second-order nonlinear polarization P_2 can now be computed from (2.1.2)

$$P_2 = \varepsilon_0 \chi_2 E^2$$
$$= \varepsilon_0 \chi_2 [2 E_0^* E_0 + E_0^2 e^{-i(2\omega_p)t} + E_0^2 e^{+i(2\omega_p)t}] \qquad (2.2.3)$$

The first term is a time-independent factor that produces no oscillating electromagnetic radiation. The second and third terms can be seen to contain frequencies that are exactly twice the frequency of the fundamental wave. These terms lead to a significant output from the material at an angular frequency of $2\omega_p$. Such output is referred to as *second harmonic generation* (SHG).

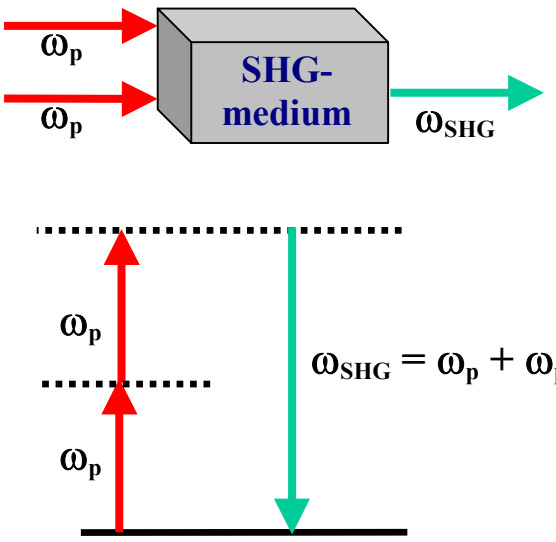

Fig. 2.1: *Second harmonic generation (SHG).*

Fig. 2.1 shows a simple picture of second harmonic generation. It shows two photons of the fundamental frequency ω_p, each with energy $\hbar\omega_p$. They combine to produce a photon with an energy of $2\hbar\omega_p$, where $\hbar = h/2\pi$ and $h = 6.6256\ 10^{34}\ Js$, is Planck's constant. The energy levels $\hbar\omega_p$ and $2\hbar\omega_p$ are illustrated as dashed lines. They are known as virtual levels, since they are not levels to accrue population. Instead two photons of frequency ω_p are destroyed and one photon of frequency $2\omega_p$ is simultaneously created, as indicted in Fig. 2.1.

In nonlinear interaction phase-matching selects the process of interest and excludes other possible processes. Thus, if the crystal birefringence is adjusted (by temperature or angle of propagation) such that the second harmonic generation is the phase-matched process. It proceeds with relatively high efficiency compared to the remaining processes involving sum and difference frequency generation.

2.3 χ_3 - Raman scattering

The third-order nonlinear processes can be applied to all optical materials, centrosymmetric or non-centrosymmetric. As mentioned before the third-order susceptibility is responsible for Raman scattering. We will study spontaneous Raman scattering, SRS and Raman four wave mixing (RFWM) processes. In this work, we will use SRS and RFWM in crystals to generate new coherent Raman lasers.

Spontaneous Raman scattering

Spontaneous Raman scattering is an inelastic process in which scattered light undergoes a frequency change characteristic to the internal energy level of the irradiated molecules. This process happens at relatively low excitation energies. A pump wave $\boldsymbol{E} = \boldsymbol{E_p}\ sin\ (2\pi\nu_p t)$ is incident on a molecule. Under the influence of the field, the electrons of the molecule oscillate. The electric dipole moment $\boldsymbol{m}$ arises proportional to $\boldsymbol{E_p}$, [2-10]:

$$\boldsymbol{m} = \alpha \boldsymbol{E} = \alpha\, \boldsymbol{E_p}\ sin\ (2\pi\nu_p t) \qquad (2.3.1)$$

α is the polarizability of the molecule. If there are now, in addition, internal molecular vibrations with a frequency $2\pi\nu_R$, for example, due to oscillations of some nuclei against one another, the polarizability can change periodically with

$$\alpha = \alpha_0 + \alpha_1\ sin\ (2\pi\nu_R t) \qquad (2.3.2)$$

Thus from equation (2.3.1) follows:

$$\boldsymbol{m} = \alpha_0\, \boldsymbol{E_p}\ sin\ (2\pi\nu_p t) + (\alpha_1\, \boldsymbol{E_p} / 2)\{cos[2\pi(\nu_p - \nu_R)t] - cos[2\pi(\nu_p + \nu_R)t]\} \qquad (2.3.3)$$

Where α_0 is the polarizability of the molecule oscillation. Therefore, the oscillating dipole moment $\boldsymbol{m}$ of the molecule contains three frequencies that are emitted. The frequency ν_p of the incoming light appears again, this is *elastic Rayleigh scattering*. But there are still two new frequencies:

$$\nu_s = \nu_p - \nu_R, \qquad \nu_{as} = \nu_p + \nu_R \qquad (2.3.4)$$

referred to as the *Stokes* and *anti-Stokes frequencies*. The frequency ν_R is called the Raman shift which is characteristic of the material in which the Raman process is observed. Equation (2.3.4) represents, after multiplication with h, conservation of energy for the Stokes and anti-Stokes process:

$$h\nu_s = h\nu_p - h\nu_R, \qquad h\nu_{as} = h\nu_p + h\nu_R \qquad (2.3.5)$$

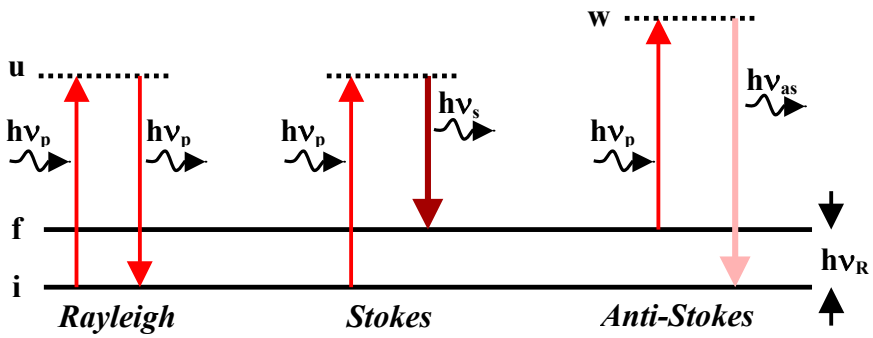

Fig. 2.2: *Spontaneous Raman scattering*

Fig. 2.2 shows a photon with energy $h\nu_p$ hits a molecule that is in the initial level i. The molecule absorbs the photon and is then in the upper virtual level u. There are two possibilities then:

1. The molecule returns into the initial level i and the whole energy $h\nu_p$ is emitted again. The photon has only changed its direction, but has transferred no energy to the molecule. This is elastic Rayleigh scattering (see Fig. 2.2).
2. The molecule returns to the final level f. Here, a photon with the energy $h\nu_s = h\nu_p - h\nu_R$ is emitted. This is the spontaneous Raman scattering in the Stokes case. The emission in Fig. 2.2 is called the first Stokes line, usually written S_1.

However, if initially the molecule is already in the final level f the molecule absorbs the photon energy $h\nu_p$ and is then in the higher energy level w. The molecule returns to the initial level i and emits a photon with energy $h\nu_{as} = h\nu_p + h\nu_R$. This is the spontaneous Raman scattering in the anti-Stokes process. The emission in Fig. 2.2 is called the first anti-Stokes, usually written AS_1. The Stokes line has lower frequency (longer wavelength) and anti-Stokes line has higher frequency (shorter wavelength) than the pump radiation. The Stokes and anti-Stokes lines are much weaker than the pump radiation. Moreover, for usual Raman active crystals there are considerably less molecules in the final level f than initial level i in thermal equilibrium at room temperature. Thus, the anti-Stokes lines are always much weaker than the Stokes lines at thermal equilibrium.

Stimulated Raman scattering

For large light intensities (laser light), besides increased spontaneous Raman scattering however, another effect occurs, the *induced* or *stimulated Raman effect*. The stimulated Raman effect is also an inelastic scattering process. An incoming photon $h\nu_p$ gives rise to the transition of the molecule from the initial level i to the upper virtual level u. It remains for a short duration. If

now within this brief time, a Stokes photon $h\nu_s$ that has been created elsewhere hits this molecule, a so-called induced emission can result. That is a Stokes photon $h\nu_s$ will be created (see Fig. 2.3a). In this case the Stokes radiation becomes amplified, while the pump radiation loses energy. It means that, the Stokes beam is generated by spontaneous Raman scattering is subsequently amplified by SRS. Then SRS is considered a two-phonon stimulated process grown out of spontaneous Raman emission. The generated Stokes photon coincides exactly with the incoming Stokes photon in direction, frequency, phase and polarization. In contrast to the incoherent spontaneous Raman emission, we have here coherent radiation. An additional line will be emitted with energy $h\nu_{as}$ which is called anti-Stokes line. It coincides exactly with the incoming anti-Stokes photon in direction, frequency, phase and polarization. As energy balance we simply have

$$h\nu_p + h\nu_s = 2h\nu_s + h\nu_R \qquad \textit{(Stokes)}$$

$$h\nu_p + h\nu_{as} = 2h\nu_{as} - h\nu_R \qquad \textit{(anti-Stokes)} \tag{2.3.6}$$

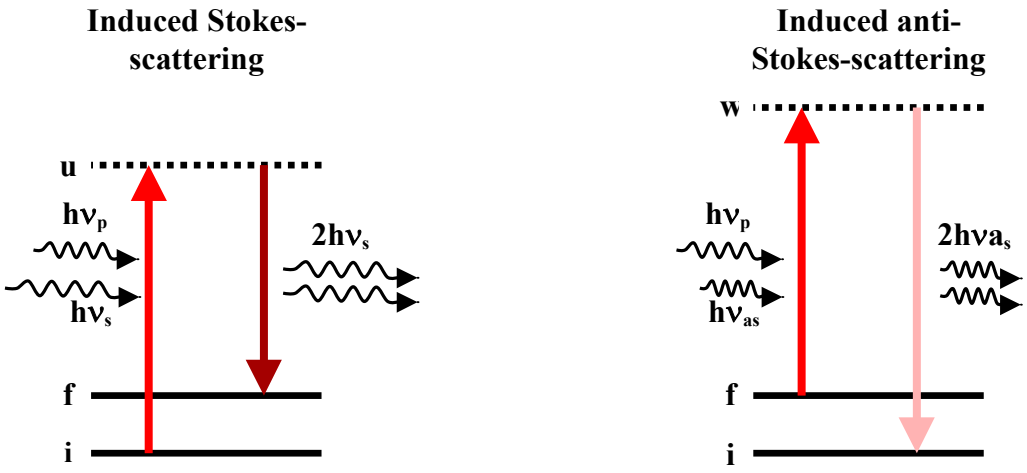

Fig. 2.3: *Level diagram for induced (or stimulated) Stokes and anti-Stokes scattering.*

Fig. 2.3 shows the induced Stokes and anti-Stokes Raman scattering. Raman process is useful in Solid-state lasers for the generation of additional spectral lines. The strongest interaction is for the output shifted towards a longer wavelength (first Stokes line). At sufficiently high pump intensities additional lines at longer as well as shorter wavelengths with respect to the pump wavelength will appear (Stokes and anti-Stokes lines).

Raman four wave mixing

Stimulated Raman scattering occur if a high power laser beam is focussed into a Raman media. The first Stokes is emitted in the direction of the incident beam and may have high power and conversion efficiency. When the first Stokes generation is strong enough, it generate the second Stokes emission and so on (see Fig. 2.4a). The Stokes frequencies are given by $h\nu_{S(n)} = h\nu_p + nh\nu_R$, where n is the Stokes order.

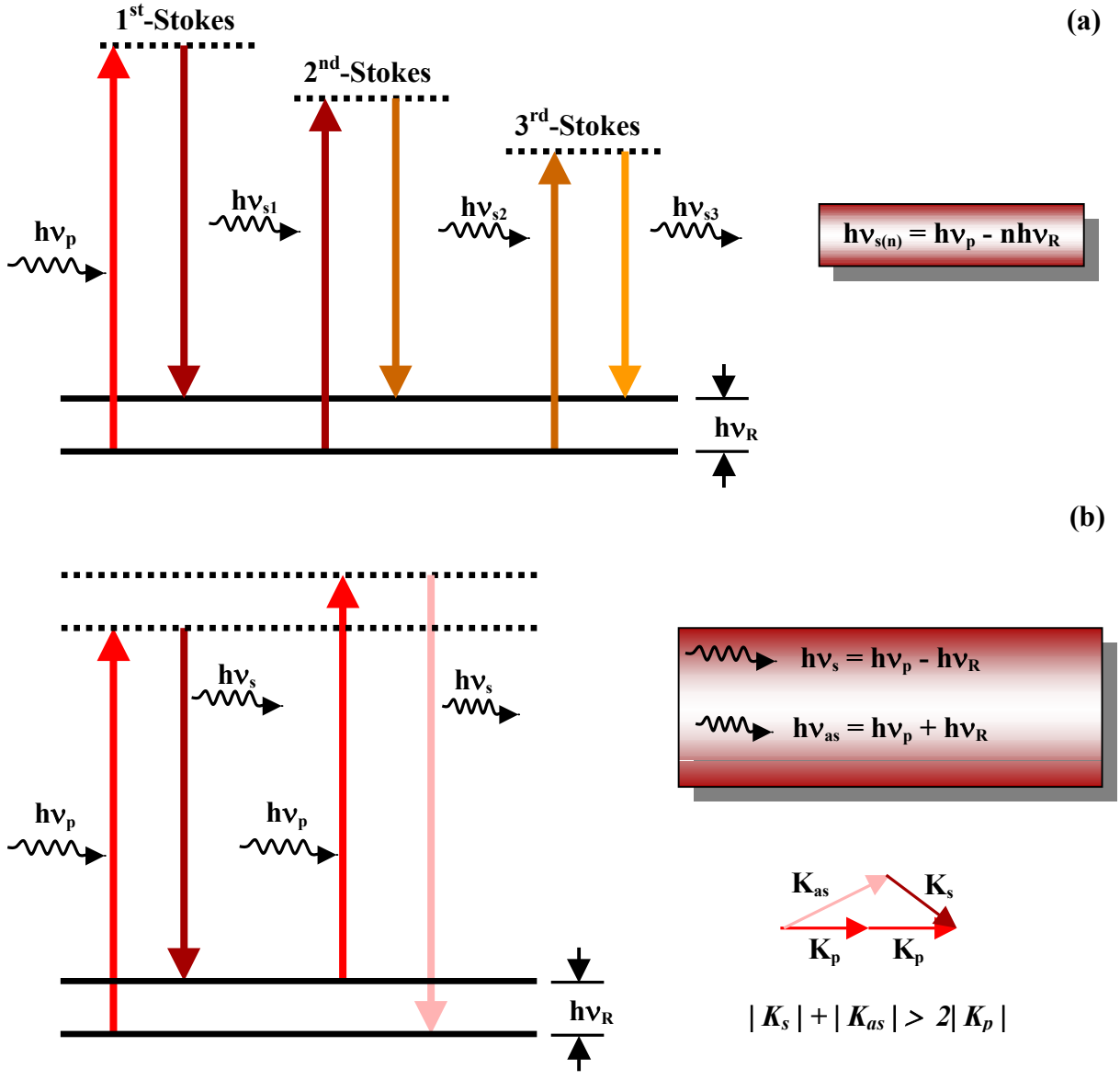

Fig. 2.4: *First and higher-order Stokes generation of stimulated Raman scattering SRS a) and combined Stokes and anti-Stokes generation of Raman four wave mixing RFWM b).*

Stokes and anti-Stokes lines can be generated simultaneously by parametric Raman four-wave mixing (RFWM). Fig. 2.4b shows parametric four-wave mixing process. This takes place as follows, after a photon with energy $h\nu_p$ has created a Stokes photon, the molecule is in excited state. This energy is immediately used by a second photon with $h\nu_p$ for the emission of an anti-Stokes photon. Then we have a Stokes-anti-Stokes coupling. Now, Stokes and anti-Stokes waves with comparable intensities are found. The frequency of the n^{th} order Stokes and anti-Stokes lines can be written as

$$\nu_{s(n)} = \nu_p - n\cdot\nu_R, \qquad \nu_{as(n)} = \nu_p + n\cdot\nu_R \qquad n = 1,2,3,\cdots \tag{2.3.7}$$

As energy balance, we simply have

$$2h\nu_p = h\nu_s + h\nu_{as} \tag{2.3.8}$$

In parametric effect, a momentum balance must be fulfilled among the propagation vectors of the participating light waves

$$2K_p = K_s + K_{as} \tag{2.3.9}$$

where

$$|K_p| = \nu_p n_p / c, \qquad |K_s| = \nu_s n_s / c, \qquad |K_{as}| = \nu_{as} n_p / c$$

and $n_{P,s,as}$: refractive index and $K_{p,s,as}$: wave vector of the pump, the Stokes and anti-Stokes waves. Because the frequencies lie very close together, one can expand in the neighborhood of $\nu = \nu_p$:

$$n_s = n(\nu_s) = n_p - \nu_R\cdot dn/d\nu, \qquad n_{as} = n(\nu_{as}) = n_p + \nu_R\cdot dn/d\nu$$

where $\nu_R = \nu_p - \nu_s = \nu_{as} - \nu_p$. Thus,

$|K_s| + |K_{as}| = 2|K_p| + \frac{4}{c}\cdot\pi\nu_R^2\cdot\frac{dn}{d\nu}$. In the region of normal dispersion $dn/d\nu > 0$, so

$$|K_s| + |K_{as}| > 2|K_p| \tag{2.3.10}$$

that is the required conservation of momentum. Stokes and anti-Stokes waves are radiated in the form of conical shell around the direction of the incidence beam with a definite aperture. Fig. 2.4a shows stimulated Raman scattering process for the first Stokes and higher-order. The first Stokes is emitted in the direction of the incident beam and may have high power and conversion efficiency. When the first Stokes generation is strong enough, it generates the second Stokes emission and so on. The Stokes frequencies are given by $\nu_{s(n)} = \nu_P - n\nu_R$, where n is the Stokes-order. Fig. 2.4b shows that Stokes and anti-Stokes lines can be generated simultaneously. This process is called also four-wave mixing because 4 photons are involved. The figure shows also the wave vectors of the pump, the first Stokes and first anti-Stokes.

2.4 Characteristics of SRS

Relaxation time

The theory of SRS is well developed and can be found [4-11, 4-12]. Here we would like to outline that depending on the pump laser pulse duration *(τ_f)*, two temporal cases can be considered. The first one is a steady state regime, when the pump pulse duration τ_p is much longer than the vibronic Raman mode dephasing (relaxation) time T_R *($\tau_f >> T_R$)*. The second case is a transient regime, when the pump pulse duration is smaller than the dephasing time ($\tau_f << T_R$) and the spectral width of pump laser $\Delta\nu_f$ is much broader than the Raman line broadening $\Delta\nu_R$. The main condition for the steady-state pumping condition, which is of more interest for many practical cases, is

$$\tau_p >> T_R = \frac{1}{\pi c \Delta\nu_R} \qquad (2.4.1)$$

where T_R, $\Delta\nu_R$ and c are the dephasing (relaxation) time of the SRS active vibration mode and the full-width half maximum (FWHM) linewidth of the corresponding spontaneous Raman scattering line and the speed of light, respectively.

Raman gain

The fundamental parameter in Raman laser is the Raman gain coefficient. Raman laser and amplifiers with gas cell have low Raman gain over long path lengths. In contrast a solid-state system has high gain over short path lengths.

If the intensity of the pump (fundamental) laser radiation I_f is much higher than the intensity of the Stokes emission $I_f >> I_S$ (steady state SRS regime without pump depletion), the SRS amplification can be written [2-13, 2-14] as,

$$\frac{dI_{S1}}{dl} = g_{ssR} I_f(l) \cdot I_{S1}(l) + I_f(l) \cdot \frac{d\sigma}{d\Omega} N_R \Delta\Omega$$

$$= g_{ssR} I_f(l)[\, I_{S1}(l) + I_{S1}(l = 0)] \qquad (2.4.2)$$

where $I_{S1}(l = 0)$ is the intensity of the spontaneous Raman scattering at the wavelength λ_{S1} of the first Stokes seed emission (in the beginning $l = 0$ of the amplified sample) and g_{ssR} is the steady-state Raman gain coefficient,

$$g_{ssR} = \frac{\lambda_f \lambda_S^2 N_{SRS}}{hc\pi n_S^2 \Delta\nu} \left(\frac{d\sigma}{d\Omega}\right) \qquad (2.4.3)$$

where, $d\sigma / d\Omega$ is the Raman scattering cross-section, N_{SRS} is the number of SRS-active atoms or structure units of the crystal, λ_f and λ_S are the pump and Stokes wavelengths, respectively, n_S the refractive index at λ_S and $\Delta\Omega$ the (small) angle of the SRS. In this SRS regime the Raman gain coefficient is linearly proportional to the scattering cross-section and inversely proportional to the line width of the spontaneous Raman scattering transition. The product $(d\sigma / d\Omega)(1/\Delta\nu_R)$ can be characterized as a peak intensity in the measured spontaneous Raman scattering spectrum [2-15]. Furthermore, the Raman linewidth (FWHM) is determined by the relaxation time T_R of the vibrational mode as $\Delta\nu = (\pi c T_R)^{-1}$. Finally, the Raman linewidth has a strong temperature dependence [2-16]. Therefore, high-gain Raman materials should have a narrow Raman line width and a high Raman scattering cross-section. In addition, the normal transparency region must also be determined to insure that the material can be used in the spectral region of interest.

The intensity of the Stokes beam is given by solving equation 2.4.2 yields [4-12]:

$$I_S(l) = I_S(0)\, exp(g_{ssR}\, I_f\, l) \qquad (2.4.4)$$

Here $I_S(l)$ is Stokes intensity at exit of the Raman medium and l the length of the active crystal. These expressions show that the intensity of the Raman beam increases with intensity of the pump laser radiation and the interaction length. SRS threshold for the first Stokes Raman generation performed when the exponent in equation 4.4.2 reaches the value of $g_{ssR}I_p l = 25\text{-}30$, which corresponds to a conversion efficiency of approximately $1\ \%\ (I_S / I_f \approx 0.01)$. Using this approximation, we have calculated the Raman gain coefficient for most of the investigated materials, under our experimental conditions.

One of the best examples of a new solid-state Raman material is barium nitrate $Ba(NO_3)_2$. The crystal provides a frequency shift of 1047 cm^{-1} with an small line width of 0.6 cm^{-1}. It has Raman gain as high as 11 cm/GW for the fundamental at 1064 nm wavelength and 47 cm/GW for its SHG at 532 nm wavelength pumping [2-17]-[2-19]. $Ba(NO_3)_2$ crystals are available in large size with high optical quality and high laser damage threshold of about 1 $GWcm^2$.

Cubic barium nitrate $Ba(NO_3)_2$ crystal is used as example for SRS and RFWM processes in crystals. Plane parallel sample without coating and with 70 mm length and 10x10 mm^2 cross-section uses to create the SRS experiment. For SRS experiment we use picosecond Nd:YAG laser excitation at the fundamental at λ_{f1} = 1064.15 nm and its SHG at λ_{f2} = 532.07 nm.

Fig. 2.5 shows first and higher-order Stokes and anti-Stokes lines in $Ba(NO_3)_2$ crystal. Stokes and anti-Stokes lines related to the SRS-active vibration mode of ν_R = 1047 cm^{-1}. Spectral composition of Stokes and anti-Stokes Raman generation and Raman shift in $Ba(NO_3)_2$ crystal were listed in Table 2.1.

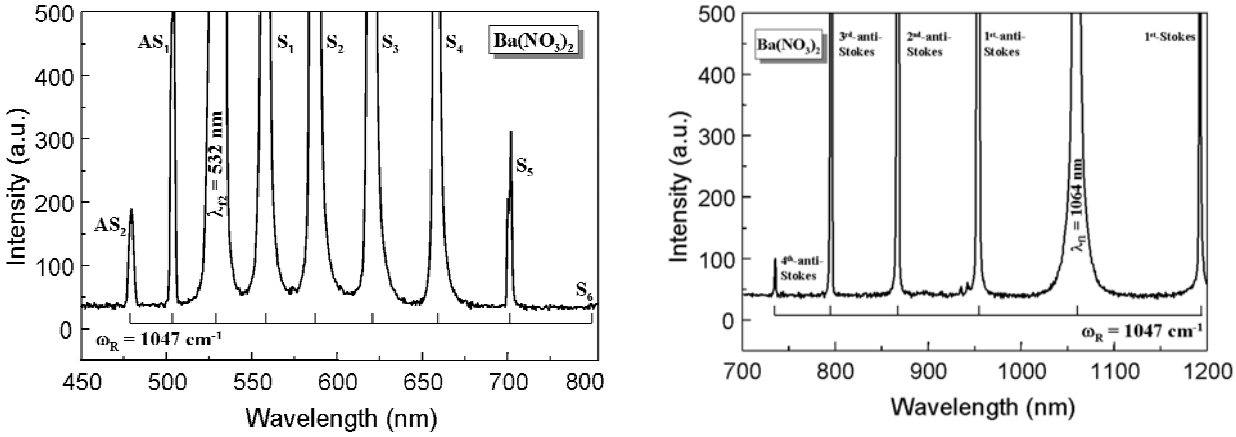

Fig. 2.5: *Room-temperature SRS and RFWM spectra of cubic $Ba(NO_3)_2$ single crystal obtained under excitation at λ_{f1} = 1064 nm wavelength and at λ_{f2} = 532 nm wavelength.*

Table 2.1: *Spectral composition of Stokes and anti-Stokes Raman generation and SRS-active vibration mode in cubic $Ba(NO_3)_2$ single crystal under picosecond excitation at λ_{f1}=1064 nm wavelength and at λ_{f2} = 532 nm wavelength.*

Pump wavelength (nm)	Stokes and anti-Stokes wavelengths (nm)	SRS-and-RFWM line attribution	line	Raman shift (cm^{-1})
1064	736	$\nu_{f1} + 4\nu_R$	AS_4	1047
	798	$\nu_{f1} + 3\nu_R$	AS_3	1047
	870	$\nu_{f1} + 2\nu_R$	AS_2	1047
	958	$\nu_{f1} + \nu_R$	AS_1	1047
	1064	ν_{f1}		
	1198	$\nu_{f1} + \nu_R$	S_1	1047
532				
	479	$\nu_{f2} + 2\nu_R$	AS_2	1047
	504	$\nu_{f2} + \nu_R$	AS_1	1047
	532	ν_{f2}		
	564	$\nu_{f2} - \nu_R$	S_1	1047
	599	$\nu_{f2} - 2\nu_R$	S_2	1047
	639	$\nu_{f2} - 3\nu_R$	S_3	1047
	685	$\nu_{f2} - 4\nu_R$	S_4	1047
	738	$\nu_{f2} - 5\nu_R$	S_5	1047
	799	$\nu_{f2} - 6\nu_R$	S_6	1047

2.5 Nonlinear optical materials

Nonlinear crystals must satisfy some criteria if they are to be useful for nonlinear optical applications. In addition to having a large nonlinearity, these materials must be transparent not only at the laser frequency but also at the newly generated frequency. They must be:

- resistant to optical damage,
- exhibit good thermal and chemical stability,
- be capable of being grown in useful size, and
- have the appropriate phase-matching properties.

Table 2.2 lists a number of second-order nonlinear optical materials. They have high nonlinear conversion coefficients as well as the necessary transparency.

Crystal	Transparency region (μm)
LiB_3O_5	0.16-2.6
β-BaB_2O_4	0.19-2.5
$KNbO_3$	0.40-5.5
$LiNbO_3$	0.40-5.0
$Ba_2NaNb_5O_{15}$	0.37-5.0
KDP	0.20-1.4
KTP	0.35-4.4

Table 2.2:
Second order nonlinear optical materials.

3 Experimental set-up

For Raman laser converters experiment single picosecond pulses from a flashlamp pumped active/passive mode-loked Nd:YAG laser are used [3-1]. An acousto-optic mode locker (AOM) is added to improve the stability of the laser output.

The experimental set-up for stimulated Raman scattering consists of an active-passive mode-locked Nd:YAG master oscillator produces picosecond pulse train. The fundamental laser beam emits at λ_{f1} = 1064.15 nm wavelength ($^4F_{3/2} \rightarrow {}^4I_{11/2}$ laser channel). Furthermore, an external pockels-cell pulse slicer transmits only the central pulse and a subsequent two-stage amplifiers to increase the energy of the single pulse. In addition, an external KD*P frequency doubler converts the fundamental to the SHG at λ_{f2} = 532.07 nm as shown in Fig. 3.1. We will study in this chapter the properties of the Gaussian beam. Finally, we report the measurements of the laser beam radius by the method of sharp-edge.

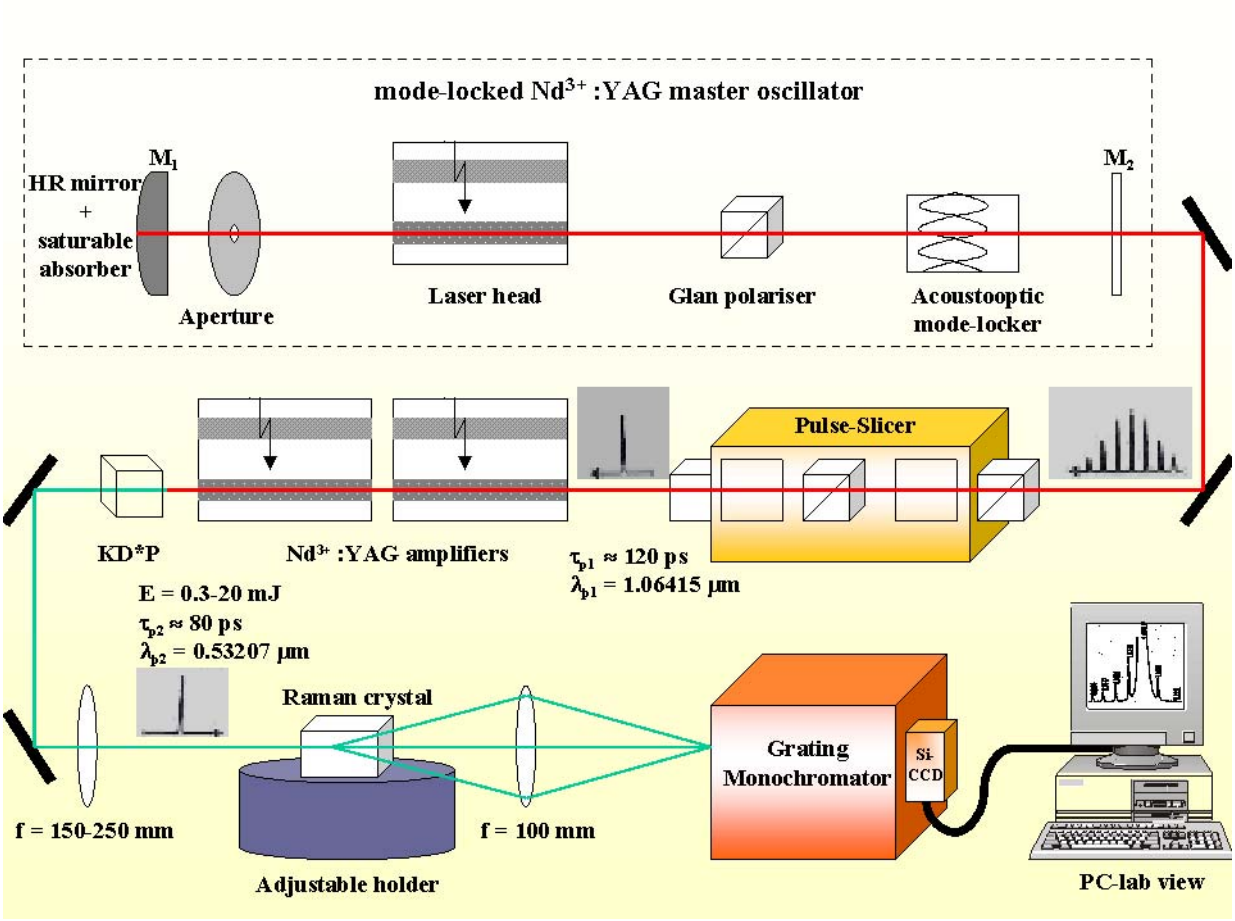

Fig. 3.1: *Experimental set-up.*

3.1 Nd:YAG-laser

Dye Q-switch and acoustooptic mode-locker

The dye Q-switch is very simple device. It consists of a dye cell which is placed between the laser rod and the rear mirror M_1. The dye uses to absorb the fluorescent emission from the laser rod to the degree that the rear mirror M_1 is optically isolated from the remainder optical cavity. When the dye bleaches, the laser radiation can reach the rear mirror and laser oscillation occurs. The generic name for the type of material which uses in the dye cell is *saturable absorber*. In these liquids the absorption coefficient decreases readily with increasing light intensity. Thus, the material becomes more transparent as the light becomes more intense. The increase in the transparency of the dye is called *bleaching* of the dye. Dye Kodak Lamda No. 26 was used [3-2]. It dissolves in 1,2-dichloroethan (laser grade) at a concentration of about 10^{-4} M [3-3]. The dye concentration depends on the lamp input energy and the resonator length. It adjusts by observing

the laser output with a fast photodiode connected to an oscilloscope. The concentration is chosen to obtain about 9 pulses. Fig. 3.2 shows the train of pulses.

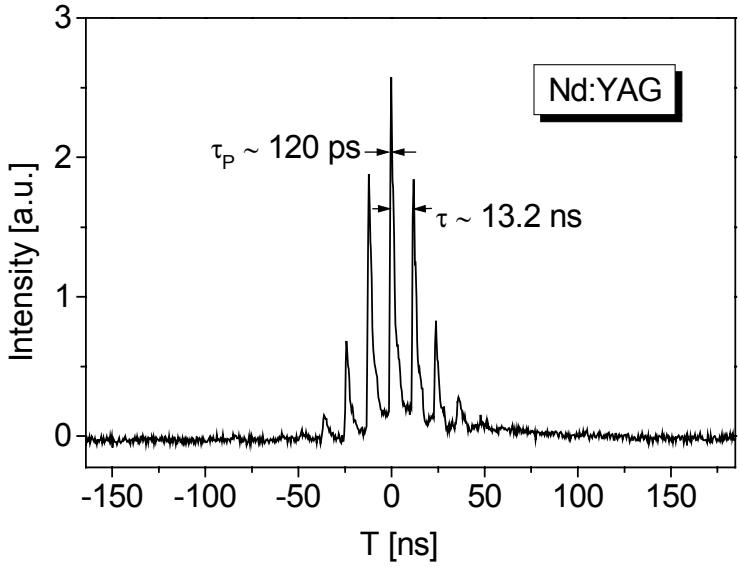

Fig. 3.2:
Pulse train of the active-passive mode-locked $Nd^{3+}:Y_3Al_5O_{12}$ laser at λ_{f1} = 1064.15 nm.

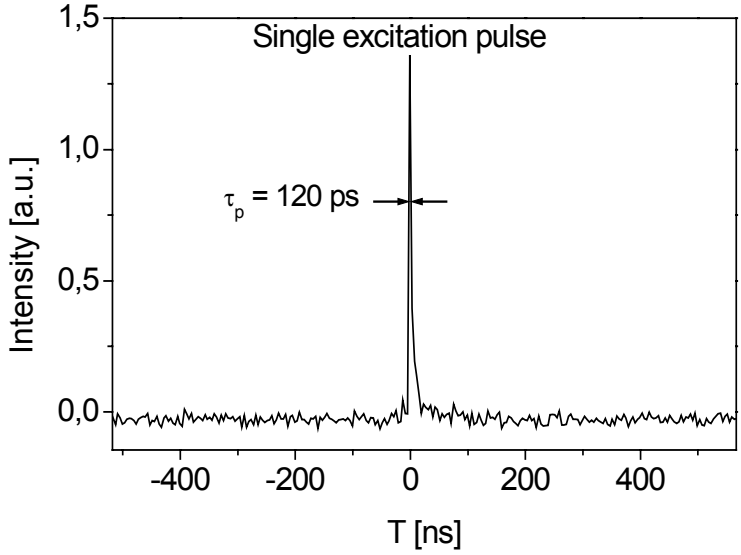

Fig. 3.3:
Single pulse with time duration 120 ps is produced by the pulse slicer.

Resonator

A plano-concave resonator with length of 1.7014 m was used. The rear mirror M_1 with radius of –8 m has high reflectivity for wavelength 1064 nm and is part of the contacted dye cell for passive mode locking. The output coupler M_2 is plane mirror and has a reflectivity of 60 %. The laser head includes a water-cooled elliptical pump cavity and a Nd:YAG laser rod. The dimensions of the laser rod are 6 mm radius and 50 mm length with plane parallel faces. It is pumped by xenon flash-lamp. A pinhole with 1.9 mm diameter places between the laser head and the dye cell to select a TEM_{00} spatial mode. The laser radiation is polarized by a Glan polariser. The acoustooptical mode-locker is located near the output coupler and driven by a

radio-frequency with power about 2 W. The round trip frequency of the circulating pulse is adjusted to match the modulation frequency of 44,08 MHz of the acousto-optical mode locker by displacement of mirror M_2. The acousto-optical modulator is temperature controlled by a water cooler. Furthermore, radio frequency generator is operating permanently with constant power to achieve a stable operation. Under this conditions the laser oscillator emits a picosecond pulse train 8-12 with a time separation given by a round-trip of 13.2 ns as shown in Fig. 3.2. The output laser beam is linearly polarized and emits with energy of about 2.5 mJ.

3.2 pulse selector and amplifiers

Pulse selector

Instead of a train of pulses of various intensity and duration, in our experiments a single pulse with favorable parameters is required. For this purpose, an appropriate pulse is separated from the train by using the pulse selector [3-4]. Fig. 3.3 shows that the pulse selector transmits only the central pulse. The pulse selector locates directly after the output coupler and triggers by a trigger unit. The trigger unit consists a photodiode and three IC-blocks forming a variable electrical time gate for the trigger signal. This selector consists of four pockels cells in conjunction with three polarizers as shown in Fig. 3.4. The polarization direction of the first two polarizers is horizontal and the last one vertical. The two pockels cell pairs switch by two pair avalanche transistor cascades. The first two polarizers are perpendicular with the third one, so that no pulse can pass through the last polarizer. After triggering, only a single pulse can pass the last polarizer, where the two Pockels cell pairs are biased with a high voltage of λ/4-voltage. The single pulse has energy about 0.12 mJ and time duration of about 120 ps (FWHM).

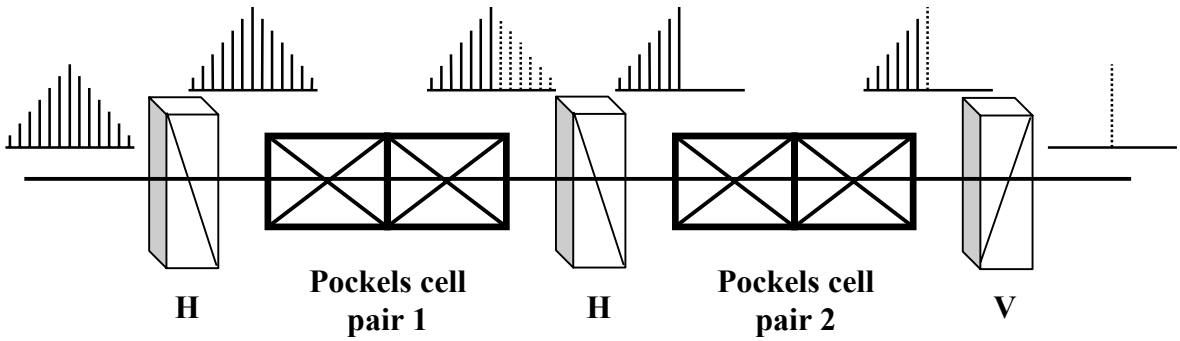

Fig. 3.4: *Single pulse selector (H) horizontal polarization (full lines in the pulse train) and (V) vertical polarization (doted lines in the pulse train).*

Amplification

The energy of the polarized single pulse increases up to 15 mJ by the following two Nd:YAG amplifiers. They are pumped with 40 J and provide energy gain 15 and 10 times respectively. The two amplifiers works exactly with the same materials as for the oscillator. The laser rods of the two amplifiers have the same geometrical parameters. The diameter of the laser rod is 6 mm and the length is 55 mm.

3.3 Beam propagation

Properties of Gaussian beams

A light beam emitted from a laser with a Gaussian intensity profile is called the fundamental mode TEM_{00} as shown in Fig. 3.5. The decrease of the intensity with distance r from the axis in a Gaussian beam is described by [3-5]

$$I = I_0 \, e^{-2r^2 / w^2(z)} \qquad (3.3.1)$$

where $w(z)$ is the beam waist radius at which the intensity drops to $1/e^2 = 13.5$ % of its value on the axis and I_0 is the maximum intensity.

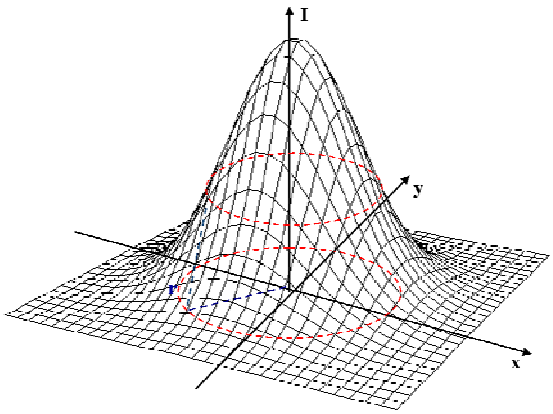

Fig. 3.5: *Gaussian beam profile with intensity I.*

Fig. 3.6 shows the Gaussian beam parameters. The Gaussian beam contracts to a minimum diameter $2w_0$ at the beam waist where the phase front is planer. The beam waist at a distance of $\pm z$ from the minimum beam waist w_0 can be described as

$$w(z) = w_0 \left[1 + \left(\frac{\lambda z}{\pi w_0^2} \right)^2 \right]^{1/2} \qquad (3.3.2)$$

equation (3.3.2) can also be expressed as

$$w(z) = w_0 \left[1 + \frac{z^2}{z_R^2}\right]^{1/2} \tag{3.3.3}$$

or, if the minimum beam waist radius w_0 occurs at a value z_0 such that $z_0 \neq 0$, then

$$w(z) = w_0 \left[1 + \left(\frac{\lambda(z - z_0)}{\pi w_0^2}\right)^2\right]^{1/2} \tag{3.3.4}$$

where

$$z_R = \frac{\pi w_0^2}{\lambda}, \tag{3.3.5}$$

$$w_0 = \sqrt{\frac{2z_R}{K}} = \sqrt{\frac{z_R \lambda}{\pi}}$$

and K is the propagation factor. The term z_R is known as the *Rayleigh range*. It is also referred to as the *depth of focus* when focusing a Gaussian beam. At $z = z_R$ then the beam waist radius is given by $w(z) = \sqrt{2}\, w_0$. An alternative term $b = 2z_R$ is referred to as the *confocal parameter*, a term that is commonly used to characterize Gaussian beams.

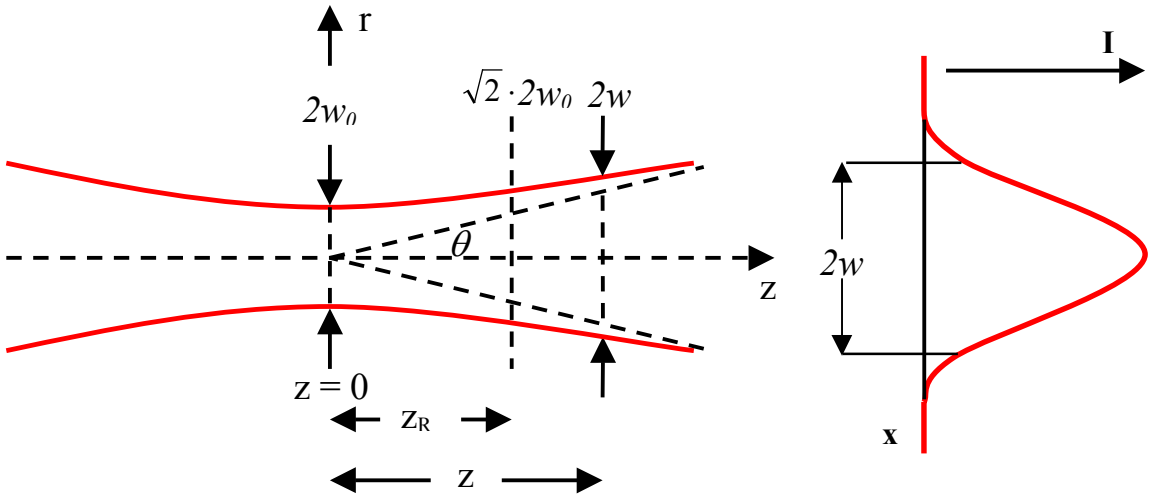

Fig.3.6: *Gaussian beam parameters associated with angular divergence θ and the beam waist diameter, in addition, the intensity distribution of Gaussian beam.*

At $z >> z_R$ the beam waist radius is written as

$$w(z) = w_0 \frac{z}{z_R} \tag{3.3.6}$$

the divergence angle of the Gaussian beam is given as

$$\theta(z) = lim\ \frac{2w(z)}{z} = \frac{2\lambda}{\pi w_0} = 1.27\frac{\lambda}{(2w_0)} \qquad (3.3.7)$$

From these considerations it follows that at large distances, the beam radius increases linearly with z, and the beam diverges at a constant cone angle θ. A most interesting point here is that the smaller the beam radius w_0 at the beam waist, the greater the divergence.

Properties of real laser beam

The previous part described the parameters associated with the dimensions and propagation of an ideal Gaussian-shaped beam TEM_{00} mode. Higher-order modes are not Gaussian-shaped. Therefore, real laser beams, operating multi-mode are not perfect Gaussian beams. A real laser beam has both a waist and divergence that are larger than that of an ideal Gaussian beam.

Let us define the divergence of a real beam as

$$\Theta = M \cdot \theta \qquad (3.3.8)$$

and the minimum waist radius of a real beam as W_0 such that

$$W_0 = M \cdot w_0 \qquad (3.3.9)$$

Thus, multiplying (3.3.8) by (3.3.9) gives the divergence of a real beam as

$$\Theta = M^2\ \frac{2\lambda}{\pi W_0} \qquad (3.3.10)$$

where $M^2 \geq 1$. Thus the factor M^2 describes the relationship of the real beam to that of an ideal Gaussian beam. This M^2 is referred to as a *propagation constant* or a *propagation factor*. For a perfect Gaussian beam $M^2 = 1$. Values of M^2 greater than unity represent laser beam with higher-order modes than the TEM_{00} Gaussian mode.

Transforming a Gaussian beam with simple lens

When a laser beam is focused by a lens, the actual focal spot, meaning the position of minimum spot size and maximum energy. This focal spot does not in fact occur exactly at the geometrical focus of the lens but is located slightly inside the lens focal length.

Assume that the waist of the input beam w_0 represents the object and the waist of the out beam $w_0^{`}$ represents the image as shown in Fig. 3.7 . Then the magnification is given by [3-6]

$$w_0^{`} = w_0\ \frac{f}{\sqrt{(s-f)^2 + z_R^2}} \qquad (3.3.11)$$

and the standard lens equation can be written as

$$\frac{1}{s}+\frac{1}{s`}=\frac{1}{f} \qquad (3.3.12)$$

the analogous formula for Gaussian beam is

$$\frac{1}{s+z_R^2/(s-f)}+\frac{1}{s`}=\frac{1}{f}$$

$$\frac{1}{(s/f)+(z_R/f)^2/(s/f-1)}+\frac{1}{s`/f}=1 \qquad (3.3.13)$$

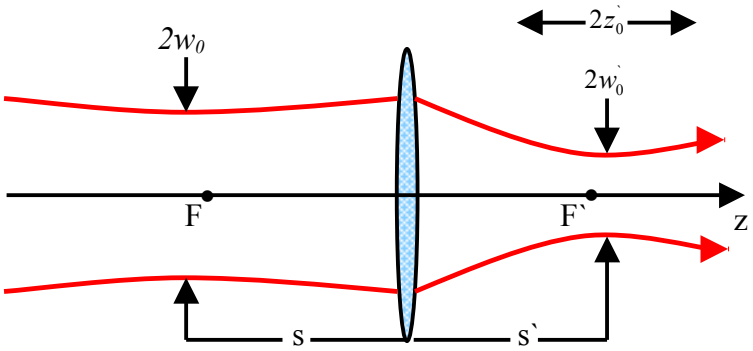

Fig. 3.7: *The beam diameter of the laser beam before and after the convex lens.*

Where s is the object distance, $s`$ is the image distance and $f$ is the focal length of the lens. In the far-field limit $(z_R \rightarrow 0)$ formula (3.10) reduces to the geometric optics equation (3.9). Special case, when the input waist is at the front focal point, $s = f$ then $s` = f$ and the waist of the out beam written as

$$w_0` = \frac{\lambda f}{\pi w_0} \qquad (3.3.14)$$

and the real waist as

$$W_0` = M^2 \frac{\lambda f}{\pi W_0} \qquad (3.3.15)$$

3.4 Beam diameter measurement

Measurement the beam radius with sharp-edge

We can measure the laser beam radius $w_0`$ after the lens by using the sharp-edge. Fig. 3.8 shows the displacement of the sharp-edge in x-direction to block the laser beam. The transmitted energy of the laser beam is measured with an energy-meter.

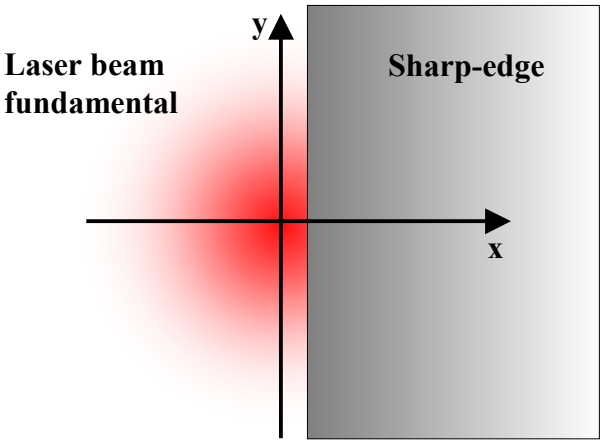

Fig. 3.8:

Sketch of determination of the laser beam radius with the sharp-edge.

The total power of the laser beam before the cutter is written as [3-7]

$$P_0 = \int_{-\infty}^{\infty}\int_{-\infty}^{\infty} I(x,y,z)dxdy = \int_{-\infty}^{\infty}\int_{-\infty}^{\infty} I_0(z)e^{-2\frac{x^2+y^2}{w^2(z)}}dxdy = \frac{\pi}{2}w(z)^2 I_0(z) \qquad (3.4.1)$$

The sharp edge move with displacement x and the transmit power is given by

$$P_T(x`,z) = \int_{-\infty}^{\infty}\int_{-\infty}^{x`} I(x,y,z)dxdy = P_0 \cdot \Phi[2x`/w_s(z)] \qquad (3.4.2)$$

where w_s is the beam radius and Φ is the integration error.

At $x_1` = w_s / 2$ then the transmitted power is given by $P_T = 0.84 \cdot P_0$ and at $x_2` = - w_s / 2$ then $P_T = (1 - 0.84) \cdot P_0$. By measuring the displacements at 84 % and 16 % of the total power of the transmitted laser beam we can calculate the beam radius using the formula

$$w_s(z) = x_1` - x_2` \qquad (3.4.3)$$

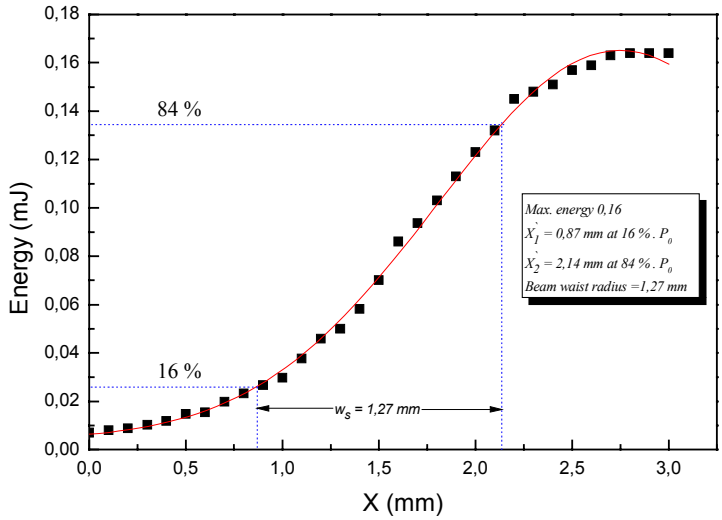

Fig. 3.9:

The transmitted energy of the fundamental beam after the edge agents the displacement of the edge.

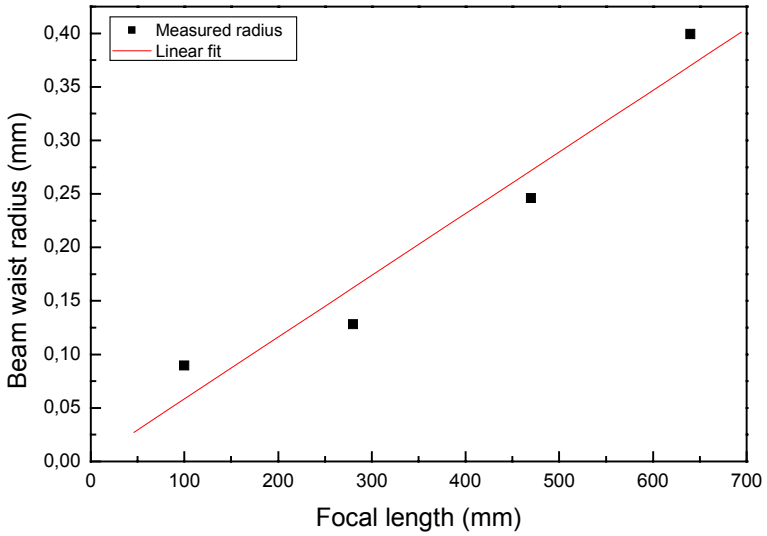

Fig. 3.10:
The laser beam waist radius against the focal length of the convex lens.

Fig. 3.9 shows the transmitted energy versus the displacement X of the cutter without lens. The measured beam radii of the laser beam against the focal length of different lenses are shown in Fig. 3.10. The M^2 of the laser beam was calculated to be 2.22. Beam waist radius range from 61 to 370 μm with different convex lenses with focal length from 100 to 600 mm are measured. The experimental results are agree well with the calculated results using equation (3.3.16).

3.5 Single-pass SRS and spectral analysis

Single pass SRS

In single pass SRS the investigated crystal is positioned between two convex lenses. The laser beam focuses into the Raman-active crystal with the first lens of focal length from f = 100 mm to f = 600 cm. The lens can vary the laser beam intensity into the crystal through variation of the focal length and the beam waist-diameter for the suitable crystal. The small pump beam waist-diameter inside the crystal leads to intensities in the high GW/cm^2 range which is enough to generate efficient scattering into the first Stokes component. The second lens with focal length of f =100 mm collects the scattered beam from the crystal and focuses it onto the spectrometer to measure the spectral composition of the Stokes and anti-Stokes generation.

Spectral analysis

The spectral composition of the Stokes and anti-Stokes generation components, as well as other parametric generation lines investigates with a grating monochromator and a silicon-CCD

sensor. The grating monochromator (McPherson-218) records a wavelength range of 400-1200 nm. A grating with 150 lines/mm was used. Behind the monochromator, a silicon CCD-sensor from Hamamatsu (model S3923-1024Q) with 1024 pixel and a length of 25 mm detects the shifted lines.

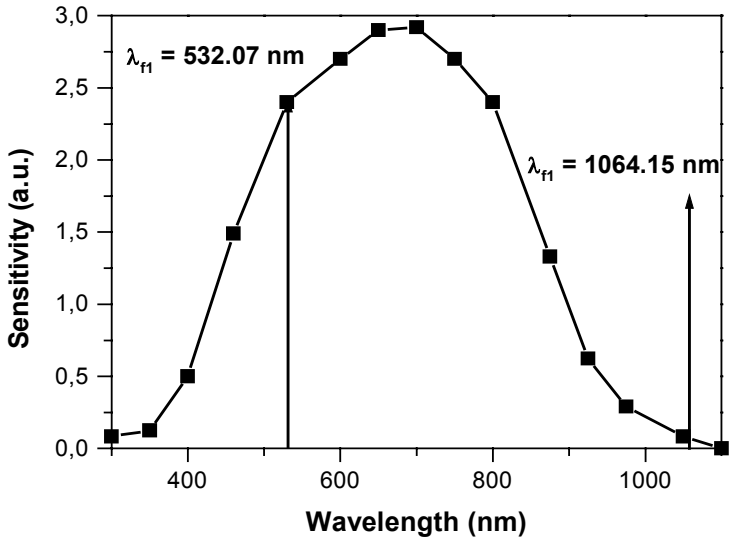

Fig. 3.11:
The spectral sensitivity of the used analyzing system.

The sensitivity of this system shown in Fig. 3.11, is mainly given by the sensitivity of Si-CCD. The sensitivity range from UV to near IR and the maximum at 650 nm wavelength. Due to the restricted sensitivity of the analyzing system, we observe the Stokes lines of the investigated Raman medium mainly with excitation at λ_{f2} = 532 nm, whereas the anti-Stokes components measures with excitation at λ_{f1} = 1064.15 nm wavelength.

4 Stimulated Raman scattering in inorganic and organic crystals and glassy materials

Stimulated Raman scattering SRS is one of the few nonlinear effects discovered in the early 1960s [1-2]. Over the years, many useful applications have been developed out of this process. Some of them are discussed in this chapter. For example, SRS is widely used nowadays to shift the frequency of laser radiation. This has led to a search for new solid-state Raman materials. The goal of investigation of optical and Raman properties of the Raman materials is developing compact, reliable and efficient SRS shifters. SRS in inorganic, organic crystals and glasses is of topical interest in modern solid state laser physics. In this thesis, 18 Raman active materials are investigated using fundamental and second harmonic lines of a picosecond Nd:YAG laser [4-1]-[4-15]. Physical properties, spontaneous Raman scattering and applications for investigated materials are presented in sections 4.1. In section 4.2, SRS wavelengths λ_R, self-frequency doubling (SFD), self-sum frequency mixing (SSFM) and SRS-active vibration modes (ν_R) are discussed and illustrated. Furthermore, relaxation time and Raman gain in active materials were reported. Finally, in section 4.5 full of new lines are listed.

4.1 Physical properties of used materials

Most of Raman active crystals investigated in this work were provided by the cooperation with Prof. Kaminskii from the Institute of Crystallography in Moscow to perform our investigations. Furthermore, barium nitrate crystals were provided from Orlovich from B. I. Stepanov Institute of Physics, Minsk, Belarus, lead tungstate crystals were provided from TU-Berlin and Alum crystal from Egypt.

Some physical properties and dimensions of inorganic and organic crystals and glasses materials are illustrated in Table 4.1. $Bi_4Ge_3O_{12}$, $KAl(SO_4)_2{\cdot}12H_2O$ and $Y_3Al_5O_{12}$ have cubic structure with space group T_d^6, *Pa3* (T_h^6) and O_h^{10} respectively. Some of investigated organic crystals {$C_{15}H_{19}N_3O_2$ (AANP), $C_{13}H_{10}O$ and $C(NH_2)_3]Zr[N(CH_2COO)_3]_2.H_2O$} have orthorhombic structure and the α-$C_{14}H_{12}O$ and $C_{16}H_{15}N_3O_4$ (MNBA) have monoclinic structure.

Table 4.1: *Crystallographic data and size of the investigated crystals and glass materials.*

Crystal	Name	Symmetry	Space-group	Size (mm)	Ref.
Inorganic crystals					
BiB_3O_6	Bismuth triborate	Monoclinic	C_2^3	12x6x3	[1]
$Bi_4Ge_3O_{12}$	Bismuth germanates	Cubic	T_d^6	50	[2]
$Bi_4Si_3O_{12}$	Bismuth silicates	Cubic	T_d^6	50	[2]
$GdVO_4$	Gadolinium vanadate	Tetragonal	D_{4h}^{19}		[3]
$KAl(SO_4)_2{\cdot}12H_2O$	Alum	Cubic	*Pa3* (T_h^6)	20x20x20	[4]
$LiCaAlF_6$	Fluoride	Trigonal	D_{3d}^2	35x10x8	[5]
$Y_3Al_5O_{12}$ (single crystal)	Yttrium aluminum garnet	Cubic	O_h^{10}	∅8x90	[6, 7]
$Y_3Al_5O_{12}$ (nanocrystalline ceramic)	Yttrium aluminum garnet	Cubic	O_h^{10}	10x10x60	[6]
$PbWO_4$	Lead tungstate	Tetragonal	C_{4h}^6	10x10x100	[8]
YVO_4	Yttrium vanadate	Tetragonal	D_{4h}^{19}		[3]
Organic crystals					
α-$C_{14}H_{12}O$	α-4-Methylbenzo-phenone	Monoclinic	C_{2h}^5	≈ 15	[9]
$C_{15}H_{19}N_3O_2$ (AANP)	2-Adamantylamino-5-Nitropyridine	Orthorhombic	C_{2v}^9		[10]
$C_{13}H_{10}O$	Benzophenone	Orthorhombic	D_2^4	≈ 15	[9]
$[C(NH_2)_3]Zr[N(CH_2COO)_3]_2.H_2O$	GuZN-III	Orthorhombic	D_2^5	8	[11]
$C_{16}H_{15}N_3O_4$ (MNBA)	4´-Nitrobenzylidene-3-Acetamino-4-Methoxyaniline	Monoclinic	C_c^4	12x15x1	[12]
Inorganic bulk glasses					
$Ca(NO_3)_2/KNO_3$ glass	Nitrate glass			4x10x15	[13]
$(NaPO_3)_x$	Polyphosphate glass			∅15x40	[14]

$Y_3Al_5O_{12}$ single crystals and nanocrystalline ceramics

Crystal compounds with the garnet cubic structure (O_h^{10}) form the most representative class of active media among the known solid-state media generating stimulated emission. Among these, $Y_3Al_5O_{12}:Nd^{3+}$ crystals are most popular [4-16, 4-17]. Single crystals of yttrium aluminum garnet

were grown by the usual Czochralski method in Pt crucibles. The SRS experiments were accomplished with rods 6-8 mm in diameter and up to 90 mm in length and with commercial Nd^{3+}:$Y_3Al_5O_{12}$ *($C_{Nd} \approx 1$ %)* and Yb^{3+}:$Y_3Al_5O_{12}$ *($C_{Yb} \approx 5$ %)* laser crystals ≈ 120 mm in length.

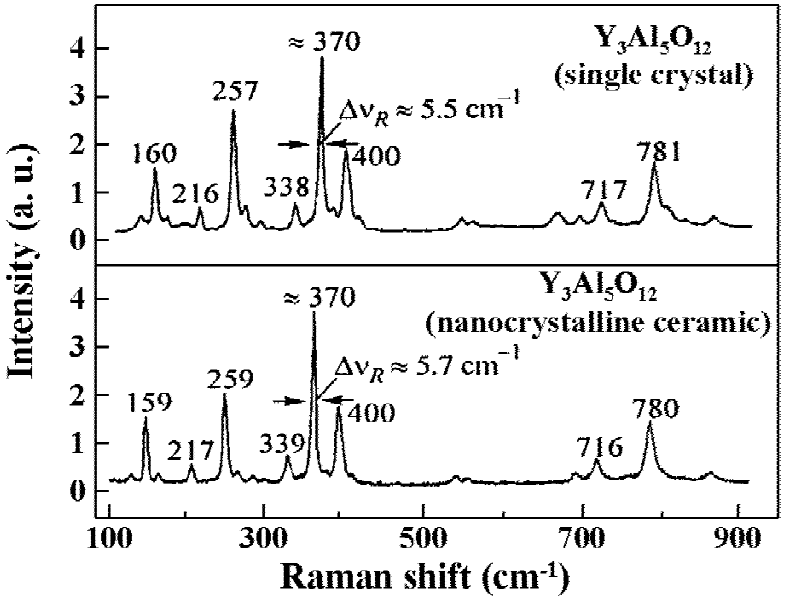

Fig. 4.1:
Spontaneous Raman spectra of the single crystal and nanocrystalline ceramic of $Y_3Al_5O_{12}$.

Optically highly transparent nanocrystalline ceramics have favorable characteristics: These laser crystals can be produced in any size and shape; fabrication is simple and inexpensive. These advantages make ceramic laser materials a powerful challenger to single-crystal laser materials, which are considerably more expensive, limited in size and difficult to grow. Nanocrystalline ceramics were prepared by the modified precipitation method using $(NH_4)_2SO_4$ urea and other additions that are necessary for this technique [4-18, 4-19]. The corresponding experimental samples were bars up to 40 mm in length with cross-section 10 x10 mm^2. The used samples of the single crystals and nanocrystalline ceramics have plane parallel endfaces and without coating.

The spontaneous Raman spectra shown in Fig. 4.1 give an indication of the spectral distribution of optical modes in the media. The strongest line $\nu_R \approx 370\ cm^{-1}$ with line width (FWHM) $\Delta\nu_{R1} \approx 5.5$ cm^{-1} and $\Delta\nu_{R2} \approx 5.7\ cm^{-1}$ of $Y_3Al_5O_{12}$ single crystal and nanocrystalline ceramics have been observed, respectively [4-20, 4-21]. Considering that the spontaneous Raman spectra of $Y_3Al_5O_{12}$ single crystals and nanocrystalline ceramics identical, as are also the other physical properties of this materials [4-18, 4-23]. It means that their SRS-active modes with frequency $\nu_R \approx 370\ cm^{-1}$ are of the same nature.

$PbWO_4$

Tetragonal $PbWO_4$ has several advantages, it is very stable (for comparison the crystal $Ba(NO_3)_2$ requires moisture protection), cheep and can be grown in big sizes with high optical quality by the ordinary Czochralski pulling technique (for growing big size of monoclinic α-$KGd(WO_4)_2$ crystals only very expensive top-seed flux method is available). The investigated tetragonal $PbWO_4$ single crystals were grown by the Czochralski method.

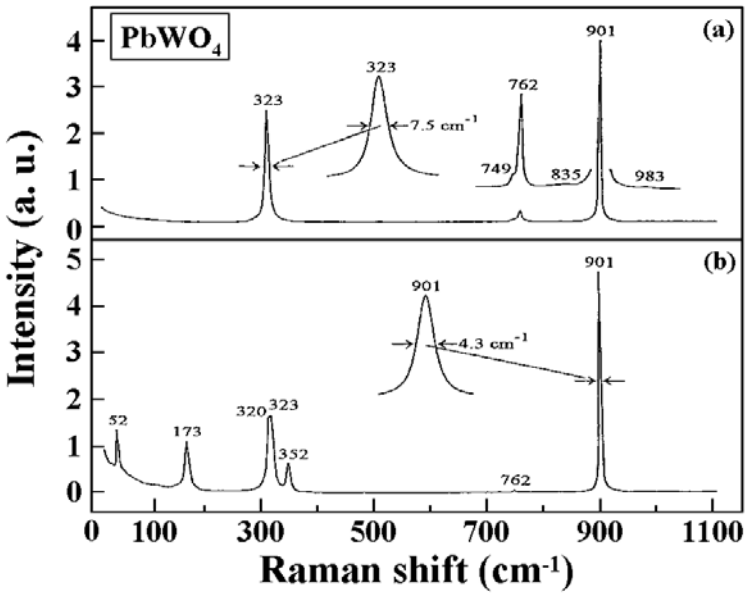

Fig. 4.2:
Spontaneous Raman spectra of the tetragonal $PbWO_4$ single crystal for two excitation geometries.

In our Raman experiments we used $PbWO_4$ crystalline bars of known crystal axis orientations and different lengths 40-100 mm with 10 x 10 mm^2 cross-section. Their endfaces were polished, plane-parallel and without antireflection coating. The refractive index is $n \approx 2.2$ for the c-axis in our experiments. Fig 4.2 illustrates spontaneous Raman spectra of $PbWO_4$ at 300 K for two different excitation geometries. Under this excitation conditions the tetragonal $PbWO_4$ display very strong peaks in two Raman shifts at $\nu_{R1} = 901$ $(\Delta\nu_{R1} \approx 4.3\ cm^{-1})$ and $\nu_{R2} = 323\ cm^{-1}$ $(\Delta\nu_{R1} \approx 7.5\ cm^{-1})$. The analysis reported in Refs. [4-24] – [4-26] concluded that these Raman lines connected with the vibrational modes of tetrahedral WO_4^{2-} ions. In the stimulated Raman scattering processes, spontaneous Raman scattering is a key factor, because the frequency-shifted emission on the intense lines acts as a seed for SRS amplification and generation [2-12, 2-13].

$C_{13}H_{10}O$

Benzophenone ($C_{13}H_{10}O$), is well-known since more than hundred years. The single crystal of benzophenone was grown from supercooled melts [4-27]. The samples for SRS experiments and

spontaneous Raman scattering measurements are in the form of rectangular bars with dimension of 20-mm along the crystallographic axes. The spontaneous Raman scattering spectrum of the $C_{13}H_{10}O$ single crystal is shown in Fig. 4.3. The strongest lines are: doublet at 3070 cm^{-1} and 3059 cm^{-1}, singles at 1650 cm^{-1} and multiples at 1032, 1001, 998, 986 cm^{-1}. The spontaneous Raman scattering results were obtained [4-28]-[4-30].

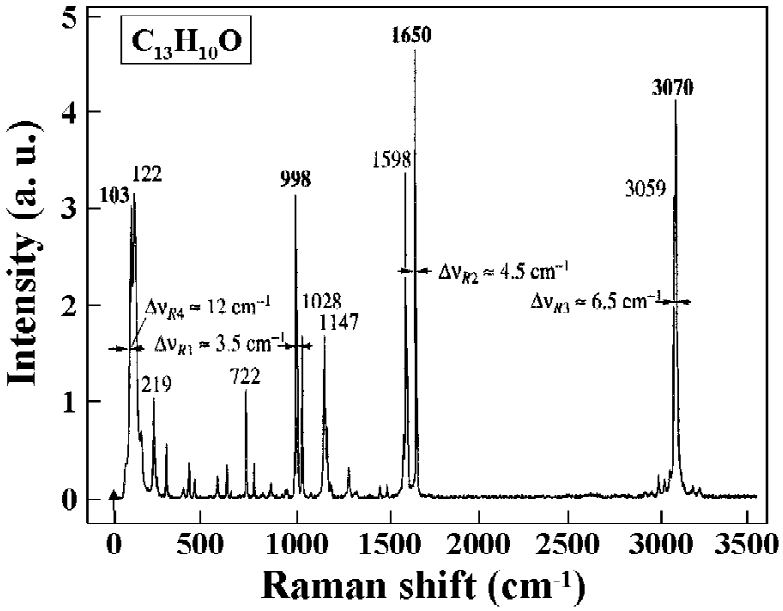

Fig. 4.3: *Spontaneous Raman scattering for the orthorhombic Benzophenone ($C_{13}H_{10}O$) single crystal (random orientation). Zero corresponds to Ar-ion laser excitation at λ = 0.51445 μm (indicated by arrow).*

4.2 Survey of investigated crystals and observed nonlinear effects

Table 4.2 shows experimentally measured Raman shifts for different types of crystalline and glassy Raman active media range from 91 to 3070 cm^{-1}. Furthermore, the observed nonlinear properties (SRS, SHG, SFG and SFM) and other applications are listed. BiB_3O_6, $Bi_4Ge_3O_{12}$, $Bi_4Si_3O_{12}$, AANP, $C_{13}H_{10}O$, GuZN-III and 4´-Nitrobenzylidene-3-Acetamino-4-Methoxyaniline are acentric crystals and showing high quadratic nonlinear susceptibilities χ_2. Therefore, crystals providing χ_2 and χ_3 properties may give rise to diverse parametric generation effects. Undoped BiB_3O_6 was used as crystal for second harmonic generation (SHG) and optical parametric oscillators (OPO) [4-31] and doped with Ln^{3+} activators as luminescense material as well [4-32]. $Bi_4Ge_3O_{12}$ and $Bi_4Si_3O_{12}$ are well characterized optical materials for physical experiments and their application. For example undoped $Bi_4Ge_3O_{12}$ and $Bi_4Si_3O_{12}$ crystals were used as self-frequency generation (SFG). In addition, $Bi_4Ge_3O_{12}$ doped with Ln^{3+} and metal ions was used as luminescense material [4-33]-[4-35].

Table 4.2: *Observed nonlinear effects and Raman shift for investigated inorganic, organic crystals and glasses materials at room temperature and some applications.*

Crystal	NLO properties	SRS-active vibration mode [cm^{-1}]	Observed nonlinear effects and other applications
Inorganic crystals			
BiB_3O_6	$\chi_2 + \chi_3$	≈ 168, ≈ 215, ≈ 374, ≈ 542, ≈ 583, ≈ 604	SRS, SHG, THG, self-SRS
$Bi_4Ge_3O_{12}$	$\chi_2 + \chi_3$	91	SRS, SHG, SFG, X- and γ-ray scintillators, electro-optics and acoustics.
$Bi_4Si_3O_{12}$	$\chi_2 + \chi_3$	97	SRS, SHG, SFG, X- and γ-ray scintillators, electro-optics and acoustics.
$GdVO_4$	$\chi^{(3)}$	882	SRS and laser-diode pumped micro-lasers
$KAl(SO_4)_2 \cdot 12H_2O$	$\chi^{(3)}$	989	SRS,
$LiCaAlF_6$	$\chi^{(3)}$	≈ 560	SRS and ultrashort-pulse lasers emitting in UV and IR.
$PbWO_4$	$\chi^{(3)}$	901, 323	SRS, self-SRS (Nd^{3+}), γ-ray scintillators and detectors in tomographic medical devices.
$Y_3Al_5O_{12}$ (single crystal)	$\chi^{(3)}$	370	SRS and solid-state laser
$Y_3Al_5O_{12}$ (nanocrystalline ceramic)	$\chi^{(3)}$	370	SRS and solid-state laser
YVO_4	$\chi^{(3)}$	890	SRS, laser diode pumped micro-lasers
Organic crystals			
α-4-Methylbenzo-phenone (α-$C_{14}H_{12}O$)	$\chi^{(3)}$	3065	SRS
AANP	$\chi_2 + \chi_3$	1280	SRS, SHG, SFG, OPO and self-SFG
Benzophenone ($C_{13}H_{10}O$)	$\chi_2 + \chi_3$	103, 998, 1650, 3070	SRS, SHG
GuZN-III	$\chi_2 + \chi_3$	≈ 1008, ≈ 2940	SRS, SHG
4′-Nitrobenzylidene-3-Acetamino-4-Methoxyaniline	$\chi_2 + \chi_3$	≈ 1587	SRS, SHG, and SFM
Inorganic bulk glasses			
$Ca(NO_3)_2/KNO_3$ glass	$\chi^{(3)}$	1053	SRS
$(NaPO_3)_x$	$\chi^{(3)}$	1165	SRS

Yttrium vanadate YVO_4 is old laser host for Nd^{3+} ions [4-36]. Nd^{3+}-doped YVO_4 has been successfully used in laser-diode pumped micro-lasers [4-37, 4-38]. Analogous laser properties have been demonstrated for the isostructural $GdVO_4$ with Nd^{3+}, Ho^{3+} and Tm^{3+}- activators [4-39]. Tetragonal lead tungstate $PbWO_4$ is promising for use as self-pumped-SRS laser media when doped with Ln^{3+} ions, in particular $PbWO_4$:Nd^{3+} [4-40]. In addition to their laser potential, some crystals of Table 4-2 posses other valuable properties for applications.

For example, various types $Y_3Al_5O_{12}$:Nd^{3+} lasers have beendeveloped for scientific, civil and military purposes, as well as for medicine. Furthermore, highly transparent $Y_3Al_5O_{12}$:Nd^{3+}

ceramic was used to develop new solid-state lasers [4-41]. $Bi_4Ge_3O_{12}$ and $Bi_4Si_3O_{12}$ are used in optical and acoustical devices [4-42, 4-43]. $PbWO_4$ and $Bi_4Ge_3O_{12}$ are widely used materials for scintillators in high-energy physics and detectors in tomographic medical devices [4-44]. The use of Raman active glasses is wide-spread, e.g., they are commonly used in optical communication systems [3-45]. However, due to a relatively low value of the χ_3 hyperpolarizibility of known glasses, practically all Raman lasers and amplifiers are built from fibers [4-46]. In the field of nonlinear optics organic crystals the attention has mainly been directed towards second harmonic generation (SHG) and third harmonic generation (THG) [4-47]-[4-49], but not towards SRS. This is rather astonishing, because the bright optical χ_3 properties, such as the SRS, were discovered in the beginning of the 1960s (nitrobenzene) [4-50].

4.3 Raman gain and relaxation time of some investigated materials

Raman gain coefficient g_{ssR}, Raman line width $\Delta\nu_R$ and relaxation time T_R of some of the used Raman-active materials are listed in Table 4.3. The relaxation time is calculated from equation *(2.4.1)* while the Raman gain coefficient is calculated using the approximation $g_{ssR}I_p l = 25\text{-}30$.

For example, for two Raman shifted lines, namely 901 and 323 cm^{-1} for tetragonal $PbWO_4$ single crystal in Fig. 4.2, the dephasing times are *2.5 ps* ($\Delta\nu_R = 4.3\ cm^{-1}$) and *1.4 ps* ($\Delta\nu_R = 7.5\ cm^{-1}$), respectively. These are considerably lower than the pumping pulse duration $\tau_f = 120\ ps$ in the near-IR. Then SRS in $PbWO_4$ takes place in the steady state case.

Raman gain coefficients of inorganic, organic and glassy materials are listed in Table 4.3. For example, the gain coefficient = 3.1 ± 0.8 cm/GW for tetragonal $PbWO_4$, which is practically the same as for the widely-used monoclinic α-$KGd(WO_4)_2$ tungstate crystal. Tetragonal vanadates YVO_4 and $GdVO_4$ have Raman gain much higher than tetragonal $PbWO_4$.

For organic crystals, we observed that the threshold intensity for the first Stokes generation is 5% to 10 % less than known for lasing of an oriented equal length reference α-$KGd(WO_4)_2$ tungstate at its first Stokes wavelength. This result allows us to estimate the Raman gain for organic crystals from 5 to 10 cm/GW.

The advantage of solid state Raman materials have higher SRS gain coefficient is due to higher concentration of Raman scattering centers than in a gas media. Due to these important reasons there is a limited number of crystals that provide high SRS gain coefficient.

Table 4.3: Spectroscopic characteristics of the Raman-active materials.

Crystal	g_{ssR} [cm/GW]	$\Delta\nu_R$ [cm^{-1}]	T_R [ps]	References
Inorganic crystals				
BiB_3O_6	2.9 ± 0.5	≈ 7-11	1.5-1	[1]
$Bi_4Ge_3O_{12}$	≈ 0.8	1.3	8	[2]
$Bi_4Si_3O_{12}$	≈ 0.8	1.4	7.6	[2]
$KAl(SO_4)_2 \cdot 12H_2O$		16.2	0.65	[4]
$LiCaAlF_6$	0.22 ± 0.07	≈ 7	1.5	[5]
Nd:YAG	0.1 ± 0.05	5.5	1.9	[6,7]
$PbWO_4$	3.1 ± 0.8	4.3	2.5	[8]
YAG-Ceramic	0.1 ± 0.05	5.7	1.8	[7]
YVO_4	4.5	3	≈ 3.5	[3]
Organic crystals				
α-4-Methylbenzo-phenone (α-$C_{14}H_{12}O$)	-	≈ 9	≈ 1.2	[9]
AANP	> 5.5	≈ 24	≈ 0.44	[10]
Benzophenone ($C_{13}H_{10}O$)	≈ 10	≈ 6.5	≈ 1.5	[9]
GuZN-III	9	≈ 5	≈ 2	[11]
MNBA	≥ 7	1.5	≈ 7	[12]
Inorganic bulk glasses				
$(NaPO_3)_x$	≈ 8	19	≈ 0.6	[14]

4.4 Experimental spectra of Raman converters

The process of SRS allows to convert laser emission wavelengths of materials providing suitable molecular or lattice modes which contribute to the third order nonlinear optical susceptibility χ_3. SRS of suggested materials can produce Stokes and/or anti-Stokes shifts in the range 91 cm^{-1} to 3070 cm^{-1}. Due to variation in crystallographic structure, different crystals have rather different Raman spectra. For the excitation of Stokes and anti-Stokes steady state single-pass SRS we use a picosecond Nd:YAG laser with the fundamental wavelength at $\lambda_{f1} = 1064.15\ nm$ and its SHG at $\lambda_{f2} = 532.07\ nm$ wavelength. The time duration of the fundamental is $\tau_{f1} \approx 120\ ps$ while $\tau_{f2} = 80\ ps$ for the SHG, which was explained in chapter 3. High-order SRS and some nonlinear effects in inorganic, organic and glasses materials are observed. Due to the CCD-sensitivity drop-off, the intensity of the of the Stokes line is strongly reduced compared to the anti-Stokes

lines when the materials under the fundamental excitation. In contrast, higher-order Stokes can easily be detected when the excitation with the SHG.

Inorganic crystals

SRS spectra for some investigated inorganic crystals ($Y_3Al_5O_{12}$-ceramic, $GdVO_4$, $KAl(SO_4)_2 \cdot 12H_2O$ and $PbWO_4$) at specific orientation and their Raman shifts are shown in Fig. 4.4. High-order Stokes and anti-Stokes lines are excited in the visible and near-IR regions YAG and nanocrystalline YAG-ceramics. SRS in these crystals are observed with Raman shift $\nu_R \approx 370$ cm^{-1}, which agrees well with spontaneous Raman scattering spectrum in Fig. 4.1. Table 4.4 shows the comparison between SRS in YAG single crystal and YAG ceramics. Due to the absorption of Nd for the green, we could not generate SRS in doped YAG single and YAG-ceramics with Nd when they pumping with the second harmonic.

Crystals	**Excitation**	
	Near-IR λ_{f1} **= 1064.15 nm**	**Green** λ_{f2} **= 532.07 nm**
Nd:YAG	SRS AS, S	No SRS
YAG-undoped	SRS AS, S	SRS AS, S
YAG-ceramics	SRS AS, S	SRS AS, S

Table 4.4: *Comparison between the SRS in doped and undoped-YAG single crystals and YAG ceramics*

Some generated Stokes and anti-Stokes lines in $Bi_4Ge_3O_{12}$ are illustrated in Fig. 4.4. All the observed Stokes and anti-Stokes lines in $Bi_4Ge_3O_{12}$ and $Bi_4Si_3O_{12}$ with Raman shifts of 91 cm^{-1} and 97 cm^{-1} are presented in Ref. [4-2]. Of course, we were very surprised to watch such rich-line Raman lasing spectra. For example, the multiple lines of the anti-Stokes wing of bismuth germanate contain 40 components and spread down to 767 nm wavelength under one-micron pumping. Due to limited spectral sensitivity of our Si-CCD sensor in the near-IR region we could not register all lines Stokes wing, but it is safe to say that their number should be essential higher than that we registered. Under pumping at λ_{f2} = 532.07 nm wavelength, the spectral composition of multiple Stokes and anti-Stokes generation of $Bi_4Ge_3O_{12}$ is not uncommon for the single-pass SRS excitation.

For tetragonal $PbWO_4$, high-order Stokes and anti-Stokes stimulated Raman scattering are generated. The known optical vibration mode at $\nu_{R1} = 901\ cm^{-1}$ and in addition, at $\nu_{R2} = 323\ cm^{-1}$ which, agree fairly well with those obtained previously in Fig. 4.2 are observed.

Analysis of our experimental data shows that these SRS-active vibration modes of the crystal are determined by the experimental conditions of excitation (direction, wavelength, polarization and power of the fundamental wave). The measurement conducted showed that the total Stokes conversion efficiency in tetragonal $PbWO_4$ crystals in our experimental conditions at pumping power density close to their optical damage threshold at $\lambda_{f2} = 532.07$ nm wavelength reached ≈ 55 %. Although we could not measure the Stokes emission in the IR wing of the SRS generation because our recording system had limited spectral sensitivity, the total conversion efficiency of the pump power density of about 1 GW/cm^2 (at $\lambda_{f1} = 1.06415$ μm) to Stokes and anti-Stokes components has been estimated to ≈ 55 %. Due to excellent crystalline and optical properties of tetragonal $PbWO_4$ crystal, we demonstrated second-Stokes Raman laser based on $PbWO_4$, in chapter 5.

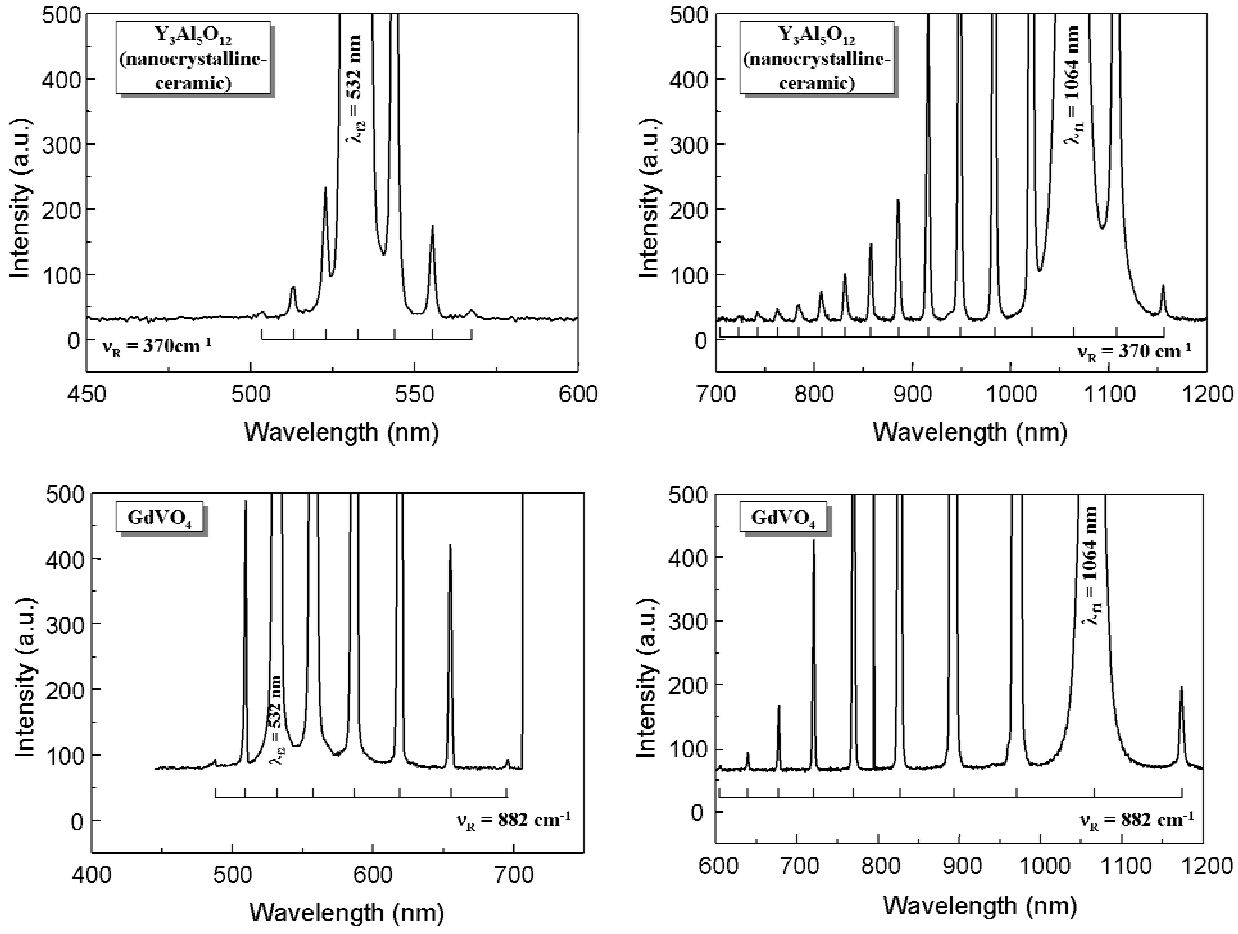

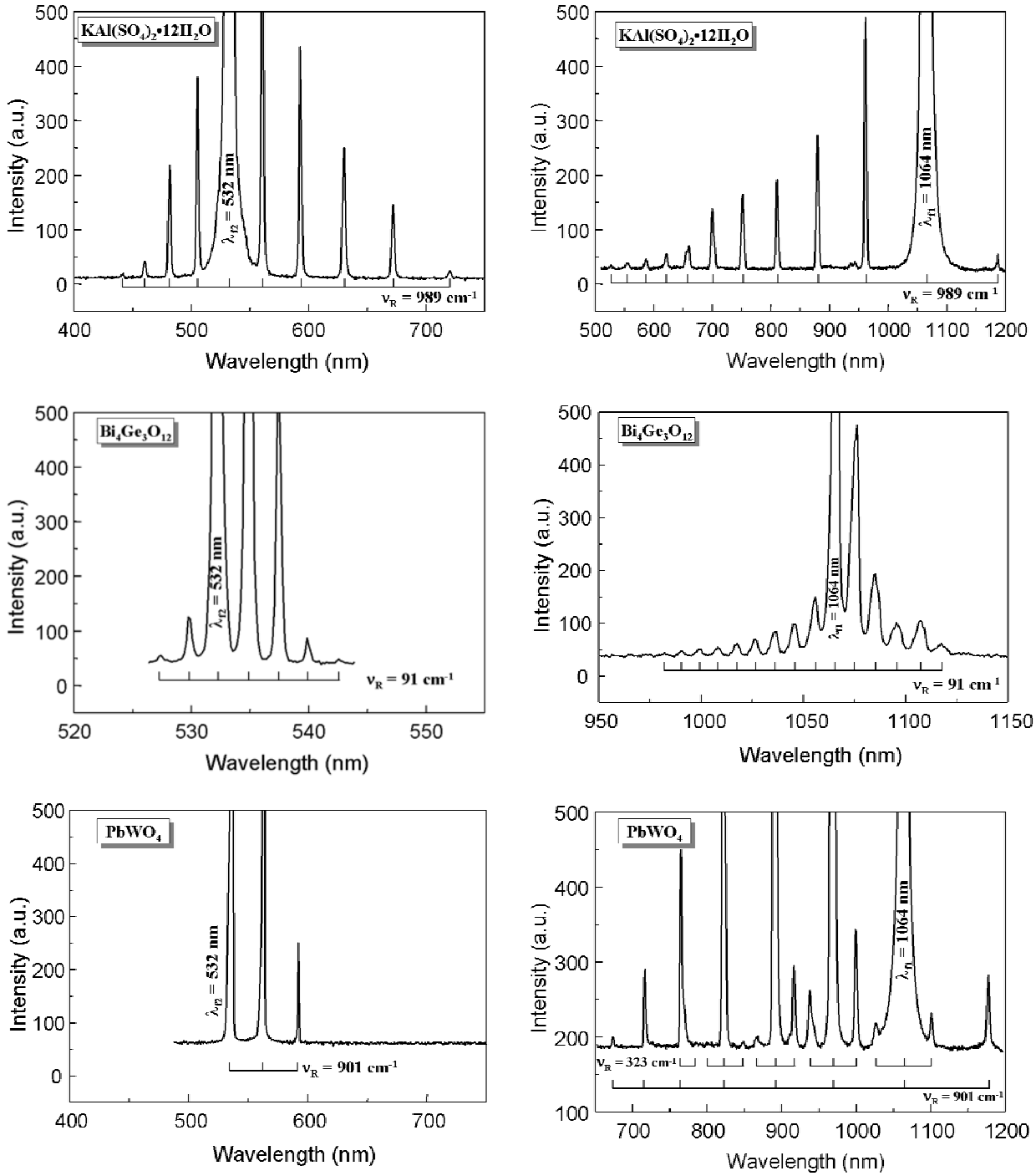

Fig. 4.4: *SRS spectra for inorganic crystals pumping with the fundamental at λ_{f1} = 1064.15 nm wavelength and with the SHG at λ_{f2} = 532.07 nm wavelength at room temperature. The relation between generated Stokes and anti-Stokes components and Raman shift ν_R of the crystals are indicated by brackets.*

Organic crystals

For SRS there is no need to have acentric materials, therefore, many of the organic crystals and polymers showing χ_3 properties may be considered for a thus far unexplored direction in the manufacturing of all-solid-state laser frequency converters. The organic crystals mentioned here were not chosen because they are the most promising ones but because they have been reported to feature χ_3 molecular properties [4-48, 4-49].

SRS based on α-$C_{14}H_{12}O$, $C_{15}H_{19}N_3O_2$, $C_{13}H_{10}O$, $[C(NH_2)_3]Zr[N(CH_2COO)_3]_2{\cdot}H_2O$ and $C_{16}H_{15}N_3O_4$ are observed. Spectra of some organic crystals are illustrated in Fig. 4.5. Our results on several organic crystal that SRS wavelength conversion is efficient and much larger Raman shifts can be obtained compared to those of most inorganic crystals.

For example, the spectral composition of the observed Stokes and anti-Stokes generation in orthorhombic benzophenone crystal is related to four SRS-active vibration modes of the crystals ν_{R1} = 103 cm^{-1}, ν_{R2} = 998 cm^{-1}, ν_{R3} = 1650 cm^{-1} and ν_{R4} = 3070 cm^{-1}. These Raman shifts are determined by the experimental excitation conditions, direction and polarization of fundamental and scattered emissions, as well as pump peak-power and active length of sample. Furthermore, total conversion efficiency at pumping energy of about 1.5 mJ at λ_{f2} = 532.07 nm wavelength into all Stokes and anti-Stokes components in a benzophenone is estimated as high as 20 %. Stokes and anti-Stokes generation and self-SHG components of $C_{15}H_{19}N_3O_2$ (AANP) single crystal are shown in Fig 4.5.

The analysis shows that the Stokes and anti-Stokes lines in $C_{15}H_{19}N_3O_2$ crystal are generated with SRS active vibration mode $\nu_{R1} \approx 1280$ cm^{-1}. Due to this large Raman shift and limited spectral sensitivity of the Si-CCD sensor we can not observe the near-IR Stokes components of $C_{15}H_{19}N_3O_2$ under excitation at λ_{f1} = 1064.15 nm wavelength. First and second Stokes lines clearly appear in the visible range as corresponding SHG lines as well as with excitation in the visible at λ_{f2} = 532.07 nm wavelength.

First anti-Stokes with Raman shift of $\nu_R \approx 2940$ cm^{-1} and self-SHG of $[C(NH_2)_3]Zr[N(CH_2COO)_3]_2{\cdot}H_2O$ (GuZN-III) single crystal were observed with excitation at λ_{f1}. Furthermore, Stokes and anti-Stokes lines of an orthorhombic GuZN-III with phonon energy of ≈ 1008 cm^{-1} were obtained under excitation at λ_{f2}. Our results on several organic crystals showed that SRS wavelength conversion is efficient and much larger Raman shifts can be obtained compared to most inorganic crystals.

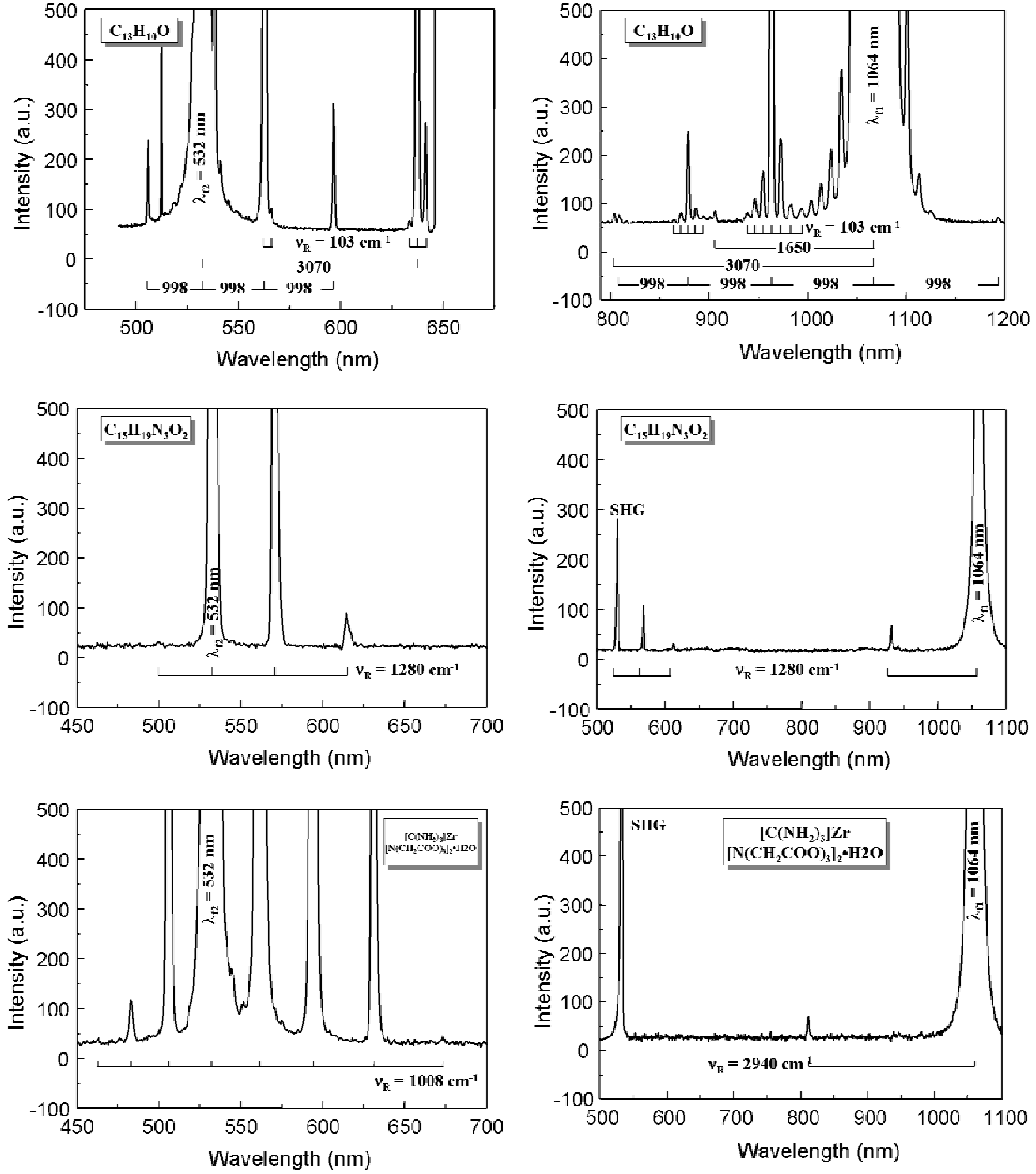

Fig. 4.5: *SRS spectra for organic crystals pumping with the fundamental at λ_{f1} = 1064.15 nm wavelength and with the SHG at λ_{f2} = 532.07 nm wavelength at room temperature. The relation between generated Stokes and anti-Stokes components and Raman shift ν_R of the crystals are indicated by brackets.*

Glassy materials

Glasses materials are promising SRS media for new laser applications including fibers. Efficient SRS has been demonstrated in inorganic bulk glasses $Ca(NO_3)_2/KNO_3$ and $(NaPO_3)_x$ with phonon energy of 1053 and 1165 cm^{-1}. Up to 10 and 8 anti-Stokes components of $Ca(NO_3)_2/KNO_3$ and $(NaPO_3)_x$ are observed under pumping at λ_{f1}. Multiple Stokes and anti-Stokes lines have been detected under excitation at λ_{f2} and are presented in Fig. 4.6.

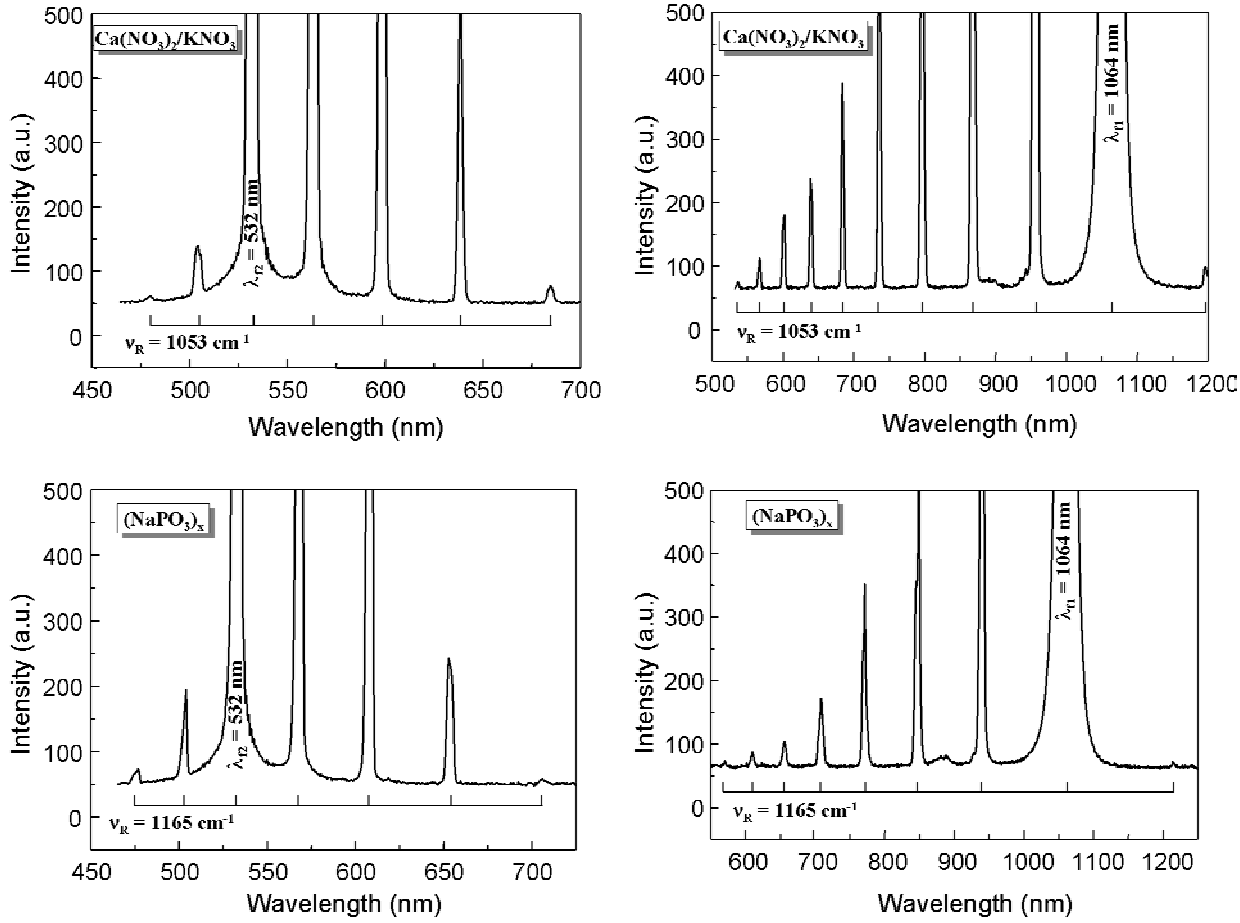

Fig. 4.6: *SRS spectra for glasses materials pumping with the fundamental at λ_{f1} = 1064.15 nm wavelength and with the SHG at λ_{f2} = 532.07 nm wavelength at room temperature. The relation between generated Stokes and anti-Stakes components and Raman shift ν_R of the crystals are indicated by brackets.*

4.5 Survey of all observed Raman lines

Up to 401 Stokes, anti-Stokes and other Raman effects lines are observed in inorganic and organic crystals and glasses materials under picosecond Nd:YAG laser fundamental at λ_{f1} = 1064.15 nm and its SHG at λ_{f2} = 532.07 nm. Experimental data resulting from our measurements, including an identification of all Stokes and anti-Stokes components with SRS-active vibration modes ω_R of selected active materials have been listed in Table 4.5. High-order SRS, self-frequency doubling, and self-sum frequency mixing in inorganic crystals [BiB_3O_6, $Bi_4Ge_3O_{12}$, $Bi_4Si_3O_{12}$, $GdVO_4$, $KAl(SO_4)_2{\cdot}12H_2O$, $LiCaAlF_6$, $Y_3Al_5O_{12}$ (single crystal), $Y_3Al_5O_{12}$ (nanocrystalline ceramic), $PbWO_4$ and YVO_4], organic crystals [α-$C_{14}H_{12}O$, $C_{15}H_{19}N_3O_2$, $C_{13}H_{10}O$, $[C(NH_2)_3]Zr[N(CH_2COO)_3]_2.H_2O$ and $C_{16}H_{15}N_3O_4$] and glasses materials [$Ca(NO_3)_2/KNO_3$ and $(NaPO_3)_x$] have been published [4-1]-[4-15]. Furthermore, multiple Stokes and anti-Stokes generation in triclinic γ-KIO_3 and hexagonal α-$LiIO_3$ [4-51], dibenzoyl $C_{14}H_{10}O_2$ [4-52], Nd^{3+}-doped $CaMoO_4$, $SrMoO_4$ and $SrWO_4$ [4-53] and $Ba(NO_3)_2$ [4-54] crystals are added to Table 4.5.

Besides the multiple ordinary SRS generation in the $(\chi_2 + \chi_3)$ active crystal MNBA $C_{16}H_{15}N_3O_4$ we have observed new nonlinear phenomena: SHG of the first (λ_{S1} = 1280.4 nm) and second (λ_{S2} = 1606.9 nm) Stokes generations at λ_{SHG} = 640.2 nm and at λ_{SHG} = 803.4 nm, respectively. This is the first observation of self-FD effect in organic single crystals. In addition, the efficient Stokes generation and a high χ_2 made it possible to observe other efficient parametric effects in MNBA –the self-sum-frequency conversion at λ_{SFM} = 581.1 nm resulting from interaction between frequency of fundamental (pumping) laser emission ω_{f1} and the frequency of first Stokes emission ν_{S1} and self-sum-frequency mixing at λ_{SFM} = 712.6 nm resulting from sum of frequency of first and second Stokes., i.e. the interaction between fundamental (pumping) laser emission and the first and second Stokes generations.

From Table 4.5, 40 components spread to 767 nm wavelength of the anti-Stokes wing and up to 9 Stokes lines of BiB_3O_6 were observed under fundamental excitation. Furthermore, second harmonic generation of the fundamental radiation and the sum-frequency generation of the fundamental and multiple Stokes emission have been observed in BiB_3O_6. It is probable that these evidences are the first observation of the self-frequency doubling and the self-frequency summing effects in cubic acentric crystals. For tetragonal $PbWO_4$ second-Stokes at wavelength

of λ_{S2} = 1316.6 nm with energy phonon of 901 cm^{-1} was observed. In addition, lead tungstate was used to generate the second-Stokes line in the next chapter.

Table 4.5: *SRS wavelengths λ_R, self-frequency doubling (SFD), self-sum frequency mixing (SSFM) and SRS-active vibration modes (ν_R) in inorganic and organic crystals and glasses materials under picosecond Nd:YAG laser fundamental at λ_{f1} = 1064.15 nm with frequency ν_{f1} and its SHG at λ_{f2} = 532.07 nm with frequency ν_{f2}.*

λ_R (nm)	Line	SRS-and RFWM-line attribution	Raman shift ν_R (cm^{-1})	Crystal	Pump (nm)	Ref.
421.2	AS_5	$\nu_{f2}+5\nu_R$	989	$KAl(SO_4)_2{\cdot}12H_2O$	532.07	[4]
431	AS_5	$\nu_{f2}+5\nu_R$	882	$GdVO_4$	532.07	[3]
438.1	AS_4	$\nu_{f2}+4\nu_R$	≈1008	$[C(NH_2)_3]_2Zr[N(CH_2COO)_3]_2{\cdot}H_2O$	532.07	[11]
439.6	AS_4	$\nu_{f2}+4\nu_R$	989	$KAl(SO_4)_2{\cdot}12H_2O$	532.07	[4]
448	AS_4	$\nu_{f2}+4\nu_R$	882	$GdVO_4$	532.07	[3]
451.4	AS_6	$\nu_{f2}+6\nu_R$	≈ 560	$LiCaAlF_6$	532.07	[5]
455.5	AS_3	$\nu_{f1}+3\nu_R$	1053	$Ca(NO_3)_2/KNO_3$	1064.15	[13]
458.3	AS_3	$\nu_{f2}+3\nu_R$	≈1008	$[C(NH_2)_3]_2Zr[N(CH_2COO)_3]_2{\cdot}H_2O$	532.07	[11]
459.5	AS_3	$\nu_{f2}+3\nu_R$	989	$KAl(SO_4)_2{\cdot}12H_2O$	532.07	[4]
460.1	AS_1	$\nu_{f2}+\nu_R$	≈2940	$[C(NH_2)_3]_2Zr[N(CH_2COO)_3]_2{\cdot}H_2O$	532.07	[11]
463.1	AS_5	$\nu_{f2}+5\nu_R$	≈ 560	$LiCaAlF_6$	532.07	[5]
466.4	AS_3	$\nu_{f2}+3\nu_R$	882	$GdVO_4$	532.07	[3]
473.4	AS_2	$\nu_{f2}+\nu_R$	1165	$(NaPO_3)_x$	532.07	[14]
475.4	AS_4	$\nu_{f2}+4\nu_R$	≈ 560	$LiCaAlF_6$	532.07	[5]
478.5	AS_2	$\nu_{f1}+2\nu_R$	1053	$Ca(NO_3)_2/KNO_3$	1064.15	[13]
478.7	AS_2	$\nu_{f2}+2\nu_R$	1047	$Ba(NO_3)_2$	532.07	[54]
480.5	AS_2	$\nu_{f2}+2\nu_R$	≈1008	$[C(NH_2)_3]_2Zr[N(CH_2COO)_3]_2{\cdot}H_2O$	532.07	[11]
481.4	AS_2	$\nu_{f2}+2\nu_R$	989	$KAl(SO_4)_2{\cdot}12H_2O$	532.07	[4]
484.4	AS_5	$\nu_{f2}+5\nu_R$	370	$Y_3Al_5O_{12}$	532.07	[7]
484.4	AS_5	$\nu_{f2}+5\nu_R$	370	$Y_3Al_5O_{12}$ ceramic	532.07	[7]
485.5	AS_2	$\nu_{f2}+2\nu_R$	901	$PbWO_4$	532.07	[8]
486	AS_1	$\nu_{f2}+\nu_R$	890	YVO_4	532.07	[3]
486.4	AS_2	$\nu_{f2}+2\nu_R$	882	$GdVO_4$	532.07	[3]
488.4	AS_3	$\nu_{f2}+3\nu_R$	≈ 560	$LiCaAlF_6$	532.07	[5]
489.5	AS_2	$\nu_{f2}+2\nu_R$	818	α-$LiIO_3$	532.07	[51]
491.2	AS_1	$\nu_{f2}+\nu_R$	781	γ-KIO_3	532.07	[51]
493.2	AS_4	$\nu_{f2}+3\nu_R$	370	$Y_3Al_5O_{12}$	532.07	[7]
493.2	AS_4	$\nu_{f2}+3\nu_R$	370	$Y_3Al_5O_{12}$ ceramic	532.07	[7]
501	AS_1	$\nu_{f2}+2\nu_R$	1165	$(NaPO_3)_x$	532.07	[14]
501.8	AS_{10}	$\nu_{f1}+10\nu_R$	1053	$Ca(NO_3)_2/KNO_3$	1064.15	[13]
502.2	AS_2	$\nu_{f2}+2\nu_R$	≈ 560	$LiCaAlF_6$	532.07	[5]
502.4	AS_3	$\nu_{f2}+3\nu_R$	370	$Y_3Al_5O_{12}$	532.07	[7]
502.4	AS_3	$\nu_{f2}+3\nu_R$	370	$Y_3Al_5O_{12}$ ceramic	532.07	[7]
503.1	SHG, AS_2	$2\nu_{f1}+2\nu_R$	≈ 542	BiB_3O_6	1064.15	[1]
503.8	AS_1	$\nu_{f1}+\nu_R$	1053	$Ca(NO_3)_2/KNO_3$	1064.15	[13]
504	AS_1	$\nu_{f2}+\nu_R$	1047	$Ba(NO_3)_2$	532.07	[54]

505	AS_1	$\nu_{f2}+\nu_R$	≈1008	$[C(NH_2)_3]_2Zr[N(CH_2COO)_3]_2\cdot H_2O$	532.07	[11]
505.5	AS_1	$\nu_{f2}+\nu_R$	989	$KAl(SO_4)_2\cdot 12H_2O$	532.07	[4]
507.7	AS_1	$\nu_{f2}+\nu_R$	901	$PbWO_4$	532.07	[8]
508	AS_2	$\nu_{f2}+\nu_R$	890	YVO_4	532.07	[3]
508.2	AS_1	$\nu_{f2}+\nu_R$	882	$GdVO_4$	532.07	[3]
508.3	AS_1	$\nu_{f2}+\nu_R$	≈ 879	$CaMoO_4$	532.07	[53]
509.9	AS_1	$\nu_{f2}+\nu_R$	818	α-$LiIO_3$	532.07	[51]
510.8	AS_1	$\nu_{f2}+\nu_R$	781	γ-KIO_3	532.07	[51]
511.9	AS_2	$\nu_{f2}+2\nu_R$	370	$Y_3Al_5O_{12}$	532.07	[7]
511.9	AS_2	$\nu_{f2}+2\nu_R$	370	$Y_3Al_5O_{12}$ ceramic	532.07	[7]
512.1	AS_1	$\nu_{f2}+\nu_{R2}$	733	γ-KIO_3	532.07	[51]
516.7	AS_1	$\nu_{f2}+\nu_R$	≈ 560	$LiCaAlF_6$	532.07	[5]
517.2	SHG, AS_1	$2\nu_{f1}+\nu_R$	≈ 542	BiB_3O_6	1064.15	[1]
518.5	AS_{10}	$\nu_{f1}+10\nu_R$	989	$KAl(SO_4)_2\cdot 12H_2O$	1064.15	[4]
521.8	AS_1	$\nu_{f2}+\nu_R$	370	$Y_3Al_5O_{12}$	532.07	[7]
521.8	AS_1	$\nu_{f2}+\nu_R$	370	$Y_3Al_5O_{12}$ ceramic	532.07	[7]
524.5	AS_3	$\nu_{f2}+3\nu_R$	91	$Bi_4Ge_3O_{12}$	532.07	[2]
527.0	AS_2	$\nu_{f2}+2\nu_R$	91	$Bi_4Ge_3O_{12}$	532.07	[2]
529.5	AS_1	$\nu_{f2}+\nu_R$	91	$Bi_4Ge_3O_{12}$	532.07	[2]
529.8	AS_9	$\nu_{f1}+9\nu_R$	1053	$Ca(NO_3)_2/KNO_3$	1064.15	[13]
532.07	SHG	$2\nu_{f1}$	-	BiB_3O_6	1064.15	[1]
532.07	SHG	$2\nu_{f1}$	-	$Bi_4Ge_3O_{12}$	1064.15	[2]
532.07	SHG	$2\nu_{f1}$	-	$C_{16}H_{15}N_3O_4$	1064.15	[12]
532.07	SHG	$2\nu_{f1}$	-	$C_{15}H_{19}N_3O_2$	1064.15	[10]
532.07	SHG	$2\nu_{f1}$	-	$[C(NH_2)_3]_2Zr[N(CH_2COO)_3]_2\cdot H_2O$	1064.15	[11]
534.3	AS_8	$\nu_{f1}+8\nu_R$	1165	$(NaPO_3)_x$	1064.15	[14]
534.7	S_1	$\nu_{f2}-\nu_R$	91	$Bi_4Ge_3O_{12}$	532.07	[2]
534.7	SHG, S_1	$2\nu_{f1}-\nu_R$	91	$Bi_4Ge_3O_{12}$	1064.15	[2]
537.3	S_2	$\nu_{f2}-2\nu_R$	91	$Bi_4Ge_3O_{12}$	532.07	[2]
537.3	SHG, S_2	$2\nu_{f1}-2\nu_R$	91	$Bi_4Ge_3O_{12}$	1064.15	[2]
539.9	S_3	$\nu_{f2}-3\nu_R$	91	$Bi_4Ge_3O_{12}$	532.07	[2]
539.9	SHG, S_3	$2\nu_{f1}-3\nu_R$	91	$Bi_4Ge_3O_{12}$	1064.15	[2]
542.6	S_4	$\nu_{f2}-4\nu_R$	91	$Bi_4Ge_3O_{12}$	532.07	[2]
542.6	SHG, S_4	$2\nu_{f1}-4\nu_R$	91	$Bi_4Ge_3O_{12}$	1064.15	[2]
542.8	S_1	$\nu_{f2}-\nu_R$	370	$Y_3Al_5O_{12}$	532.07	[7]
542.8	S_1	$\nu_{f2}-\nu_R$	370	$Y_3Al_5O_{12}$ ceramic	532.07	[7]
543.3	AS_{10}	$\nu_{f1}+10\nu_R$	901	$PbWO_4$	1064.15	[8]
545.3	SHG, S_5	$2\nu_{f1}-5\nu_R$	91	$Bi_4Ge_3O_{12}$	1064.15	[2]
546.5	AS_9	$\nu_{f1}+9\nu_R$	989	$KAl(SO_4)_2\cdot 12H_2O$	1064.15	[4]
547.9	SHG, S_1	$2\nu_{f1}-\nu_R$	≈ 542	BiB_3O_6	1064.15	[1]
548	SHG, S_6	$2\nu_{f1}-6\nu_R$	91	$Bi_4Ge_3O_{12}$	1064.15	[2]
548.4	S_1	$\nu_{f2}-\nu_R$	≈ 560	$LiCaAlF_6$	532.07	[5]
550.7	SHG, S_7	$2\nu_{f1}-7\nu_R$	91	$Bi_4Ge_3O_{12}$	1064.15	[2]
553.5	SHG, S_8	$2\nu_{f1}-8\nu_R$	91	$Bi_4Ge_3O_{12}$	1064.15	[2]
553.7	S_1	$\nu_{f2}-\nu_{R2}$	733	γ-KIO_3	532.07	[51]
553.9	S_2	$\nu_{f2}-2\nu_R$	370	$Y_3Al_5O_{12}$	532.07	[7]
553.9	S_2	$\nu_{f2}-2\nu_R$	370	$Y_3Al_5O_{12}$ ceramic	532.07	[7]
555.1	S_1	$\nu_{f2}-\nu_R$	781	γ-KIO_3	532.07	[51]
555.9	AS_{11}	$\nu_{f1}+11\nu_R$	781	γ-KIO_3	1064.15	[51]
556.3	S_1	$\nu_{f2}-\nu_R$	818	α-$LiIO_3$	532.07	[51]
556.3	SHG, S_9	$2\nu_{f1}-9\nu_R$	91	$Bi_4Ge_3O_{12}$	1064.15	[2]
571.0	SHG, S_1	$2\nu_{f1}-\nu_R$	≈ 1280	$C_{15}H_{19}N_3O_2$	1064.15	[10]
558.2	S_1	$\nu_{f2}-\nu_R$	≈ 879	$CaMoO_4$	532.07	[53]
558.3	S_1	$\nu_{f1}-\nu_R$	882	$GdVO_4$	1064.15	[3]

558.5	S_1	ν_{f2}-ν_R	890	YVO_4	532.07	[3]
558.9	S_1	ν_{f2}-ν_R	901	$PbWO_4$	532.07	[8]
559.1	SHG, S_{10}	$2\nu_{f1}$-$10\nu_R$	91	$Bi_4Ge_3O_{12}$	1064.15	[2]
561.1	AS_8	ν_{f1}+$8\nu_R$	1053	$Ca(NO_3)_2/KNO_3$	1064.15	[13]
561.6	S_1	ν_{f2}-ν_R	989	$KAl(SO_4)_2{\cdot}12H_2O$	532.07	[4]
562.0	SHG, S_{11}	$2\nu_{f1}$-$11\nu_R$	91	$Bi_4Ge_3O_{12}$	1064.15	[2]
562.2	S_1	ν_{f2}-ν_R	≈1008	$[C(NH_2)_3]_2Zr[N(CH_2COO)_3]_2{\cdot}H_2O$	532.07	[11]
563.5	S_1	ν_{f2}-ν_R	1047	$Ba(NO_3)_2$	532.07	[54]
563.7	S_1	ν_{f2}-ν_R	1053	$Ca(NO_3)_2/KNO_3$	532.07	[13]
564.7	SHG, S_2	$2\nu_{f1}$-$2\nu_R$	≈ 542	BiB_3O_6	1064.15	[1]
565.4	AS_9	ν_{f1}+$9\nu_R$	≈ 921	$SrMoO_4:Nd^{3+}$	1064.15	[53]
565.5	S_3	ν_{f2}-$3\nu_R$	370	$Y_3Al_5O_{12}$	532.07	[7]
565.5	S_3	ν_{f2}-$3\nu_R$	370	$Y_3Al_5O_{12}$ ceramic	532.07	[7]
565.8	S_2	ν_{f2}-$2\nu_R$	≈ 560	$LiCaAlF_6$	532.07	[5]
567.2	S_1	ν_{f2}-ν_R	1165	$(NaPO_3)_x$	532.07	[14]
569.7	AS_7	ν_{f1}+$7\nu_R$	1165	$(NaPO_3)_x$	1064.15	[14]
571.2	AS_9	ν_{f1}+$9\nu_R$	901	$PbWO_4$	1064.15	[8]
577.1	S_2	ν_{f2}-$2\nu_{R2}$	733	γ-KIO_3	532.07	[51]
577.6	S_4	ν_{f2}-$4\omega_R$	370	$Y_3Al_5O_{12}$	532.07	[7]
577.6	S_4	ω_{f2}-$4\nu_R$	370	$Y_3Al_5O_{12}$ ceramic	532.07	[7]
577.7	AS_8	ν_{f1}+$8\nu_R$	989	$KAl(SO_4)_2{\cdot}12H_2O$	1064.15	[4]
580.3	S_2	ν_{f2}-$2\nu_R$	781	γ-KIO_3	532.07	[51]
581.1	SFM	ν_{f1}+ν_{S1}		$C_{16}H_{15}N_3O_4$	1064.15	[12]
581.1	S_1	ν_{f2}-ν_R	≈1587	$C_{16}H_{15}N_3O_4$	532.07	[12]
581.2	AS_{10}	ν_{f1}+$10\nu_R$	781	γ-KIO_3	1064.15	[51]
582.5	SHG, S_3	$2\nu_{f1}$-$3\nu_R$	≈ 542	BiB_3O_6	1064.15	[1]
582.8	S_2	ν_{f2}-$2\nu_R$	818	α-$LiIO_3$	532.07	[51]
584.3	S_3	ν_{f2}-$3\nu_R$	≈ 560	$LiCaAlF_6$	532.07	[5]
587.0	S_2	ν_{f2}-$2\nu_R$	≈ 879	$CaMoO_4$	532.07	[53]
587.2	S_2	ν_{f2}-$2\nu_R$	882	$GdVO_4$	532.07	[3]
587.7	S_2	ν_{f2}-ν_R	890	YVO_4	532.07	[3]
588.5	S_2	ν_{f2}-$2\nu_R$	901	$PbWO_4$	532.07	[8]
590.2	S_5	ν_{f2}-$5\nu_R$	370	$Y_3Al_5O_{12}$	532.07	[7]
590.2	S_5	ν_{f2}-$5\nu_R$	370	$Y_3Al_5O_{12}$ ceramic	532.07	[7]
594.7	S_2	ν_{f2}-$2\nu_R$	989	$KAl(SO_4)_2{\cdot}12H_2O$	532.07	[4]
596.0	S_2	ν_{f2}-$2\nu_R$	≈1008	$[C(NH_2)_3]_2Zr[N(CH_2COO)_3]_2{\cdot}H_2O$	532.07	[11]
596.4	AS_7	ν_{f1}+$7\nu_R$	1053	$Ca(NO_3)_2/KNO_3$	1064.15	[13]
596.5	AS_8	ν_{f1}+$8\nu_R$	≈ 921	$SrMoO_4:Nd^{3+}$	1064.15	[53]
598.8	S_1	ν_{f2}-$2\nu_R$	1047	$Ba(NO_3)_2$	532.07	[54]
599.2	S_2	ν_{f2}-$2\nu_R$	1053	$Ca(NO_3)_2/KNO_3$	532.07	[13]
602.2	AS_8	ν_{f1}+$8\nu_R$	901	$PbWO_4$	1064.15	[8]
604.1	S_4	ν_{f2}-$4\nu_R$	≈ 560	$LiCaAlF_6$	532.07	[5]
605.4	AS_8	ν_{f1}+$8\nu_R$	890	YVO_4	1064.15	[3]
607.4	S_2	ν_{f2}-$2\nu_R$	1165	$(NaPO_3)_x$	532.07	[14]
607,8	AS_8	ν_{f1}+$8\nu_R$	882	$GdVO_4$	1064.15	[3]
607.9	S_3	ν_{f2}-$3\nu_R$	781	γ-KIO_3	532.07	[51]
608.8	AS_9	ν_{f1}+$9\nu_R$	781	γ-KIO_3	1064.15	[51]
610.2	AS_6	ν_{f1}+$6\nu_R$	1165	$(NaPO_3)_x$	1064.15	[14]
612.0	S_3	ν_{f2}-$3\nu_R$	818	α-$LiIO_3$	532.07	[51]
612.7	AS_7	ν_{f1}+$7\nu_R$	989	$KAl(SO_4)_2{\cdot}12H_2O$	1064.15	[4]
616.0	SHG, S_2	$2\nu_{f1}$-$2\nu_R$	≈ 1280	$C_{15}H_{19}N_3O_2$	1064.15	[10]
618.9	S_3	ν_{f2}-$3\nu_R$	≈ 879	$CaMoO_4$	532.07	[53]
619.3	S_3	ν_{f2}-$3\nu_R$	882	$GdVO_4$	532.07	[3]
620.2	S_3	ν_{f2}-ν_R	890	YVO_4	532.07	[3]

621.5	S_3	ν_{f2}-3ν_R	901	$PbWO_4$	532.07	[8]
625.2	S_5	ν_{f2}-5ν_R	≈ 560	$LiCaAlF_6$	532.07	[5]
627.3	AS_8	ν_{f1}+8ν_R	818	α-$LiIO_3$	1064.15	[51]
630.7	S_1	ν_{f2}-ν_R	≈2940	$[C(NH_2)_3]_2Zr[N(CH_2COO)_3]_2{\cdot}H_2O$	532.07	[11]
631.2	AS_7	ν_{f1}+7ν_R	≈ 921	$SrMoO_4$:Nd^{3+}	1064.15	[53]
631.8	S_3	ν_{f2}-3ν_R	989	$KAl(SO_4)_2{\cdot}12H_2O$	532.07	[4]
634.1	S_3	ν_{f2}-3ν_R	≈1008	$[C(NH_2)_3]_2Zr[N(CH_2COO)_3]_2{\cdot}H_2O$	532.07	[11]
636.3	AS_6	ν_{f1}+6ν_R	1053	$Ca(NO_3)_2/KNO_3$	1064.15	[13]
636.8	AS_7	ν_{f1}+7ν_R	901	$PbWO_4$	1064.15	[8]
638.1	S_4	ν_{f2}-4ν_R	781	γ-KIO_3	532.07	[51]
638.8	S_3	ν_{f2}-3ν_R	1047	$Ba(NO_3)_2$	532.07	[54]
639.2	AS_8	ν_{f1}+8ν_R	781	γ-KIO_3	1064.15	[51]
639.6	S_3	ν_{f2}-3ν_R	1053	$Ca(NO_3)_2/KNO_3$	532.07	[13]
639.9	AS_7	ν_{f1}+7ν_R	890	YVO_4	1064.15	[3]
640.2	SHG	2ν_{S1}		$C_{16}H_{15}N_3O_4$	1064.15	[12]
642.2	AS_7	ν_{f1}+7ν_R	882	$GdVO_4$	1064.15	[3]
644.2	S_4	ν_{f2}-4ν_R	818	α-$LiIO_3$	532.07	[51]
652.3	AS_6	ν_{f1}+6ν_R	989	$KAl(SO_4)_2{\cdot}12H_2O$	1064.15	[4]
653.6	S_3	ν_{f2}-3ν_R	1165	$(NaPO_3)_x$	532.07	[14]
654.5	S_4	ν_{f2}-4ν_R	≈ 879	$CaMoO_4$	532.07	[53]
656.4	S_4	ν_{f2}-ν_R	890	YVO_4	532.07	[3]
656.9	AS_5	ν_{f1}+5ν_R	1165	$(NaPO_3)_x$	1064.15	[14]
661.2	AS_7	ν_{f1}+7ν_R	818	α-$LiIO_3$	1064.15	[51]
669.0	AS_{15}	ν_{f1}+15ν_R	370	$Y_3Al_5O_{12}$	1064.15	[6]
670.1	AS_6	ν_{f1}+6ν_R	≈ 921	$SrMoO_4$:Nd^{3+}	1064.15	[53]
671.6	S_5	ν_{f2}-5ν_R	781	γ-KIO_3	532.07	[51]
672.8	AS_7	ν_{f1}+7ν_R	781	γ-KIO_3	1064.15	[51]
673.9	S_4	ν_{f2}-4ν_R	989	$KAl(SO_4)_2{\cdot}12H_2O$	532.07	[4]
674.9	AS_{10}	ν_{f1}+10ν_R	≈ 542	BiB_3O_6	1064.15	[1]
675.5	AS_6	ν_{f1}+6ν_R	901	$PbWO_4$	1064.15	[8]
677.4	S_4	ν_{f2}-4ν_R	≈1008	$[C(NH_2)_3]_2Zr[N(CH_2COO)_3]_2{\cdot}H_2O$	532.07	[11]
678.7	AS_6	ν_{f1}+6ν_R	890	YVO_4	1064.15	[3]
680.8	AS_6	ν_{f1}+6ν_R	882	$GdVO_4$	1064.15	[3]
681.6	AS_6	ν_{f1}+ν_R	≈ 879	$CaMoO_4$:Nd^{3+}	1064.15	[53]
682.0	AS_5	ν_{f1}+5ν_R	1053	$Ca(NO_3)_2/KNO_3$	1064.15	[13]
684.6	S_4	ν_{f2}-4ν_R	1047	$Ba(NO_3)_2$	532.07	[54]
685.8	S_4	ν_{f2}-4ν_R	1053	$Ca(NO_3)_2/KNO_3$	532.07	[13]
686.0	AS_{14}	ν_{f1}+ν_R	370	$Y_3Al_5O_{12}$	1064.15	[6]
686.0	AS_{14}	ν_{f1}+ν_R	370	$Y_3Al_5O_{12}$ ceramic	1064.15	[7]
692.2	AS_5	ν_{f1}+5ν_R	1010	$C_{14}H_{10}O_2$	1064-15	[52]
697.0	AS_3	ν_{f1}+3ν_R	1650	$C_{13}H_{10}O$	1064.15	[9]
697.1	S_5	ν_{f2}-ν_R	890	YVO_4	532.07	[3]
697.2	AS_5	ν_{f1}+5ν_R	989	$KAl(SO_4)_2{\cdot}12H_2O$	1064.15	[4]
699.1	AS_6	ν_{f1}+6ν_R	818	α-$LiIO_3$	1064.15	[51]
700.5	AS_9	ν_{f1}+9ν_R	≈ 542	BiB_3O_6	1064.15	[1]
703.9	AS_{13}	ν_{f1}+ν_R	370	$Y_3Al_5O_{12}$	1064.15	[6]
703.9	AS_{13}	ν_{f1}+ν_R	370	$Y_3Al_5O_{12}$ ceramic	1064.15	[7]
710.1	AS_6	ν_{f1}+6ν_R	781	γ-KIO_3	1064.15	[51]
711.4	AS_4	ν_{f1}+4ν_R	1165	$(NaPO_3)_x$	1064.15	[14]
712.6	SFM	ν_{S1}+ν_{S2}		$C_{16}H_{15}N_3O_4$	1064.15	[12]
714.2	AS_5	ν_{f1}+5ν_R	≈ 921	$SrWO_4$:Nd^{3+}	1064.15	[51]
719.3	AS_5	ν_{f1}+5ν_R	901	$PbWO_4$	1064.15	[8]
722.1	S_5	ν_{f2}-5ν_R	989	$KAl(SO_4)_2{\cdot}12H_2O$	532.07	[4]
722.2	AS_5	ν_{f1}+5ν_R	890	YVO_4	1064.15	[3]

722.7	AS_{12}	$\nu_{fl}+\nu_R$	370	$Y_3Al_5O_{12}$	1064.15	[6]
722.7	AS_{12}	$\nu_{fl}+\nu_R$	370	$Y_3Al_5O_{12}$ ceramic	1064.15	[7]
723.2	AS_5	$\nu_{fl}+5\nu_R$	≈ 886	$SrMoO_4:Nd^{3+}$	1064.15	[53]
724.3	AS_5	$\nu_{fl}+5\nu_R$	882	$GdVO_4$	1064.15	[3]
725.1	AS_5	$\nu_{fl}+\nu_R$	≈ 879	$CaMoO_4:Nd^{3+}$	1064.15	[53]
728.2	AS_8	$\nu_{fl}+8\nu_R$	≈ 542	BiB_3O_6	1064.15	[1]
734.8	AS_4	$\nu_{fl}+4\nu_R$	1053	$Ca(NO_3)_2/KNO_3$	1064.15	[13]
736.1	AS_4	$\nu_{fl}-4\nu_R$	1047	$Ba(NO_3)_2$	1064.15	[54]
737.5	S_5	$\nu_{fl2}-5\nu_R$	1047	$Ba(NO_3)_2$	532.07	[54]
741.5	AS_5	$\nu_{fl}+5\nu_R$	818	α-$LiIO_3$	1064.15	[51]
742.6	AS_{11}	$\nu_{fl}+\nu_R$	370	$Y_3Al_5O_{12}$	1064.15	[6]
742.6	AS_{11}	$\nu_{fl}+\nu_R$	370	$Y_3Al_5O_{12}$ ceramic	1064.15	[7]
744.2	AS_4	$\nu_{fl}+4\nu_R$	1010	$C_{14}H_{10}O_2$	1064-15	[52]
748.9	AS_4	$\nu_{fl}+4\nu_R$	989	$KAl(SO_4)_2\cdot12H_2O$	1064.15	[4]
751.8	AS_5	$\nu_{fl}+5\nu_R$	781	γ-KIO_3	1064.15	[51]
758.1	AS_7	$\nu_{fl}+7\nu_R$	≈ 542	BiB_3O_6	1064.15	[1]
763.5	AS_{10}	$\nu_{fl}+\nu_R$	370	$Y_3Al_5O_{12}$	1064.15	[6]
763.5	AS_{10}	$\nu_{fl}+\nu_R$	370	$Y_3Al_5O_{12}$ ceramic	1064.15	[7]
764.5	AS_4	$\nu_{fl}+4\nu_R$	≈ 921	$SrWO_4:Nd^{3+}$	1064.15	[53]
767.0	AS_{40}	$\nu_{fl}+40\nu_R$	91	$Bi_4Ge_3O_{12}$	1064.15	[2]
769.2	AS_4	$\nu_{fl}+4\nu_R$	901	$PbWO_4$	1064.15	[8]
771.8	AS_4	$\nu_{fl}+4\nu_R$	890	YVO_4	1064.15	[3]
772.4	AS_{39}	$\nu_{fl}+39\nu_R$	91	$Bi_4Ge_3O_{12}$	1064.15	[2]
772.7	AS_4	$\nu_{fl}+4\nu_R$	≈ 886	$SrMoO_4:Nd^{3+}$	1064.15	[53]
773.7	AS_4	$\nu_{fl}+4\nu_R$	882	$GdVO_4$	1064.15	[3]
774.3	S_2	$\nu_{fl2}-2\nu_R$	≈2940	$[C(NH_2)_3]_2Zr[N(CH_2COO)_3]_2\cdot H_2O$	532.07	[11]
774.4	AS_4	$\nu_{fl}+\nu_R$	≈ 879	$CaMoO_4:Nd^{3+}$	1064.15	[53]
775.7	AS_3	$\nu_{fl}+3\nu_R$	1165	$(NaPO_3)_x$	1064.15	[14]
777.9	AS_{38}	$\nu_{fl}+38\nu_R$	91	$Bi_4Ge_3O_{12}$	1064.15	[2]
783.4	AS_{37}	$\nu_{fl}+37\nu_R$	91	$Bi_4Ge_3O_{12}$	1064.15	[2]
785.7	AS_9	$\nu_{fl}+9\nu_R$	370	$Y_3Al_5O_{12}$	1064.15	[6]
785.7	AS_9	$\nu_{fl}+9\nu_R$	370	$Y_3Al_5O_{12}$ ceramic	1064.15	[7]
787.6	AS_2	$\nu_{fl}+2\nu_R$	1650	$C_{13}H_{10}O$	1064.15	[9]
788.8	S_1 from AS_4	$(\nu_{fl}+4\nu_{R1})-\nu_{R2}$	ω_{R1}=901 ω_{R2}=323	$PbWO_4$	1064.15	[8]
789.1	AS_{36}	$\nu_{fl}+36\nu_R$	91	$Bi_4Ge_3O_{12}$	1064.15	[2]
789.3	AS_4	$\nu_{fl}+4\nu_R$	818	α-$LiIO_3$	1064.15	[51]
790.6	AS_6	$\nu_{fl}+6\nu_R$	≈ 542	BiB_3O_6	1064.15	[1]
794.8	AS_{35}	$\nu_{fl}+35\nu_R$	91	$Bi_4Ge_3O_{12}$	1064.15	[2]
795.5	AS_2	$\nu_{fl}+2\nu_R$	≈1587	$C_{16}H_{15}N_3O_4$	1064.15	[12]
796.4	AS_3	$\nu_{fl}+3\nu_R$	1053	$Ca(NO_3)_2/KNO_3$	1064.15	[13]
797.6	AS_3	$\nu_{fl}-3\nu_R$	1047	$Ba(NO_3)_2$	1064.15	[54]
798.7	AS_4	$\nu_{fl}+4\nu_R$	781	γ-KIO_3	1064.15	[51]
799.2	S_6	$\nu_{fl2}-6\nu_R$	1047	$Ba(NO_3)_2$	532.07	[54]
800.6	AS_{34}	$\nu_{fl}+34\nu_R$	91	$Bi_4Ge_3O_{12}$	1064.15	[2]
802.1	AS_1	$\nu_{fl}+\nu_R$	3070	$C_{13}H_{10}O$	1064.15	[9]
803.4	SHG	$2\nu_{S1}$		$C_{16}H_{15}N_3O_4$	1064.15	[12]
804.7	AS_3	$\nu_{fl}+3\nu_R$	1010	$C_{14}H_{10}O_2$	1064-15	[52]
804.9	AS_1 from AS_3	$(\nu_{fl}+3\nu_{R1})+\nu_{R2}$	ω_{R1}=901 ω_{R2}=323	$PbWO_4$	1064.15	[8]
805.3	AS_5	$\nu_{fl}+5\nu_R$	≈ 604	BiB_3O_6	1064.15	[1]
808.8	AS_3	$\nu_{fl}+3\nu_R$	989	$KAl(SO_4)_2\cdot12H_2O$	1064.15	[4]
809.3	AS_8	$\nu_{fl}+8\nu_R$	370	$Y_3Al_5O_{12}$	1064.15	[6]
809.3	AS_8	$\nu_{fl}+8\nu_R$	370	$Y_3Al_5O_{12}$ ceramic	1064.15	[7]

810.6	AS_1	$\nu_{fl}+\nu_R$	≈2940	$[C(NH_2)_3]_2Zr[N(CH_2COO)_3]_2\cdot H_2O$	1064.15	[11]
812.4	AS_{32}	$\nu_{fl}+32\nu_R$	91	$Bi_4Ge_3O_{12}$	1064.15	[2]
818.5	AS_{31}	$\nu_{fl}+31\nu_R$	91	$Bi_4Ge_3O_{12}$	1064.15	[2]
822.4	AS_3	$\nu_{fl}+3\nu_R$	≈ 921	$SrWO_4:Nd^{3+}$	1064.15	[53]
824.6	AS_{30}	$\nu_{fl}+30\nu_R$	91	$Bi_4Ge_3O_{12}$	1064.15	[2]
826.0	AS_5	$\nu_{fl}+5\nu_R$	≈ 542	BiB_3O_6	1064.15	[1]
826.4	AS_3	$\nu_{fl}+3\nu_R$	901	$PbWO_4$	1064.15	[8]
828.7	AS_3	$\nu_{fl}+3\nu_R$	890	YVO_4	1064.15	[3]
829.5	AS_3	$\nu_{fl}+3\nu_R$	≈ 886	$SrMoO_4:Nd^{3+}$	1064.15	[53]
830.2	S from AS	$(\nu_{fl}+\nu_{R2})-\nu_{R1}$	998, 1650	$C_{13}H_{10}O$	1064.15	[9]
830.4	AS_3	$\nu_{fl}+3\nu_R$	882	$GdVO_4$	1064.15	[3]
830.8	AS_{29}	$\nu_{fl}+29\nu_R$	91	$Bi_4Ge_3O_{12}$	1064.15	[2]
831.0	AS_3	$\nu_{fl}+\nu_R$	≈ 879	$CaMoO_4:Nd^{3+}$	1064.15	[53]
834.2	AS_7	$\nu_{fl}+7\nu_R$	370	$Y_3Al_5O_{12}$	1064.15	[6]
834.2	AS_7	$\nu_{fl}+7\nu_R$	370	$Y_3Al_5O_{12}$ ceramic	1064.15	[7]
836.3	AS_2	$\nu_{fl}+2\nu_R$	≈ 1280	$C_{15}H_{19}N_3O_2$	1064.15	[10]
837.2	AS_{28}	$\nu_{fl}+28\nu_R$	91	$Bi_4Ge_3O_{12}$	1064.15	[2]
843.6	AS_{27}	$\nu_{fl}+27\nu_R$	91	$Bi_4Ge_3O_{12}$	1064.15	[2]
843.8	AS_3	$\nu_{fl}+3\nu_R$	818	α-$LiIO_3$	1064.15	[51]
846.5	AS_4	$\nu_{fl}+4\nu_R$	≈ 604	BiB_3O_6	1064.15	[1]
849.1	S_1 from AS_3	$(\nu_{fl}+3\nu_{R1})-\nu_{R2}$	ω_{R1}=901 ω_{R2}=323	$PbWO_4$	1064.15	[8]
850.1	AS_{26}	$\nu_{fl}+26\nu_R$	91	$Bi_4Ge_3O_{12}$	1064.15	[2]
851.8	AS_3	$\nu_{fl}+3\nu_R$	781	γ-KIO_3	1064.15	[51]
852.7	AS_2	$\nu_{fl}+2\nu_R$	1165	$(NaPO_3)_x$	1064.15	[14]
856.7	AS_{25}	$\nu_{fl}+25\nu_R$	91	$Bi_4Ge_3O_{12}$	1064.15	[2]
860.8	AS_6	$\nu_{fl}+6\nu_R$	370	$Y_3Al_5O_{12}$	1064.15	[6]
860.8	AS_6	$\nu_{fl}+6\nu_R$	370	$Y_3Al_5O_{12}$ ceramic	1064.15	[7]
863.5	AS_{24}	$\nu_{fl}+24\nu_R$	91	$Bi_4Ge_3O_{12}$	1064.15	[2]
864.7	AS_4	$\nu_{fl}+4\nu_R$	≈ 542	BiB_3O_6	1064.15	[1]
867.9	AS_1 from AS_2	$(\nu_{fl}+2\nu_{R1})+\nu_{R2}$	ω_{R1}=901 ω_{R2}=323	$PbWO_4$	1064.15	[8]
869.3	AS_2	$\nu_{fl}+2\nu_R$	1053	$Ca(NO_3)_2/KNO_3$	1064.15	[13]
870.2	AS_2	$\nu_{fl}-2\nu_R$	1047	$Ba(NO_3)_2$	1064.15	[54]
870.3	AS_{23}	$\nu_{fl}+23\nu_R$	91	$Bi_4Ge_3O_{12}$	1064.15	[2]
875.9	AS_2	$\nu_{fl}+2\nu_R$	1010	$C_{14}H_{10}O_2$	1064-15	[52]
877.3	AS_{22}	$\nu_{fl}+22\nu_R$	91	$Bi_4Ge_3O_{12}$	1064.15	[2]
877.7	AS_2	$\nu_{fl}+2\nu_R$	998	$C_{13}H_{10}O$	1064.15	[9]
879.1	AS_2	$\nu_{fl}+2\nu_R$	989	$KAl(SO_4)_2\cdot 12H_2O$	1064.15	[4]
884.3	AS_{21}	$\nu_{fl}+21\nu_R$	91	$Bi_4Ge_3O_{12}$	1064.15	[2]
889.1	AS_5	$\nu_{fl}+5\nu_R$	370	$Y_3Al_5O_{12}$	1064.15	[6]
889.1	AS_5	$\nu_{fl}+5\nu_R$	370	$Y_3Al_5O_{12}$ ceramic	1064.15	[7]
889.8	AS_2	$\nu_{fl}+2\nu_R$	≈ 921	$SrWO_4:Nd^{3+}$	1064.15	[53]
891.5	AS_{20}	$\nu_{fl}+20\nu_R$	91	$Bi_4Ge_3O_{12}$	1064.15	[2]
892.1	AS_3	$\nu_{fl}+3\nu_R$	≈ 604	BiB_3O_6	1064.15	[1]
892.9	AS_2	$\nu_{fl}+2\nu_R$	901	$PbWO_4$	1064.15	[8]
894.7	AS_2	$\nu_{fl}+2\nu_R$	890	YVO_4	1064.15	[3]
895.3	AS_2	$\nu_{fl}+2\nu_R$	≈ 886	$SrMoO_4:Nd^{3+}$	1064.15	[53]
896.0	AS_2	$\nu_{fl}+2\nu_R$	882	$GdVO_4$	1064.15	[3]
896.5	AS_2	$\nu_{fl}+\nu_R$	≈ 879	$CaMoO_4:Nd^{3+}$	1064.15	[53]
898.8	AS_{19}	$\nu_{fl}+19\nu_R$	91	$Bi_4Ge_3O_{12}$	1064.15	[2]
905.2	AS_1	$\nu_{fl}+\nu_R$	1650	$C_{13}H_{10}O$	1064.15	[9]
906.2	AS_{18}	$\nu_{fl}+18\nu_R$	91	$Bi_4Ge_3O_{12}$	1064.15	[2]
906.4	AS_2	$\nu_{fl}+2\nu_R$	818	α-$LiIO_3$	1064.15	[51]

907.2	AS_3	$\nu_{fl}+3\nu_R$	≈ 542	BiB_3O_6	1064.15	[1]
910.4	AS_1	$\nu_{fl}+\nu_R$	≈1587	$C_{16}H_{15}N_3O_4$	1064.15	[12]
912.5	AS_2	$\nu_{fl}+2\nu_R$	781	γ-KIO_3	1064.15	[51]
913.7	AS_{17}	$\nu_{fl}+17\nu_R$	91	$Bi_4Ge_3O_{12}$	1064.15	[2]
919.4	S_1 from AS_2	$(\nu_{fl}+2\nu_{R1})-\nu_{R2}$	ω_{R1}=901 ω_{R2}=323	$PbWO_4$	1064.15	[8]
919.4	AS_4	$\nu_{fl}+4\nu_R$	370	$Y_3Al_5O_{12}$	1064.15	[6]
919.4	AS_4	$\nu_{fl}+4\nu_R$	370	$Y_3Al_5O_{12}$ ceramic	1064.15	[7]
921.4	AS_{16}	$\nu_{fl}+16\nu_R$	91	$Bi_4Ge_3O_{12}$	1064.15	[2]
929.2	AS_{15}	$\nu_{fl}+15\nu_R$	91	$Bi_4Ge_3O_{12}$	1064.15	[2]
936.6	AS_1	$\nu_{fl}+\nu_R$	≈ 1280	$C_{15}H_{19}N_3O_2$	1064.15	[10]
937.1	AS_{14}	$\nu_{fl}+14\nu_R$	91	$Bi_4Ge_3O_{12}$	1064.15	[2]
941.6	AS_1 from AS_1	$(\nu_{fl}+\nu_{R1})+\nu_{R2}$	ω_{R1}=901 ω_{R2}=323	$PbWO_4$	1064.15	[8]
942.9	AS_2	$\nu_{fl}+2\nu_R$	≈ 604	BiB_3O_6	1064.15	[1]
945.2	AS_{13}	$\nu_{fl}+13\nu_R$	91	$Bi_4Ge_3O_{12}$	1064.15	[2]
946.7	AS_2	$\nu_{fl}+\nu_R$	≈ 583	BiB_3O_6	1064.15	[1]
946.8	AS_1	$\nu_{fl}+\nu_R$	1165	$(NaPO_3)_x$	1064.15	[14]
951.7	AS_3	$\nu_{fl}+3\nu_R$	370	$Y_3Al_5O_{12}$	1064.15	[6]
951.7	AS_3	$\nu_{fl}+3\nu_R$	370	$Y_3Al_5O_{12}$ ceramic	1064.15	[7]
953.4	AS_{12}	$\nu_{fl}+12\nu_R$	91	$Bi_4Ge_3O_{12}$	1064.15	[2]
954.1	AS_2	$\nu_{fl}+2\nu_R$	≈ 542	BiB_3O_6	1064.15	[1]
956.9	AS_1	$\nu_{fl}+\nu_R$	1053	$Ca(NO_3)_2/KNO_3$	1064.15	[13]
957.5	AS_1	$\nu_{fl}-\nu_R$	1047	$Ba(NO_3)_2$	1064.15	[54]
960.9	AS_1	$\nu_{fl}+\nu_R$	1010	$C_{14}H_{10}O_2$	1064-15	[52]
961.7	AS_{11}	$\nu_{fl}+11\nu_R$	91	$Bi_4Ge_3O_{12}$	1064.15	[2]
962.0	AS_1	$\nu_{fl}+\nu_R$	998	$C_{13}H_{10}O$	1064.15	[9]
962.8	AS_1	$\nu_{fl}+\nu_R$	989	$KAl(SO_4)_2\cdot12H_2O$	1064.15	[4]
969.2	AS_1	$\nu_{fl}+\nu_R$	≈ 921	$SrWO_4:Nd^{3+}$	1064.15	[53]
970.2	AS_{10}	$\nu_{fl}+10\nu_R$	91	$Bi_4Ge_3O_{12}$	1064.15	[2]
971.1	AS_1	$\nu_{fl}+\nu_R$	901	$PbWO_4$	1064.15	[8]
972.1	AS_1	$\nu_{fl}+\nu_R$	890	YVO_4	1064.15	[3]
972.5	AS_1	$\nu_{fl}+\nu_R$	≈ 886	$SrMoO_4:Nd^{3+}$	1064.15	[53]
972.8	AS_1	$\nu_{fl}+\nu_R$	882	$GdVO_4$	1064.15	[3]
973.1	AS_1	$\nu_{fl}+\nu_R$	≈ 879	$CaMoO_4:Nd^{3+}$	1064.15	[53]
978.8	AS_9	$\nu_{fl}+9\nu_R$	91	$Bi_4Ge_3O_{12}$	1064.15	[2]
978.9	AS_1	$\nu_{fl}+\nu_R$	818	α-$LiIO_3$	1064.15	[51]
982.5	AS_1	$\nu_{fl}+\nu_R$	781	γ-KIO_3	1064.15	[51]
986.5	AS_2	$\nu_{fl}+2\nu_R$	370	$Y_3Al_5O_{12}$	1064.15	[6]
986.5	AS_2	$\nu_{fl}+2\nu_R$	370	$Y_3Al_5O_{12}$ ceramic	1064.15	[7]
987.6	AS_8	$\nu_{fl}+8\nu_R$	91	$Bi_4Ge_3O_{12}$	1064.15	[2]
995.1	S_1 from AS_1	$(\nu_{fl}+\nu_{R2})-\nu_{R1}$	ω_{R1}=998, ω_{R2}=1650	$C_{13}H_{10}O$	1064.15	[9]
999.9	AS_1	$\nu_{fl}+\nu_R$	≈ 604	BiB_3O_6	1064.15	[1]
1002.0	AS_1	$\nu_{fl}+\nu_R$	≈ 583	BiB_3O_6	1064.15	[1]
1002.6	S_1 from AS_1	$(\nu_{fl}+\nu_{R1})-\nu_{R2}$	ω_{R1}=901 ω_{R2}=323	$PbWO_4$	1064.15	[8]
1005.7	AS_6	$\nu_{fl}+6\nu_R$	91	$Bi_4Ge_3O_{12}$	1064.15	[2]
1006.1	AS_1	$\nu_{fl}+\nu_R$	≈ 542	BiB_3O_6	1064.15	[1]
1015.0	AS_5	$\nu_{fl}+5\nu_R$	91	$Bi_4Ge_3O_{12}$	1064.15	[2]
1022.0	AS_4	$\nu_{fl}+4\nu_R$	97	$Bi_4Si_3O_{12}$	1064.15	[2]
1023.4	AS_1	$\nu_{fl}+\nu_R$	≈ 374	BiB_3O_6	1064.15	[1]
1023.8	AS_1	$\nu_{fl}+\nu_R$	370	$Y_3Al_5O_{12}$	1064.15	[6]
1023.8	AS_1	$\nu_{fl}+\nu_R$	370	$Y_3Al_5O_{12}$ ceramic	1064.15	[7]
1024.5	AS	$\nu_{fl}+4\nu_R$	91	$Bi_4Ge_3O_{12}$	1064.15	[2]

1028.8	AS_1	$\nu_{fl}+\nu_R$	323	$PbWO_4$	1064.15	[8]
1032.2	AS_3	$\nu_{fl}+3\nu_R$	97	$Bi_4Si_3O_{12}$	1064.15	[2]
1034.1	AS_3	$\nu_{fl}+3\nu_R$	91	$Bi_4Ge_3O_{12}$	1064.15	[2]
1042.6	AS_2	$\nu_{fl}+2\nu_R$	97	$Bi_4Si_3O_{12}$	1064.15	[2]
1043.9	AS_2	$\nu_{fl}+2\nu_R$	91	$Bi_4Ge_3O_{12}$	1064.15	[2]
1045.5	AS_1	$\nu_{fl}+\nu_R$	≈ 168	BiB_3O_6	1064.15	[1]
1053.3	AS_1	$\nu_{fl}+\nu_R$	97	$Bi_4Si_3O_{12}$	1064.15	[2]
1053.9	AS_1	$\nu_{fl}+\nu_R$	91	$Bi_4Ge_3O_{12}$	1064.15	[2]
1074.6	S_1	$\nu_{fl}-\nu_R$	91	$Bi_4Ge_3O_{12}$	1064.15	[2]
1075.3	S_1	$\nu_{fl}-\nu_R$	97	$Bi_4Si_3O_{12}$	1064.15	[2]
1083.5	S_1	$\nu_{fl}-\nu_R$	≈ 168	BiB_3O_6	1064.15	[1]
1085.2	S_2	$\nu_{fl}-2\nu_R$	91	$Bi_4Ge_3O_{12}$	1064.15	[2]
1086.6	S_2	$\nu_{fl}-2\nu_R$	97	$Bi_4Si_3O_{12}$	1064.15	[2]
1089.1	S_1	$\nu_{fl}-\nu_R$	≈ 215	BiB_3O_6	1064.15	[1]
1096	S_3	$\nu_{fl}-3\nu_R$	91	$Bi_4Ge_3O_{12}$	1064.15	[2]
1098.2	S_3	$\nu_{fl}-3\nu_R$	97	$Bi_4Si_3O_{12}$	1064.15	[2]
1102.0	S_1	$\nu_{fl}-\nu_R$	323	$PbWO_4$	1064.15	[8]
1107.0	S_4	$\nu_{fl}-4\nu_R$	91	$Bi_4Ge_3O_{12}$	1064.15	[2]
1107.8	S_1	$\nu_{fl}-\nu_R$	370	$Y_3Al_5O_{12}$	1064.15	[6]
1107.8	S_1	$\nu_{fl}-\nu_R$	370	$Y_3Al_5O_{12}$ ceramic	1064.15	[7]
1108.3	S_1	$\nu_{fl}-\nu_R$	≈ 374	BiB_3O_6	1064.15	[1]
1110.0	S_4	$\nu_{fl}-4\nu_R$	97	$Bi_4Si_3O_{12}$	1064.15	[2]
1118.3	S_5	$\nu_{fl}-5\nu_R$	91	$Bi_4Ge_3O_{12}$	1064.15	[2]
1129.3	S_1	$\nu_{fl}-\nu_R$	≈ 542	BiB_3O_6	1064.15	[1]
1129.8	S_6	$\nu_{fl}-6\nu_R$	91	$Bi_4Ge_3O_{12}$	1064.15	[2]
1134.5	S_1	$\nu_{fl}-\nu_R$	≈ 583	BiB_3O_6	1064.15	[1]
1137.3	S_1	$\nu_{fl}-\nu_R$	≈ 604	BiB_3O_6	1064.15	[1]
1141.5	S_7	$\nu_{fl}-7\nu_R$	91	$Bi_4Ge_3O_{12}$	1064.15	[2]
1153.5	S_8	$\nu_{fl}-8\nu_R$	91	$Bi_4Ge_3O_{12}$	1064.15	[2]
1155.1	S_2	$\nu_{fl}-2\nu_R$	370	$Y_3Al_5O_{12}$	1064.15	[6]
1155.1	S_2	$\nu_{fl}-2\nu_R$	370	$Y_3Al_5O_{12}$ ceramic	1064.15	[7]
1160,6	S_1	$\nu_{fl}-\nu_R$	781	γ-KIO_3	1064.15	[51]
1165.2	S1	$\nu_{fl}-\nu_{R2}$	ω_{R2}=815	YVO_4	1064.15	[3]
1165.6	S_1	$\nu_{fl}-\nu_R$	818	α-$LiIO_3$	1064.15	[51]
1165.8	S_9	$\nu_{fl}-9\nu_R$	91	$Bi_4Ge_3O_{12}$	1064.15	[2]
1174.0	S_1	$\nu_{fl}-\nu_R$	≈ 879	$CaMoO_4:Nd^{3+}$	1064.15	[53]
1174.4	S1	$\nu_{fl}-\nu_R$	882	$GdVO_4$	1064.15	[3]
1174.9	S_1	$\nu_{fl}-\nu_R$	≈ 886	$SrMoO_4:Nd^{3+}$	1064.15	[53]
1175.5	S1	$\nu_{fl}-\nu_R$	890	YVO_4	1064.15	[3]
1177	S_1	$\nu_{fl}-\nu_R$	901	$PbWO_4$	1064.15	[8]
1179.8	S_1	$\nu_{fl}-\nu_R$	≈ 921	$SrMoO_4:Nd^{3+}$	1064.15	[53]
1189.3	S_1	$\nu_{fl}-\nu_R$	989	$KAl(SO_4)_2\cdot 12H_2O$	1064.15	[4]
1190.6	S_1	$\nu_{fl}-\nu_R$	998	$C_{13}H_{10}O$	1064.15	[9]
1192.3	S_1	$\nu_{fl}-\nu_R$	1010	$C_{14}H_{10}O_2$	1064-15	[52]
1197.6	S_1	$\nu_{fl}-\nu_R$	1047	$Ba(NO_3)_2$	1064.15	[54]
1198.4	S_1	$\nu_{fl}-\nu_R$	1053	$Ca(NO_3)_2/KNO_3$	1064.15	[13]
1214.8	S_1	$\nu_{fl}-\nu_R$	1165	$(NaPO_3)_x$	1064.15	[14]
1316.6	S_2	$\nu_{fl}-2\nu_R$	901	$PbWO_4$	1064.15	[15]
1369.3	S_2	$\nu_{fl}-2\nu_R$	1047	$Ba(NO_3)_2$	1064.15	[54]

5 Second-Stokes Raman lasers

Frequency shifting of pico and nanosecond laser pulses by stimulated Stokes and anti-Stokes scattering in solid-state crystals is of interest for many applications. It allows to design solid-state Raman lasers emitting radiation in specified spectral region. A Raman laser is constructed similarly as a conventional laser i.e. an optical resonator is formed placing two mirrors at both sides of the active medium. The optical resonator includes a number of passes of scattering radiation through the interaction region in the pumped nonlinear medium. The special properties of solid-state Raman lasers make them useful in many different types of applications [5-1]-[5-4]. High efficiency and excellent beam quality are important laser properties for any application. Some current applications of Raman lasers are described below:

1. Pumping a barium nitrate Raman crystal with a Nd:YAG-laser results in a Raman laser output at 1560 nm. This is an optimum wavelength for atmospheric propagation and eye-safe operation. Therefore this type of Raman laser is ideal as a transmitter for atmospheric LIDAR system.
2. One important current area of laser development is for sodium guidestar applications. In this case a laser is projected through a telescope to the upper atmosphere where it is resonantly absorbed by a layer of sodium atoms. The sodium fluorescence acts like an artificial star and the atmospheric distortion of its image is detected for astronomical propose.
3. The spectral range of output wavelengths and the variety of output configurations demonstrate the potential for Raman laser in military applications such as range finder, target designators and munitions guidance.
4. In medical applications requiring specific wavelengths in the visible and near infrared spectral regions. One particular application is application is the removal of vascular lesions. For which the main requirement for the laser is strong absorption by haemoglobin, with minimal absorption by the melanin pigment in tissue.

Raman laser can be based on a wide variety of active Raman crystals. Then it is possible to envision many more applications in future.

The most used materials in Raman lasers are cubic $Ba(NO_3)_2$, monoclinic α-$KGd(WO_4)_2$, and tetragonal $PbWO_4$ crystals. Among them $PbWO_4$ has several advantages, it is very stable (e.g., $Ba(NO_3)_2$ requires moisture protection), cheep and can be grown in big sizes with high optical quality by the ordinary Czochralski pulling technique (for growing big size of α-$KGd(WO_4)_2$ crystals only very expensive top-seed flux method is available). During last years many versions of Stokes Raman lasers have been developed based on these crystals. For example, first, second and third-Stokes SRS nonlinear processes in high gain and high effective solid state $Ba(NO_3)_2$ Raman material was used for laser light frequency shifting to a spectral range of 1200-1500 nm [5-5]. Nanosecond Nd:YAG laser pumping was used for generation theses Raman lasers. Raman laser was performed in $PbWO_4$ in the nanosecond temporal regime which demonstrate the efficient generation of first Stokes wavelengths in the near-IR region (with a 3-mirror ring resonator) and in the visible region (using a linear optical resonator) [4-8]. Raman lasers on the first Stokes line of $KGd(WO_4)_2$ and $PbWO_4$ were demonstrated inside the laser cavity as well as in an external cavity [5-6]. The Stokes Raman lasers were converted to the yellow spectral region, e.g. 580 nm or 590 nm with a doubler crystal. Recently, first Stokes Raman lasers based on the $BaWO_4$ crystal have been investigated in the near infrared, visible, and ultraviolet regions [5-7].

We discuss in this chapter a second-Stokes Raman laser based on $PbWO_4$ and $Ba(NO_3)_2$ crystals pumped by a picosecond Nd:YAG laser at 1064.15 nm. Conversion efficiency of the second-Stokes Raman lasers dependence of $PbWO_4$ crystal length have been studied. We have used the doubler crystal to convert the Raman lines to the red spectral region. Finally, beam profile of the generated Raman lasers is reported.

5.1 Experimental set-up

Raman laser can be constructed in a variety of configurations: single pass Raman shifter, Raman laser with an external pumping or with an intracavity pumping optical scheme. We perform SRS experiment in an external cavity to allow an independent optimization of the pump laser and the SRS process. Furthermore, Raman laser in an external cavity can give a significant increase of conversion efficiency and intensity of SRS with respect to single pass.

The simplest scheme of Raman conversion can be realized in conditions where a nonlinear medium is placed inside a laser resonator having a high-reflectivity mirror for the pump wavelength but a semitransparent mirror for the Raman shifted wavelength. By building a resonator around the Raman medium, the pump threshold is greatly reduced, the conversion efficiency is increased and better spatial quality is obtained. To obtain high energy conversion efficiency in the Raman cavity it was necessary to optimize pump pulse energy and duration, input beam waist diameter and interaction length. Furthermore, Raman shifter with external cavity concentrate SRS radiation in a narrow angle beam close to the diffraction limited one. A short plano-concave cavity is chosen to achieve small output beam size, small divergent angle, easy alignment and overall compactness.

With one flat mirror with radius of curvature $R_1 = \infty$ and one curved mirror with radius of curvature $R_2 = R$, the Raleigh range Z_R for the cavity is written as [5-8]

$$Z_R = \sqrt{L(R-L)} \qquad (5.1.1)$$

then the Gaussian beam waist diameter is

$$2w_0 = 2\sqrt{Z_R \lambda / \pi} \qquad (5.1.2)$$

where λ is the Raman shift wavelength.

The beam diameter at the output coupler is

$$2w_Z = 2w_0 \sqrt{1 + (L / Z_R)^2} \qquad (5.1.3)$$

It is possible to prepare dichroic mirrors with optimal reflectivity for the second Stokes wavelength and low for first Stokes components. This can increase the intensity in the second component. By varying the reflectivity of the cavity mirrors it is possible to prepare laser cavity working only at the first or only at the third Stokes component, independently.

For generation of second-Stokes Raman laser we use picosecond Nd:YAG laser at wavelength $\lambda_{fl} = 1064.15$ nm with pulse duration 120 ps. The experimental set-up was discussed in details in chapter 2. To achieve efficient second-Stokes Raman laser based on $PbWO_4$ and $Ba(NO_3)_2$ at $\lambda_{St2} = 1316.6$ nm and at $\lambda_{St2} = 1369$ nm wavelength respectively, with high beam quality, a plano-concave cavity is used. The schematic of the Raman resonator for the second-Stokes Raman laser is shown in Fig. 5.1. The Gaussian beam waist diameter at the plane mirror *M* with radius $R_1 = \infty$ and at the output coupler *OC* with radius of curvature $R_2 = R = -250$ mm were calculated to be about 0,41 and 1 mm, respectively. Optical characteristics of used cavity mirrors are shown in Table 5.1. We use the same resonator for second-Stokes Raman lasers in $PbWO_4$ and $Ba(NO_3)_2$ crystals.

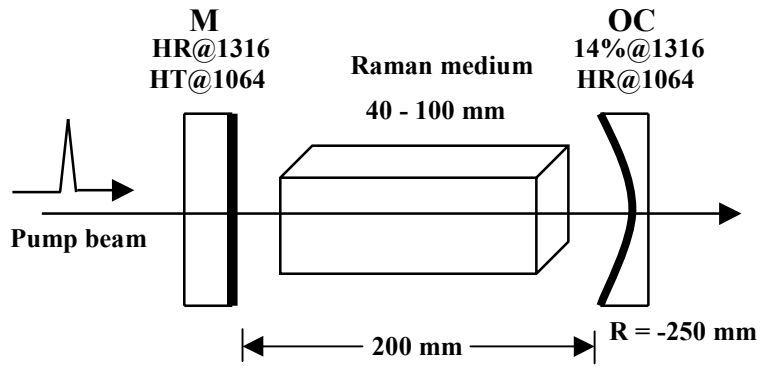

Fig. 5.1: *Plano-concave linear resonator for Raman laser.*

Table 5.1: *Mirror reflectivities of the Raman resonator.*

Crystal	Size (mm)	Raman shift (cm^{-1})	R @ Output coupler			R @ End mirror
			R @ 1064 nm	1^{st}-Stokes	2^{nd}-Stokes	
$PbWO_4$	10x10x100	901	HR	HR	12 %	HT @ 1064 nm HR @ 1316.6 nm HR @ 1369 nm
$Ba(NO_3)_2$	10x10x70	1047	HR	HR	11 %	

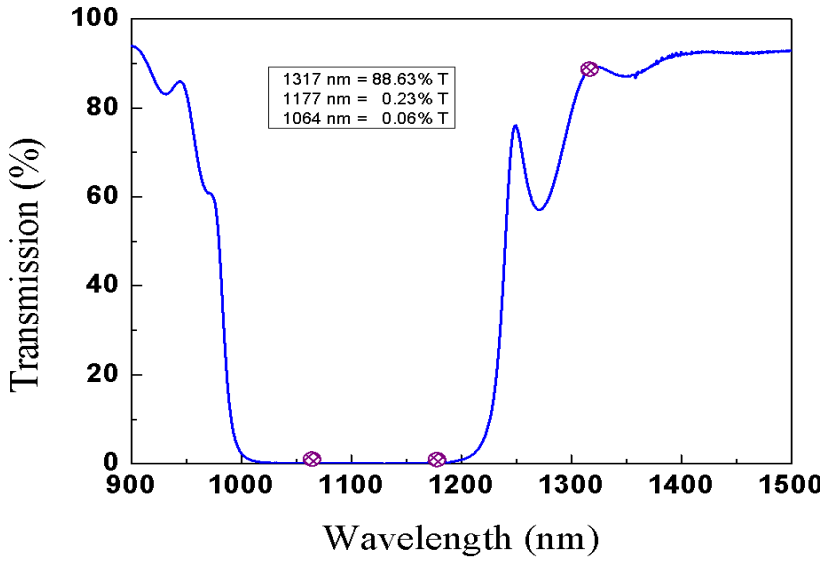

Fig. 5.2: *Transmission characteristics of the output coupler of the second-Stokes Raman laser using $PbWO_4$ or $Ba(NO_3)_2$ crystal.*

The transmission characteristics of the output coupler are shown in Fig 5.2. The mirrors are separated by 200 mm and the investigated $PbWO_4$ Raman crystal (10 mm x 10 mm x 40-100 mm) is placed between them to form the resonator. The intensity of the pump beam in the Raman resonator with pump pulse duration $\tau_p \approx 120\ ps$, threshold energy $E_{thr} \approx 0.35\ mJ$ and beam waist diameter $d \approx 100\ \mu m$ was calculated by using $I_{P(0)} = E/\tau.d^2 = 1\ GW/cm^2$.

5.2 Operation of second-Stokes Raman laser

Tetragonal $PbWO_4$ and cubic $Ba(NO_3)_2$ crystals have been investigated to generate second-Stokes Raman laser at λ_{St2} = 1316.6 nm and at λ_{St2} = 1369 nm wavelength respectively. The used Raman active crystals are polished with plane-parallel end faces and without coating. Different $PbWO_4$ bars with 40, 56 and 100 mm length and cross-section of 10x10 mm^2 have been used. The dimension of the $Ba(NO_3)_2$ sample is 70 mm length and 10x10x mm^2 cross-section. The laser axis was perpendicular to the optical c-axis of the $PbWO_4$ crystal. The Raman active materials are placed in the cavity constructed with dichroic mirrors *M* and *OC*. In the beginning, first-Stokes is generated in the Raman cavity. It is amplified and becomes the pump for the second-Stokes scattering. After that the second-Stokes component is amplified in the Raman cavity. Then during further passes of the first-Stokes, the pump emission is considerably reduced and the energy of the outcoming Raman pulses is therefore decreasing. This shows that the second-Stokes oscillation does not start from spontaneous level of Raman scattering but is amplified in the intensive field of Raman oscillations stimulated by the pump and first Stokes components with the frequencies ν_{f1} and ν_{S1} defined as $\nu_{S1} - \nu_{S2} = \nu_R = \nu_{f1} - \nu_{S1}$. Fig. 5.3 shows second-Stokes Raman spectra in addition, the fundamental and first Stokes lines of $PbWO_4$ crystal with phonon energy of 901 cm^{-1}.

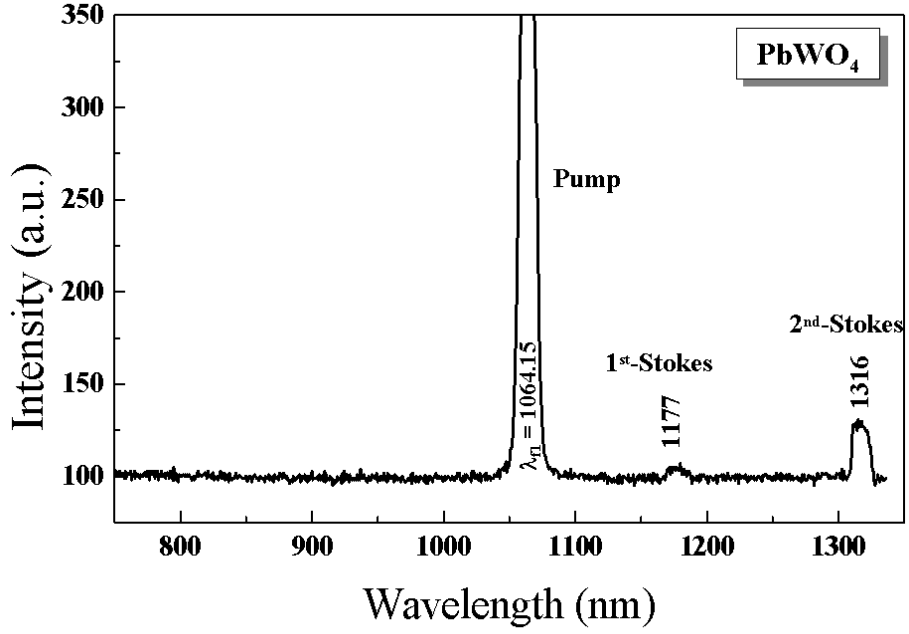

Fig. 5.3: *Second-Stokes Raman emission in tetragonal $PbWO_4$ single crystal.*

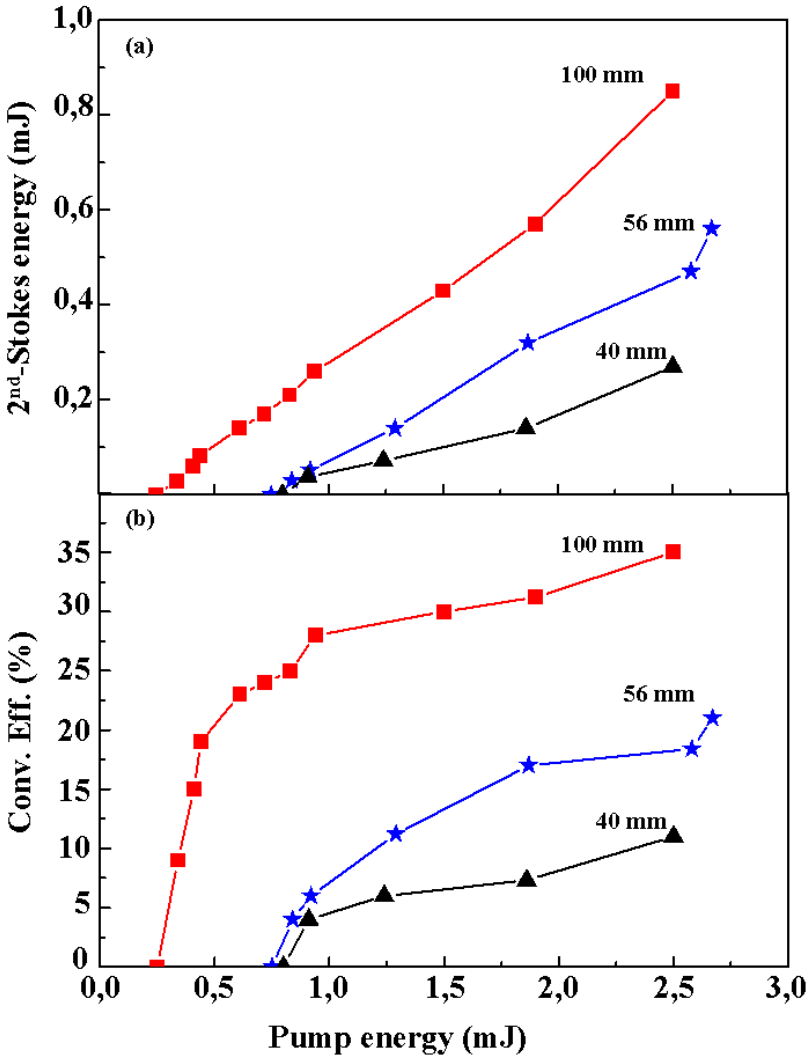

Fig. 5.4:

Second-Stokes energy a) and conversion efficiency b) dependence on the pump energy for $PbWO_4$ crystals of different lengths 100 mm, 56 mm and 40 mm.

The output energy of the Raman laser behind the output-coupler was selected by a plane mirror with high reflectivity for the fundamental and first-Stokes wavelengths and high transmission for the second-Stokes and measured with calibrated energy meter (Rj-7200). In this arrangement we obtain a laser energy of more than 0.85 mJ for $PbWO_4$ crystal. Maximum conversion efficiency of about 11, 21 and 35 % at the second-Stokes wavelength of a 40, 56 and 100 mm crystals length of 10 x 10 mm^2 cross-section are observed. We estimate the conversion efficiency by taking the ratio of the second-Stokes output energy to the pump energy [5-9]. Fig. 5.4 shows the second-Stokes energy and conversion efficiency against the pump energy for Raman crystals with different lengths. The conversion efficiency of the second-Stokes depends of the Raman crystal length. Very similar behavior of Stokes generation was earlier obtained in a $Ba(NO_3)_2$ Raman laser [5-5].

The conversion efficiency for individual Raman shifts drops slightly when we increase the pump energy over the saturation level (2 – 2.5 mJ). This phenomena may be due to the higher crystal temperature which lowers the efficiency and the unwanted higher and/or lower-order Stokes shifts. Like other crystals involving vibration transitions, the maximum gain in the $PbWO_4$ crystal occurs for pump and Stokes polarizations that are linear and parallel [5-10]. In our case, the Raman laser output is almost linearly polarized for a linearly polarized pump beam.

Fig. 5.4 shows second-Stokes $Ba(NO_3)_2$ Raman laser at wavelength 1369 nm with phonon energy of 1047 cm^{-1}. We obtain maximum output energy about 2 mJ for $Ba(NO_3)_2$ crystal. Maximum conversion efficiency of about 21 % is observed at the second-Stokes line of a 70 mm crystal length and 10 x 10 mm^2 cross-section.

Although, the $PbWO_4$ samples is longer than the $Ba(NO_3)_2$ crystal and it shows stable Raman laser operation, it generates second-Stokes Raman laser line with energy less than $Ba(NO_3)_2$. So, it is not possible to directly compare these materials since they posses many different properties including different crystal structures, indices of refraction and Raman gain.

5.3 Frequency doubling

We applied the second harmonic generation SHG method for accurate measurement of the wavelength of the second-Stokes Raman laser emission. KD*P was chosen as the SHG materials because of its high damage threshold and large acceptance angle. The highest conversion efficiency was obtained in an KD*P crystal (10x10x40 mm), cut for type I. The second-Stokes output was focussed using a 100 mm lens to produce a beam waist diameter of about 150 μm.

Due to considerable energy of the second-Stokes $PbWO_4$ line (0.85 mJ) strong SHG at 658.5 nm wavelength is observed. Maximum average output energy of about 0.08 mJ at the SHG wavelengths of 658.5 nm is achieved, with conversion efficiency of about 10 %. Fig. 5.5 shows second-Stokes Raman laser spectrum in $PbWO_4$ crystal and its SHG.

In Fig. 5.5 the Raman emission spectrum of $Ba(NO_3)_2$ crystal and its second harmonic is shown. SHG wavelengths at 684.5 nm of the second-Stokes $Ba(NO_3)_2$ line is observed with maximum output energy 0.23 mJ, and conversion efficiency of about 12 %. Due to the reflectivity of the output coupler the first anti-Stokes at 958 nm wavelength is observed.

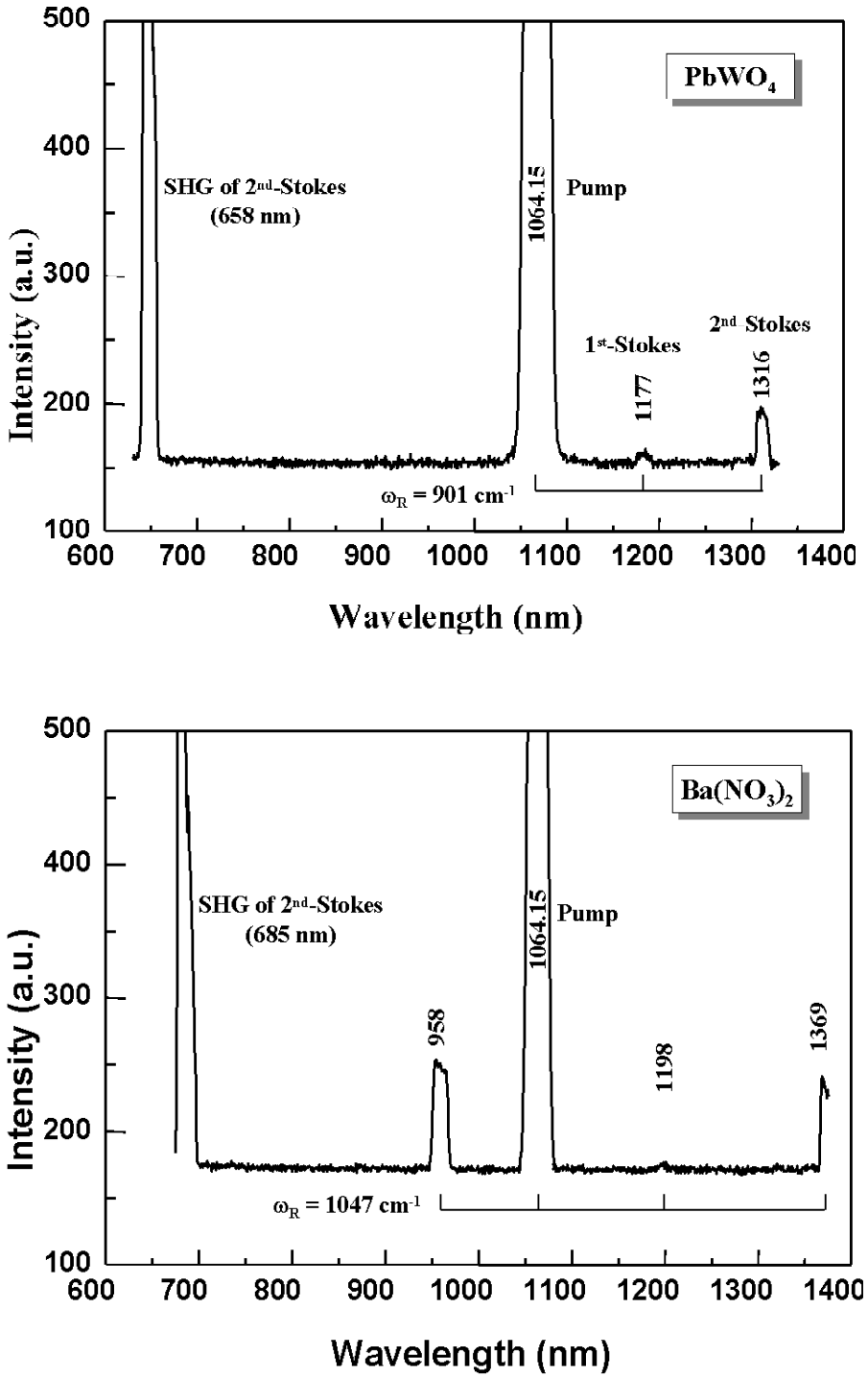

Fig. 5.5:
Second-Stokes Raman laser spectrum and its second harmonic emission in the visible in $PbWO_4$ and $Ba(NO_3)_2$ crystals. The spectral sensitivity for the two Stokes lines is strongly reduced.

Table 5.2 illustrates the maximum output energy of the second-Stokes Raman line and the energy of the corresponding SHG of the tetragonal $PbWO_4$ and $Ba(NO_3)_2$ crystals. In addition, the maximum conversion efficiency of the second-Stokes $PbWO_4$ and $Ba(NO_3)_2$ lines are listed. Doubling the Raman line from 1064 nm efficiently converts Nd:YAG laser radiation to the red spectral region. Furthermore, first and higher order-Stokes stimulated Raman scattering pumped at 532 nm covers the green and yellow spectral regions.

Table 5.2: *Investigated Raman active crystals for second-Stokes Raman lasers. E_{out} is the maximum output energy of the second-Stokes line, η is the conversion efficiency of this line and E_{out} (SHG) is the output energy of the SHG of the second-Stokes line.*

Crystal	Size [mm]	E_{out} [mJ]	η (%)	E_{out} [mJ] (SHG)
$PbWO_4$	10x10x100	0.85	35@1316.6 nm	0.08
$Ba(NO_3)_2$	10x10x70	2	21@1369 nm	0.22

5.4 Spatial emission of 2nd-Stokes $PbWO_4$ Raman laser

The spatial-beam profile of the second-Stokes $PbWO_4$ laser at 1316.6 nm wavelength is recorded using by a Si-CCD array-camera (EHD Kam07CL). In addition, a lens with focal length *f = 100* mm is positioned behind the output coupler. A mirror with optimized reflectivities is used to suppress the fundamental and first Stokes lines. Fig. 5.6a,b show the beam-profile of the Raman line. The beam-profile which is fitted with a Gaussian function is shown in Fig.5.6a. The output-beam shape was always near-Gaussian. Furthermore, it is observed that the quality of the second-Stokes beam, expressed by M^2, is often roughly the same as the M^2 of the pump beam [5-11].

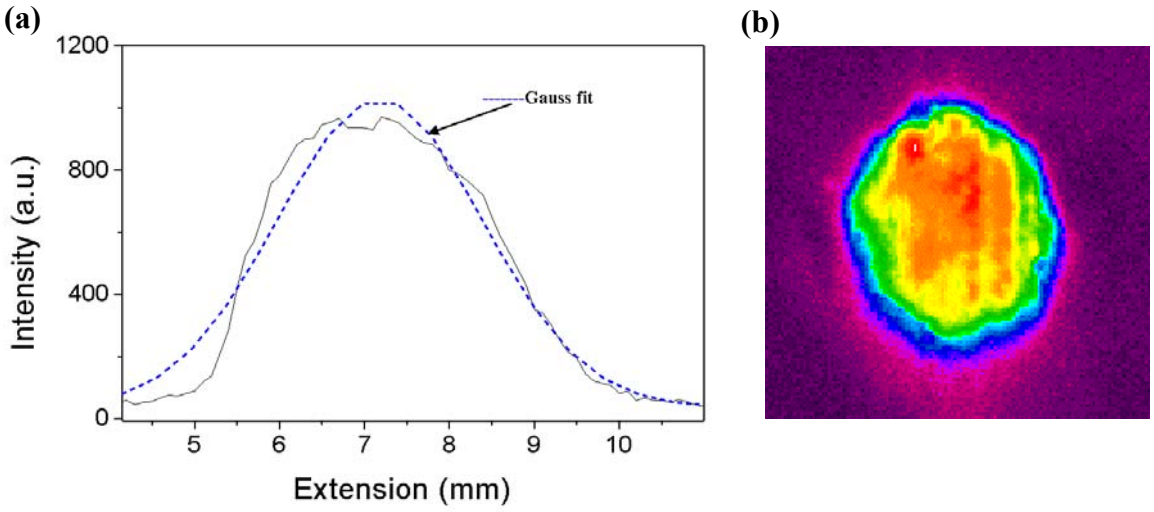

Fig. 5.6a,b: *Beam profile of second-Stokes $PbWO_4$ Raman laser.*

The radius of the second-Stokes line after the lens is measured as discussed in chapter 3. From Fig. 5.6a we can calculate the extension at two positions, one at 16 % of the total output energy and the second at 84 %. The difference between them gives the radius of the Raman line after the lens. By applying equation 3.15, we calculate the real waist radius of the second-Stokes $PbWO_4$ Raman laser behind the output-coupler. The pump beam diameter was 2.54 mm, while the second-Stokes generated output beam diameter was 2.2 mm. The quality of the generated Stokes beam will depend on the quality of the pump beam [5-12]. In addition, for many applications a good beam quality is essential.

5.5 Temporal profile

The pulse emitted by the resonator is measured with a Si-photodiode and an oscilloscope (Tektronix 7104). Single pulse with pulse duration $\tau_p = 120\ ps$ was used to generate SRS by the circulating pump pulse in the external resonator. The pump pulse duration is much longer than the Raman transition response time T_R, i.e. laser activity is generated in the steady-state limit $T_R << \tau_p$. The cavity round-trip-time τ_e is calculated using the relation:

$$\tau_e = \frac{2[l_r + (n-1)L]}{c} \qquad (4.3.1)$$

Where $l_r = 200\ mm$ the resonator length and L and n are the length and the refractive index of the Raman active crystal, respectively. The calculated cavity round-trip-time τ_e of the second-Stokes Raman laser based on $PbWO_4$ and $Ba(NO_3)_2$ crystals are listed in Table 5.3.

Table 5.3: *Cavity round-trip-time τ_e, relaxation time T_R, length L and the refractive index n of $PbWO_4$ and $Ba(NO_3)_2$ crystals.*

Crystal	*λ_{S2} (nm)*	*T_R (ns)*	*n*	*L (mm)*	*τ_e (ns)*
$PbWO_4$	1316.6	2.5	2.15	100	2
$Ba(NO_3)_2$	1369	18	1.6	70	1.61

Fig. 5.7 shows the time distribution of the second-Stokes $PbWO_4$ Raman line generated in an external cavity arrangement. The Raman line is observed with total duration of τ = 17.7 ns. The cavity round-trip-time τ_e of the Raman laser emission is about 2 ns so that about 9 round-trips

take place before laser action stops. The double peak of the start of laser emission is believed to be due to SRS in the two opposite directions of the crystal which causes a delay of about 1 ns. The time dependence of the second-Stokes $Ba(NO_3)_2$ Raman laser emission is shown in Fig. 5.7. The laser emission in the external cavity generates a Raman pulses with time separation of 0.83 ns. The total duration of the emitted Raman pulses is 9.76 ns. Then, about 12 Raman pulses will emit, corresponding to the external Raman resonator arrangement.

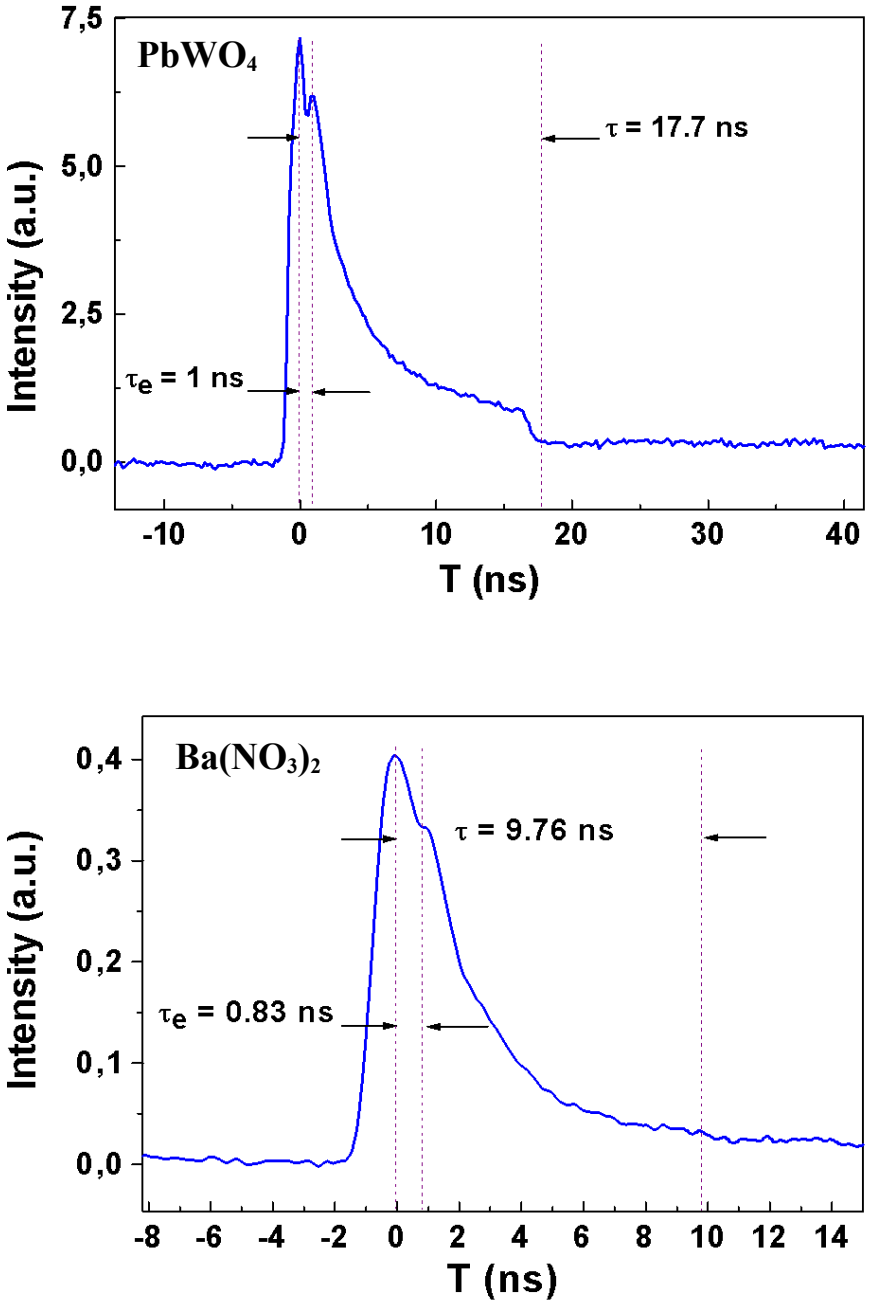

Fig. 5.7:

Time resolved SRS laser emission and single excitation pulse in $PbWO_4$ and $Ba(NO_3)_2$ crystals.

6 First-anti-Stokes $Ba(NO_3)_2$ Raman laser

Raman Stokes shifting of laser light has been studied extensively in many crystals [1-7]-[1-13], [4-8, 4-15] and [5-5]-[5-7]. By contrast, the anti-Stokes Raman process has received relatively little attention as a method of frequency conversion. The most important reason for this neglect is that the conversion efficiency of anti-Stokes is low. A well-known technique for shifting a laser beam to shorter wavelengths makes use of the anti-Stokes-shifted light produced when the pump beam is focused into a Raman active medium (single pass-SRS) [6-1]-[6-4]. This technique has the advantage that even low-power laser sources may be used, since high intensity are attainable in a tightly focused spot. However, it has the disadvantages that the distribution of energy into the various anti-Stokes and Stokes orders is not easily controlled. Furthermore, the anti-Stokes beam comes out in the form of rings and it is not scalable to arbitrarily high energies. In addition, this technique produces a beam that is generally not suitable for propagating more than a few meters and hence is inappropriate for many laser applications. Hence, this technique is most commonly used in low-power applications for which high conversion efficiency is not essential, such as coherent anti-Stokes Raman spectroscopy.

First anti-Stokes-shifted light in hydrogen has been generated by using collimated pump and first Stokes seed beams, slightly crossed within a Raman active medium [6-5]-[6-7]. In this technique, the highest demonstrated conversion efficiency in H_2 is 10 % [6-5, 6-6], while typical efficiencies are near 1 % [6-1, 6-4]. The advantages of this technique are that the generated anti-Stokes beam is energy scalable and suitable for propagating over long distances. The disadvantages of this technique are that, the total long of the cell more than 2500 mm and high-quality pump and first-Stokes beams should be used. Furthermore, up to three cells and a lot of optical components are used to generate the first-anti-Stokes laser.

Compact, efficient, energy scalable, suitable for propagating over long distances and easy alignment first-anti-Stokes Raman laser in solids can be generated by using multi-passes SRS. The active Raman crystal is positioned between two mirrors as a Raman resonator. This technique can be used as an efficient method of up-converting useful, high-intensity laser light.
In this chapter, single-pass SRS under nanosecond Nd:YAG laser excitation is investigated. Furthermore, first-anti-Stokes $Ba(NO_3)_2$ Raman laser with maximum conversion efficiency up to 4.7 % has been demonstrated.

6.1 Investigated crystal

For demonstration of an anti-Stokes Raman laser we use a cubic Barium nitrate $Ba(NO_3)_2$ crystal. $Ba(NO_3)_2$ crystal is one of the promising solid-state Raman materials. It possesses a strong Raman mode with frequency of about 1047 cm^{-1}. The investigated crystal is polished with plane-parallel end faces and has 35 mm length and a cross-section of 7 x 7 mm^2 without antireflection coatings.

6.2 Experimental set-up and results

Single-pass stimulated Raman scattering

For SRS-experiment we use nanosecond Nd:YAG laser at a wavelength of 1064 nm, a pulse duration of 8-9 ns (FWHM) and energy up to 275 mJ. The pump beam is focussed into the sample of $Ba(NO_3)_2$ with a lens f_1 = 100 mm. The second lens with focal length f_2 =100 mm collects the scattered beam from the crystal and focuses it into the spectrometer. The spectral composition of the generated Stokes and anti-Stokes lines is investigated with a grating monochromator and Si-CCD sensor (see Fig. 6.1a). Fig. 6.2 shows the generated Stokes and anti-Stokes components connected with a Raman shift of 1047 cm^{-1}. Because of a drop in the CCD-sensitivity, the intensity of the Stokes line is strongly reduced compared with the intensities of the anti-Stokes lines. The first-anti-Stokes line at 957 nm wavelength is selected using two mirrors F1 and F2 with characteristics listed in Table 6.1. The energy of the first anti-Stokes line is measured by an energy-meter (Rj-7200). In this arrangement we obtained a first-anti-Stokes energy of more than 1.8 mJ for $Ba(NO_3)_2$ crystal. Maximum conversion efficiency of 1.5 % with single-pass SRS is observed. Emission took place in form of a cone with an angle of 1.1°.

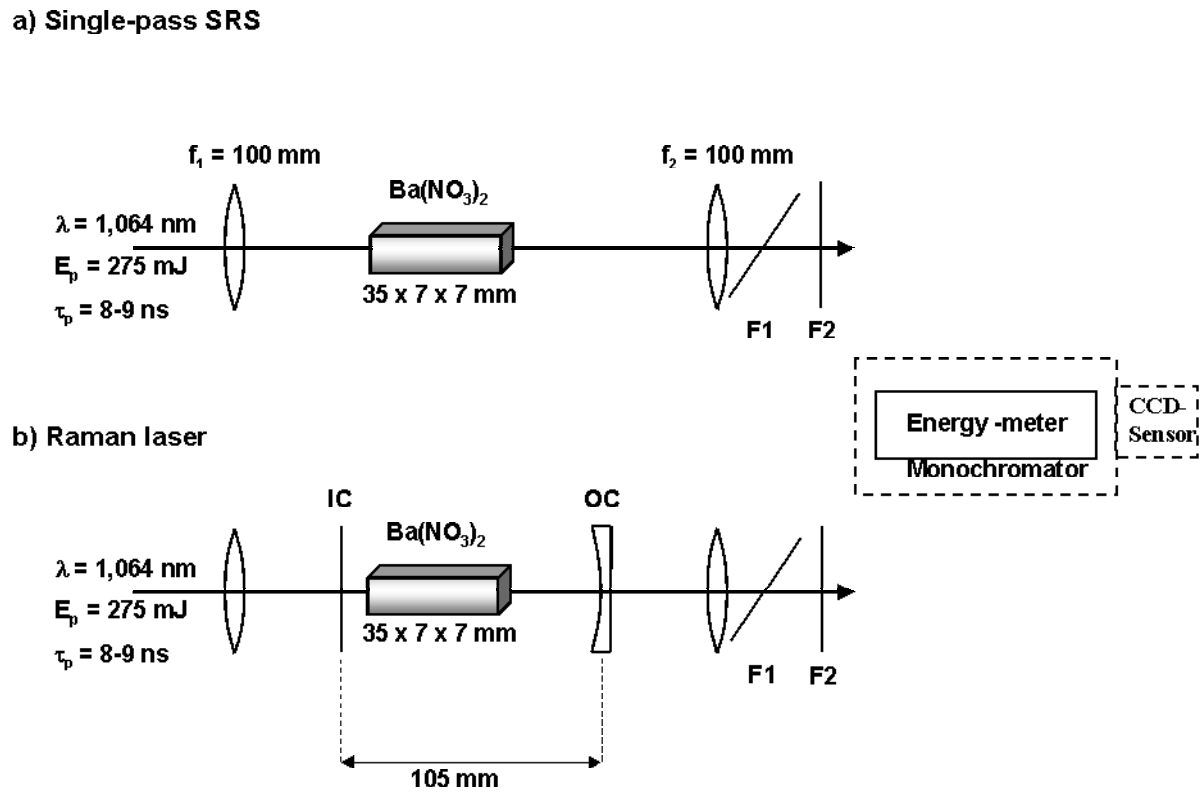

Fig. 6.1: *Experimental set-up for a) single-pass stimulated Raman scattering, b) first anti-Stokes Raman laser in $Ba(NO_3)_2$ single crystal.*

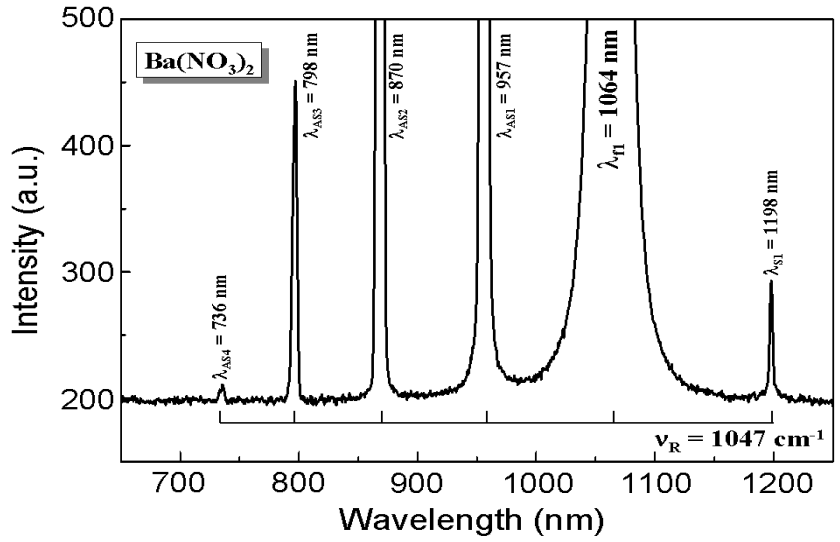

Fig. 6.2:

Single-pass stimulated Raman spectrum of $Ba(NO_3)_2$ single crystal with Raman shift of $\nu_R = 1047\ cm^{-1}$.

Table 6.1: *Transmissions for input-coupler (IC), output-coupler (OC), mirror F1 and mirror F2 for selected wavelengths.*

Mirror name	Incident angle [°]	Transmission at selected wavelengths [%]				
		870 nm	957 nm	1064 nm	1198 nm	1369 nm
IC	0		HR	HT		
OC	0	90	73	3	95	96
F1	0	80.3	68.0	0.22	0.22	89.6
F2	35	0.27	94.3	65.4	3.65	5.15

First-anti-Stokes Raman laser

To build-up a first anti-Stokes $Ba(NO_3)_2$ Raman laser, a 105-mm long plano-concave cavity was placed around the Raman crystal. Optical characteristics of the used cavity mirrors are shown in Table 6.1. The output coupler OC has HR for the pump beam, HT for the second-anti-Stokes line and for the first and second Stokes lines and 73 % transmission for the first-anti-Stokes line. The characteristics of the OC is shown in Fig. 6.3. This external Raman cavity is optimized to yield maximal output energy at the first-anti-Stokes wavelength at 957 nm by choosing the output coupler and by adjusting the mirrors distance and the barium nitrate crystal position. The optimization has shown that it is favorable to provide lower feedback to the higher order anti-Stokes radiation. The best performance is accomplished in a 105 mm long cavity with the barium nitrate crystal placed near from the input mirror as seen in Fig. 6.1. Nd:YAG laser pumping at 1064 nm wavelength with about 8-9 ns pulse duration and up to 275 mJ energy is used.

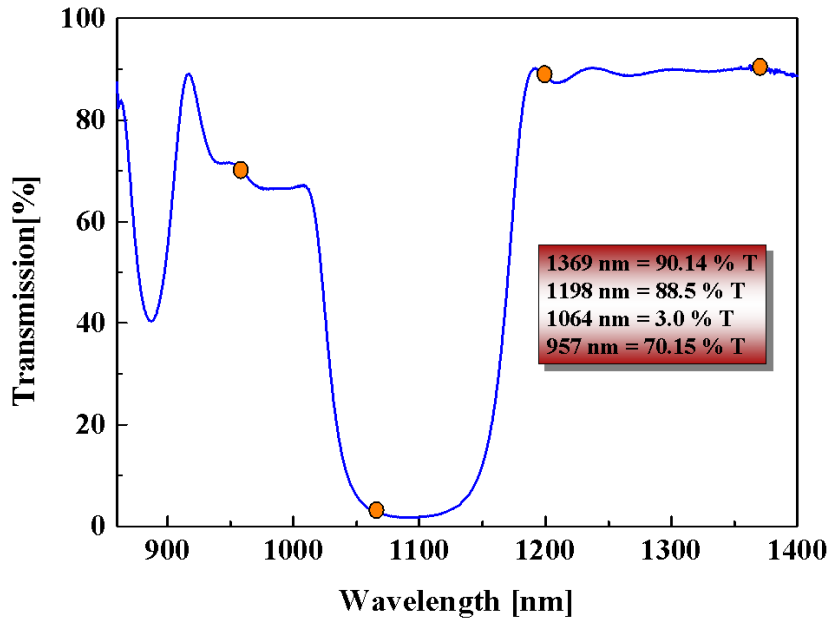

Fig. 6.3: *Transmission characteristics of the output-coupler of the first-anti-Stokes $Ba(NO_3)_2$ Raman laser at λ_{AS1} = 957 nm wavelength.*

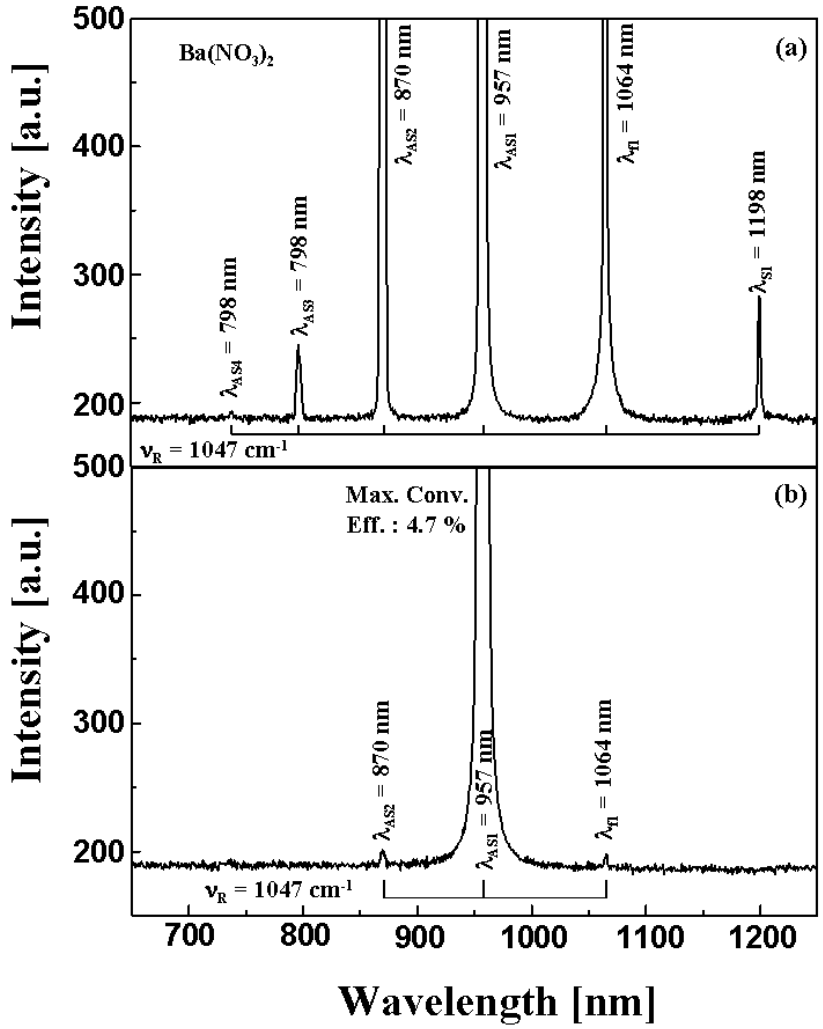

Fig. 6.4:
The generated spectrum a) and selected Raman emission b) of $Ba(NO_3)_2$ in external cavity with phonon interaction at $\nu_R = 1047\ cm^{-1}$.

In the beginning, the first-Stokes line with λ_{S1} = 1198 nm is created. Increasing the pump energy, the higher order Stokes lines and anti-Stokes lines are generated by parametric four-wave-mixing in the Raman active crystal. First-Stokes, pump beam and up to the fourth anti-Stokes lines are shown in Fig. 6.4a. Since the cavity mirrors are chosen for the first-anti-Stokes line at 957 nm wavelength, this line is amplified in the Raman cavity. Then, during further passes of the first-anti-Stokes, the pump emission is considerably reduced and the energy of the outcoming Raman pulses therefore decreases. Fig. 6.4b shows the generated first anti-Stokes $Ba(NO_3)_2$ Raman laser emission at 957 nm wavelength selected with mirrors F1 and F2. Since the mirrors F1 and F2 have high transmission for the first-anti-Stokes and high reflectivity for the other lines, the fundamental and the second-anti-Stokes are hardly observed and the other lines are totally omitted. The output energy of the first-Stokes Raman laser behind the mirrors F1 and F2 is measured with energy meter (laser Precision Rj-7200). In Fig. 6.5 we see the output energy of

the first anti-Stokes line versus input energy. We observed maximum output energy of 5.5 mJ at 120 mJ pump energy. The conversion efficiency against the input energy is shown in Fig. 6.5. Maximum conversion efficiency (output energy of the first-anti-Stokes / input energy of the pump beam) of 4.7 % is obtained. In comparison with single-pass SRS the maximum conversion efficiency is 3 times higher with a resonator.

Longer crystals with anti-reflection coating are expected to increase the conversion efficiency of the first anti-Stokes $Ba(NO_3)_2$ Raman laser.

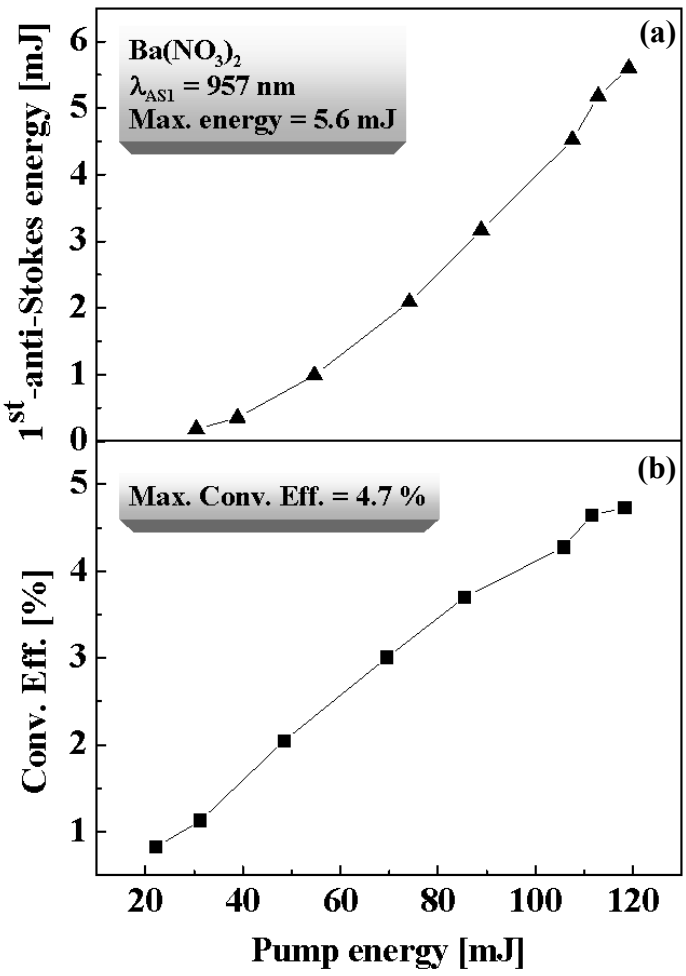

Fig. 6.5: *dependence of a) first-anti-Stokes energy and b) conversion efficiency on the pump energy for $Ba(NO_3)_2$ Raman crystal.*

6.3 Temporal profile

The time dependence of the Q-switch Nd:YAG pump radiation is shown in Fig. 6.6. The temporal distribution of this radiation was measured with a Si-photodiode (Siemens BPX 65) and

an oscilloscope (Tektronix TDS 680B). Fig. 6.6. shows the pulse train emitted by the master oscillator of the Nd:YAG laser. More than 40 pulses were emitted with a time separation given by a round-trip time of 4.9 ns. The total duration of the 40 emitted pulses was 195.5 ns. Single-pulse of pump radiation with 8-9 ns pulse duration (FWHM) and the time distribution of the first-anti-Stokes $Ba(NO_3)_2$ Raman laser at λ_{AS1} = 957 nm wavelength could not be resolved with the available photodiode. Pulse-train of first-anti-Stokes Raman laser with time separation of 0.8 ns corresponding to the Raman cavity with 105 mm length and 35 mm crystal length is expected.

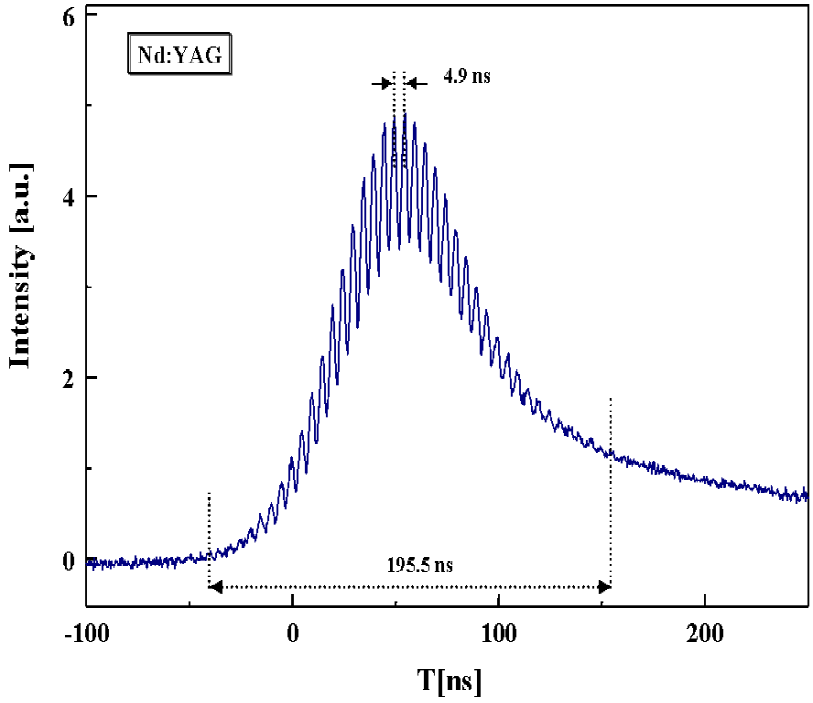

Fig. 6.6:
Pulse train of Nd:YAG laser at λ_{fl} = 1064.15 nm.

7. Conclusions and outlook

The goals of the thesis are verified. New materials for SRS experiment were discovered. Raman lasers with wavelength longer or shorter than the pump have been demonstrated.

Stimulated Raman scattering

single-pass SRS

First, about 18 crystals have been shown to exhibit SRS on about 401 lines covering the whole visible and near-infrared spectrum. The range of the observed Stokes and anti-Stokes lines are between 421 nm and 1369 nm. The range of observed lines are listed in Table 7.1.

Table 7.1: *List of observed Stokes and anti-Stokes lines. More details about these wavelengths are listed in Table 4.5.*

Wavelength (nm)	Line	Crystal
421	AS	$KAl(SO_4)_2 \cdot 12H_2O$
27 lines (Blue)		
503	AS	BiB_3O_6
504	AS	$Ba(NO_3)_2$
174 lines (Green & Red)		
771	AS	YVO_4
772	AS	$Bi_4Ge_3O_{12}$
773	AS	$GdVO_4$

Wavelength (nm)	Line	Crystal
774	AS	$CaMoO_4:Nd^{3+}$
102 lines (Near-IR)		
951	S	$Y_3Al_5O_{12}$
953	S	$Bi_4Ge_3O_{12}$
956	S	$Ca(NO_3)_2/KNO_3$
957	S	$Ba(NO_3)_2$
80 lines (Near-IR)		
1,369	S	$Ba(NO_3)_2$

We have discovered the new χ_3 nonlinear properties of the $Y_3Al_5O_{12}$-based crystalline materials that are most popular in laser physics and excited the multi-frequency SRS by picosecond pumping. In spite of the relatively low Raman gain in these materials, one should consider this phenomena as a possible stray effect when developing laser for generating ultrashort pulses. At the same time, the observed SRS seems to be intense enough for developing new SRS laser in themselves.

We have discovered the new χ_3 nonlinear properties for tetragonal YVO_4 and $GdVO_4$ crystals as efficient Raman laser converter in the visible and near-IR. We also believe that the doped vanadates YVO_4 :Nd^{3+} and $GdVO_4$:Nd^{3+}, are promising for use as self-SRS laser media.

High-order multi-phonon stimulated Raman scattering was excited under picosecond pumping in the visible and near-IR on the Stokes and anti-Stokes lines of $C_{13}H_{10}O$ and α-$C_{14}H_{12}O$ single crystals. Both crystals offer largest known Raman frequency shifts of ν_{R3} = 3070 and ν_{R3} = 3065 cm^{-1} among other SRS-active solids crystalline materials.

New efficient shifter e.g. BiB_3O_6, $Bi_4Ge_3O_{12}$, $Bi_4Si_3O_{12}$, AANP, $C_{13}H_{10}O$, GuZN-III and 4′-Nitrobenzylidene-3-Acetamino-4-Methoxyaniline crystals were investigated. They combine SRS and SHG nonlinear frequency conversion in the same crystal and allow to efficiently shift the Nd:YAG laser emission to discrete lines in the visible.

Self-SHG is observed in a $C_{16}H_{15}N_3O_4$ crystal, SHG of the first (λ_{S1} = 1280.4 nm) and second (λ_{S2} = 1606.9 nm) Stokes lines generate λ_{SHG} = 640.2 nm and λ_{SHG} = 803.4 nm, respectively. This is the first observation of the self-SHG effect in organic single crystals.

Raman lasers

Raman laser increase the conversion of stimulated Raman scattering and can be constructed to emit in a single Raman line by wavelength selected through specially chosen cavity mirrors.

Second-Stokes Raman lasers

New solid-state lasers in the visible between 650 nm and 685 nm are available with $PbWO_4$ and $Ba(NO_3)_2$ crystals. Raman Stokes lines in IR at 1316.6 and 1369 nm are converted to the visible spectral region with KD*P frequency doubling conserving the good Stokes beam quality. Near-IR second-Stokes Raman laser based on $PbWO_4$ single crystal at wavelength 1316.6 nm was achieved for the first time. The second-Stokes Raman lasers with $PbWO_4$ and $Ba(NO_3)_2$ crystals are observed with energies 0.85 mJ and 2 mJ, respectively. Maximum conversion efficiency up to 35 % is observed with $PbWO_4$ crystal with 100 mm length and 21 % with $Ba(NO_3)_2$ with 35 mm crystal length. Dependence of the conversion efficiency on the $PbWO_4$ crystal with length

40-100 mm has been studied. The spatial beam profile for the second-Stokes $PbWO_4$ Raman laser was observed. The temporal emissions of the Raman laser emission with $PbWO_4$ and $Ba(NO_3)_2$ crystals were listed for 18 and 10 ns, respectively.

First-anti-Stokes Raman laser

Finally, first-anti-Stokes Raman solid state laser based on $Ba(NO_3)_2$ crystal with 957 nm wavelength has been demonstrated for the first time. The crystal was pumped by an 8-9 ns Nd-YAG laser at 1064 nm wavelength. The maximum output energy of the Raman emission was 5.5 mJ. Up to 4.7 % conversion efficiency has been observed with crystal length of 35 mm. Previous efficient anti-Stokes Raman generation was investigated in oscillator-amplifier experiment [6-5]-[6-7]. In comparison with these experiments our laser arrangement is more simple and thus more stable.

Outlook

Investigation of new Raman materials for frequency conversion processes in particular, stimulated Raman scattering is still of interest to create new coherent light sources and extend the number of currently available emission wavelengths. New Raman lasers with wavelengths shorter or longer than the pump and convert into ultra violet, yellow and red spectral regions are important for many application in spectroscopy e.g. detecting water vapour pollutants in the atmosphere by lidar techniques. Raman lasers generate coherent radiation at many wavelengths not directly available by the traditional solid-state lasers. This gives an opportunity for the future use in various applications.

8 Literature

Chapter 1-:

[1-1] **R. C. Powell, J. T. Murray, W. L. Austin, T. T. Basiev, P. G. Zverev,** *Solid state Raman lasers: materials, design and application*, **Proc. of the SPIE-The International Society for optical Engineering 3572,** 45-49 (1999).

[1-2] **E. J. Woodbury, W. K. Ng, Proc. IRE 50,** 2367 (1962).

[1-3] **W. Kaiser, M. Maier,** *Laser handbook*, **Eds. F. T. Arrecchi, E. O. Schultz-Dubo (N.-Holland, Amsterdam) 2,** 1077 (1972).

[1-4] **Y. R. Shen,** *Light scattering in solids 1*, **Ed. M. Cardona (Springer, Berlin),** 275 (1983).

[1-5] **G. Eckhardt,** *Selection of Raman laser materials*, **IEEE J. Quant. Electron. 2,** 1 (1966).

[1-6] **G. Eckhardt, D. P. Bortfeld, M. Geller,** *Stimulated emission of Stokes and anti-Stokes Raman lines from diamond, calcite and α-sulfur single crystals*, **Appl. Phys. Lett. 3,** 137 (1963).

[1-7] **S. N. Karpukhin, A. I. Stepanov,** *Generation of radiation in a resonator under conditions of stimulated Raman scattering in $Ba(NO_3)_2$, $NaNO_3$, and $CaCO_3$ crystals*, **Sov. J. Quantum Electron. 16,** 1027-131 (1986).

[1-8] **C. He, T.H. Chyba,** *Solid-state barium nitrate in the visible region*, **Opt. Comm. 135,** 273-278 (1997).

[1-9] **J.T. Murray, R.C. Powell, N. Peyghambarian, D. Smith, W. Austin, R. Stolzenberger,** *Generation of 1.5-μm radiation through intracavity solid-state Raman shifting in $Ba(NO_3)_2$ nonlinear crystals*, **Opt. Lett. 20,** 1017 (1995).

[1-10] **P.G. Zverev, T.T. Basive, Pro. On Advaced Solid-State laser, 24,** 288 (1995).

[1-11] **J. Findeisen, H.J. Eichler, P. Peuser,** *Self-stimulating, transversally diode pumped Nd^{3+}: $KGd(WO_4)_2$ Raman laser*, **Opt. Commun. 181,** 129-133 (2000).

[1-12] **A. V. Gulin, G. I. Narkhova, N. S. Ustimenko,** *Multiwave generation of the Stokes components in laser with an SRS self-converter based on Nd^{3+}: $KGd(WO_4)_2$ crystal*, **Quant. Electron. 28,** 804-805 (1998).

[1-13] **W. Chen; Y. Inagawa, T. Omatsu, M. Tateda,** *Diode-pumped, self-stimulating, passively Q-switched Nd^{3+}:$PbWO_4$ Raman laser*, **Opt. Comm. 194,** 401-407 (2001).

[1-14] **J.T. Murray, R.C. Powell, N. Peyghambarian,** *Properties of stimulated Raman*

scattering in crystals, **J. Lumin. 66-67,** 89 (1996).

[1-15] **H. P. Pask, A. Piper,** *Practical 580 nm source based on frequency doubling of an intracavity-Raman-shifted Nd:YAG laser*, **Opt. Commun. 148,** 285-288 (1998).

[1-16] **J. T. Murray, R. C. Powell, W. L. Austin, W. T. Roberts, J. Roger, P. Angel, C. T. Shelton, D. G. Sandler,** *in Proc. of the workshop on laser technology for laser guide star adaptive optics astronomy*, **Garching, Germany,** 356-365 (1997).

[1-17] **E.M. Dianov, A.A. Abrramov, M.M. Bubnov, A.M. Prokhorov, A.V. Shipulin, G.G. Devjatykh, A.N. Guryanov, V.F. Khopin,** *30 dB gain Raman amplifier at 1.3 μm in low loss high GeO_2 doped silica fibers,* **Electron. Lett., 31,** 1057 (1995).

[1-18] **T.N. Nielsen, A.J. Stentz, K. Rottwitt, D.S. Vengsarkar, Z.J. Chen, P.B. Hansen, J.H. Park, K.S. Feder, S. Cabot, S. Stulz, D.W. Peckham, L. Hsu, C.K. Kan, A.F. Judy, S.Y. Park, L.E. Nelson, L. Gruner-Nielsen,** *3.283Tb/transmission over 3 x 100 km of nonzero-dispersion fiber using dual C- and L-band distributed Raman amplification*, **IEEE Photon. Technol. Lett. 12,** 1075 (2000).

[1-19] **N. Takachio, H. Suzuki,** *Application of Raman-distributed amplification to WDM transmission system using 1.55 μm dispersion-shifted fiber*, **J. Lightwave Technol. 19,** 60 (2001).

[1-20] **R. H. Stolen, J. E. Bjorkholm, A. Ashkin,** *Phase-matched three-wave mixing in silica fiber optical waveguides*, **Appl. Phys. Lett. 24,** 308 (1974).

[1-21] **A.A. Kaminskii, H.J. Eichler, K. Ueda, N.V. Klassen, B.S. Redkin, Li LE, J. Findeisen, D. Jaque, J. Garcia-Sole, J. Fernandez, R. Balda,** *Properties of Nd^{3+}-doped and undoped tetragonal $PbWO_4$, $NaY(WO_4)_2$, $CaWO_4$, and undoped monoclinic $ZnWO_4$ and $CdWO_4$ as laser-active and stimulated Raman scattering-active crystals*, **Appl. Opt. 38,** 4533 (1999).

[1-22] **P. Cerny, P.G. Zverev, H. Jelinkova, T.T. Basiev,** *Efficient Raman shifting of picosecond pulses using $BaWO_4$ crystal*, **Opt. Commun. 177,** 397 (2000).

[1-23] **K. Andryunas, Y. Vishakas, V. Kobelka, I. V. Mochalov, A. A. Pavlyuk, G. T. Petrovskii, V. Syrus, JETP Lett. 42,** 333 (1985).

[1-24] **A.A. Kaminskii, H. J. Eichler, D. Grebe, R. Macdonald, S. N. Bagaev, A.A.Pavlyuk ,F.A. Kuznetsov,** *High-efficient stimulated-Raman scattering in ferroelectric and ferroelastic orthorhombic Gd-2(MoO_4)(3) crystals* **Phys. Stat. Solidi A 153,** 281 (1996).

[1-25] **A. A Kaminskii, S. N. Bagayev, K. Ueda, H. J. Eichler, J. Garcia-Sole, D. Jaque, J.**

J. Romero, J. Fernandez, R. Balda, A. V. Butashin, Agullo-Rueda, *Multiple Stokes and anti-Stokes picosecond generation, cw laser action at wavelengths of two stimulated-emission channels F-4(3/2) -> I-4(11/2) and F-4(3/2) -> I-4(13/2), and nanosecond self-SRS lasing in undoped and Nd^{3+}-doped tetragonal $PbMoO_4$ crystals*, **Laser Physics 11,** 1142-1146 (2001).

[1-26] **A. A Kaminskii, H. J. Eichler, D. Grebe, R. MacDonald, A. V. Butashin, S. N. Bagaev, A. A. Pavlyuk,** *New optical effects in acentric $LaBGeO_5$ and β-Gd-2(MoO_4)(3) laser crystal hosts having high $\chi^{(2)}$ and $\chi^{(3)}$ nonlinear susceptibilities* **Phys. Stat. Solidi B 198,** K9-K12 (1996).

[1-27] **A. A Kaminskii, , S. N. Bagaev, A. M. Yurkin, A. E. Kokh, H. Eichler, J. Findeisen**, *New nonlinear laser effects in $\chi^{(2)}$ + $\chi^{(3)}$-active β-BaB_2O_4 crystal*, **Doklady Akademii NAUK 367,** 468-474 (1999).

[1-28] **M. Klein**, M. **Maier,** G*iant Raman optical-activity of the 128-cm^{-1} mode in α-quartz*, **Opt. Commun. 44,** 411-414 (1983).

[1-29] **A. A Kaminskii, S. N. Bagaev, J. G. Sole, H. J. Eichler, J. Fernandez, D. Jaque , J. Findeisen, R. Balda, F. A. Rueda,** *First observations of stimulated emission and of stimulated Raman scattering in acentric cubic Nd^{3+}:$Bi_{12}SiO_{20}$ crystals*, **Quantum Electron. 29,** 6-8 (1999).

[1-30] **E. O. Ammann, C. D. Decker,** *0.9-w Raman oscillator*, **J. App. Phys. 48,** 1973-1975 (1977).

[1-31] **G. G. Grigoryan, S. B. Sogomonyan,** *A synchronously pumped SRS laser emitting picosecond light-pulses from a $LiIO_3$ crystal*, **Kvantovaya Elektronika 16,** 2180-2183 (1989).

[1-32] **J. Gelbwach, R. H. Pantel, H. E. Puthoff, J. M. Yarborou,** A *tunable stimulated Raman oscillator*, **App. Phys. Lett.**

[1-33] **A. S. Eremenko, S. N. Karpukhin, A. I. Stepanov,** *Stimulated Raman scattering of the second harmonic of a neodymium laser in nitrate crystals*, **Sov. J. Quantum Electron. 10,** 113-114 (1980).

[1-34] **S. N. Karpukhin, V.E. Yashin, Sov. J. Quantum Electron. 14,** 1337 (1984).

[1-35] **P. G. Zverev, J. T. Murray, R. C. Powell, R. J. Reeves,** *Stimulated Raman scattering of picosecond pulses in barium nitrate crystals*, **Opt. Commun. 97,** 59-64 (1993).

[1-36] **A. A Kaminskii, S. N. Bagaev, J. Hulliger, H. Eichler, J. Findeisen, R. Macdonald,** *Acentric cubic $NaClO_3$ - a new crystal for Raman lasers*, **App. Phys. B 67,** 157-162

(1998).

[1-37] **A. A Kaminskii, H. J. Eichler, J. Findeisen, C. Barta,** *Room-temperature high-order stimulated Raman scattering and stimulated emission in ultra-low-phonon energy orthorhombic $PbCl_2 : Nd^{3+}$ crystal*, **Phys. Stat. Solidi B 206,** R3-R4 (1998).

[1-38] **P. Franz, P. Egger, J. Hulliger, J. Findeisen, A.A. Kaminskii, H.J. Eichler,** *Observation of stimulated Raman scattering in orthorhombic Na_2SO_4 and cubic $NaBrO_3$ at 300 K under picosecond excitation*, **Phys. Stat. Solidi B, 210** (1998) R7.

[1-39] **A.A. Kaminskii, H.J. Eichler, D. Grebe, R. Macdonald, A.V. Butashin,** *Stimulated Raman scattering in α-Al_2O_3 leucosapphire single crystals at room temperature*, **Phys. Stat. Solidi B 199,** R3 (1997).

[1-40] **A. A. Kaminskii,** *in Raman scattering-70 years of the research* **(Ed: V. I. Gorelik), Lebedev Physical Institute, Moscow,** 206-212 (1998).

Chapter 2-:

[2-1] **P.G. Harper, B.S. Wherrett,** *Nonlinear optics*, **Academic Press** (1977).

[2-2] **P.A. Franken, A.E. Hill, C.W. Peters, G. Weinreich,** *Generation of optical harmonics*, **Phys. Rev. Lett. 7,** 118-119 (1961).

[2-3] **J.A. Giordmaine, R.C. Miller,** *Tunable coherent parametric oscillation in LiNbO3 at optical frequencies*, **Phys. Rev. Lett. 14,** 973-976 (1965).

[2-4] **C.C. Wang, G.W. Racette,** *Measurement of parametric gain accompanying optical difference frequency generation*, **Appl. Phys. Lett. 6,** 169 (1965).

[2-5] **R.W. Terhune, P.D. Maker, C.M. Savage,** *Optical harmonic generation in calcite*, **Phys. Rev. Lett. 8,** 404-406 (1962).

[2-6] **G. Eckhardt, R.W. Hellwarth, F.J. McClung, S.E. Schwarz, D. Weiner, E.J. Woodbury,** *Stimulated Raman scattering from organic liquids*, **Phys. Rev. Lett. 9,** 455-457 (1962).

[2-7] **R.Y. Chiao, C.H. Townes, B.P. Sticheff,** *Stimulated Raman scattering and coherent generation of intense hypersonic waves*, **Phys. Rev. Lett. 12,** 592 (1964).

[2-8] **D.I. Mash, V.V. Morozo, V.S. Starunov, I.L. Fabelinskii,** *Stimulated scattering of light of Rayleigh-line wing*, **JETP Lett. 2,** 25 (1965).

[2-9] **W.T. Silfvast,** *Laser fundamentals*, **Cambridge University Press** (1996).

[2-10] **E.G. Sauter,** *Nonlinear optics*, **John Wiley and Sons, Inc.** (1996).

[2-11] **Y. Wang,** *Theory of stimulated Raman scattering*, **Phys. Rev. 182,** 482-494 (1969).

[2-12] **Y. R. Shen,** *The principles of nonlinear optics*, **Wiley, New York, 1984.**

[2-13] **P. D. Maker, R. W. Terhune,** *Study of optical effects due to an induced polarization third order in the electric field strength*, **Phys. Rev. (a) 137,** 801-818 (1965).

[2-14] **A. Z. Grasyuk, S. V. Kurbasov, L. L. Losev, A. P. Lutsenko, A. A. Kaminskii, V. B. Semenov,** *Determination of Raman gain coefficient in leucosapphire*, **Quant. Electron. 28,** 162-166 (1998).

[2-15] **T.T. Basiev, A.A. Sobol, P.G. Zverev, V.V. Osiko, R.C. Powell,** *Comparative spontaneous Raman spectroscopy of crystals forv Raman lasers*, **Appl.. Opt. 38,** 594-598.

[2-16] **P.G. Zverev, W. Jia, H. Liu, T.T. Basiev,** *Vibrational dynamic of the Raman-active mode in barium nitrate crystal*, **Opt. Lett. 20** 2378 (1995).

[2-17] **M.H. Brooker, D.E. Irish G.E. Boyd,** *Ionic interactions in crystals-infrared and Raman spectra of powdered* $Ca(NO_3)_2$, $Sr(NO_3)_2$, $Ba(NO_3)_2$, *and* $Pb(NO_3)_2$, **J. Chem. Phys. 53,** 1083 (1970).

Chapter 3-:

[3-1] **M. Glotz, H. J. Eichler,** *Cavity dumping of a mode-locked pulsed Nd:YAG laser*, **J. Phys. E: Sci. Instrum. 20,** 1493-1496 (1987).

[3-2] **N.H. Schiller, M. Foresti, R.R. Alfano,** *Picosecond pulses produced by mode locking a Nd:glass laser with Kodak dye #26*, **J. Opt. Soc. Am. B 2,** 729 (1985).

[3-3] **B. Kopainsky, P. Qiu, W. Kaiser,** *Lifetime, photostability, and chemical structure of IR Heptamethine Cyanine dyes absorbtion beyond 1 μm*, **Appl. Phys. B 29,** 15-18 (1982).

[3-4] **H.J. Eichler, B. Liu,** *Picosecond NdCr:GSGG-laser system with 30 mJ energy*, **Opt. Mater. 1,** 21-25 (1992).

[3-5] **W.T. Silfvast,** *Laser fundamentals*, **Cambridge University Press** (1996).

[3-6] **J. Eichler, H.J. Eichler,** *Laser*, **Springer Verlag Berlin** (1998).

[3-7] **H.J. Eichler, H.-D. Kronfeldt, J. Sahm,** *Das Neue Physikalische Grund-Praktikum*, **Springer Verlag Berlin** (2001).

Chapter 4-:

[4-1] **A.A. Kaminskii, P. Becker, L. Bohaty, K. Ueda, K. Takichi, J. Hanuza, M. Moczka, H.J. Eichler, G.M.A. Gad,** *Monoclinic bismuth triborate* BiB_3O_6 *– a new*

efficient $\chi^{(2)}+\chi^{(3)}$ –nonlinear crystal: multiple stimulated Raman scattering and self-sum-frequency lasing effects, **Opt. Commun. 206,** 179-191 (2002).

[4-2] **A.A. Kaminskii**, **S.N. Bagayev, N.V. Kravtsov, S.N. Chekina, Ya.V. Vasiliev, N.I. Ivannikova, K. Ueda, J. Lu, H.J. Eichler, G.M.A. Gad, J. Hanuza, J. Fernandez, P. Reiche,** *Spectroscopy and cw laser action, magnetooptics and nonlinear optical frequency conversion in Ln^{3+}doped and undoped $Bi_4Ge_3O_{12}$ and $Bi_4Si_3O_{12}$ crystals*, **Laser Spectroscopy 11,** 897-918 (2001).

[4-3] **A.A. Kaminskii**, **K. Ueda, J. Lu, H.J. Eichler, Y. Kuwano, H. Kouta, S.N. Bagaev, T.H. Chyba, J.C. Branes, G.M.A. Gad, T. Murai, J. Lu,** *Tetragonal vanadates YVO_4 and $GdVO_4$-new efficient $\chi^{(3)}$-materials for Raman lasers*, **Opt. Comm. 194,** 201-206 (2001).

[4-4] **G. M. A. Gad, A. A. Kaminskii, H. J. Eichler, J. Pickardt,** *Double sulfate $KAl(SO_4)_2 \cdot 12H_2O$ single crystals (α-alum)-a new material for Raman laser converters*, **Phys. Stat. Sold. (a) 193,** R10-R12 (2002).

[4-5] **A.A. Kaminskii, H.J. Eichler, K. Ueda, P. Reiche, G.M. Gad,** *The first observation of SRS in a trigonal $LiCaAlF_6$ crystal*, **Quant. Electron. 30,** 1035-1036 (2000).

[4-6] **A.A. Kaminskii, H.J. Eichler, K. Ueda, S.N. Bagaev, G.M.A. Gad, J. Lu, T. Murai, H. Yagi, T. Yanagitani,** *Stimulated Raman scattering in $Y_3Al_5O_{12}$ single crystal*, **Phys. Stat. Sol. (a) 181** R19-R21 (2000).

[4-7] **A.A. Kaminskii, H.J. Eichler, K. Ueda, S.N. Bagaev, G.M.A. Gad, J. Lu, T. Murai, H. Yagi, T. Yanagitani,** *Observation of stimulated Raman scattering in $Y_3Al_5O_{12}$ single crystals and nanocrystalline ceramics and in these materials activated with laser ions Nd^{3+} and Yb^{3+}*, **JETP Lett. 72,** 499-502 (2000).

[4-8] **A.A. Kaminskii, C.L. McCray, H.R. Lee, S.W. Lee, D.A. Temple, T.H. Chyba, W.D. Marsh, J.C. Barnes, A.N. Annanenkov, V.D. Legun, H.J. Eichler, G.M.A. Gad, K. Ueda,** *High efficiency nanosecond Raman lasers based on tetragonal $PbWO_4$ crystals*, **Opt. Commun. 183,** 277-287 (2000).

[4-9] **A. A. Kaminskii, H. Klapper, J. Hulliger, H.J. Eichler, J. Hanuza, K. Ueda, K. Takichi, C. Wickleder, G.M.A. Gad, M. Moczka,** *High-order many-phonon stimulated Raman scattering in orthorhombic benzophenone ($C_{13}H_{10}O$) and monoclinic α-4-methylbenzophenone (α-$C_{14}H_{12}O$) crystals*, **Laser Phys. 12,** 1041-1053 (2002).

[4-10] **A.A. Kaminskii, T. Kaino, T. Taima, A. Yokoo, K. Ueda, K. Takichi, J. Hulliger, H.J. Eichler, J. Hanuza, J. Fernandez, R. Balada, M. Moczka, G.M.A. Gad,**

Monocrystalline 2-Adamantylamino-5-Nitropyridine (AANP)- a novel organic material for laser Raman converters in the visible and near-IR, **Jpn. J. Appl. Phys. 41,** 1041-1053 (2002).

[4-11] **A. A. Kaminskii, E. Haussühl, J. Hulliger, K. Ueda, K. Takichi, J. Hanuza, M. Moczka, H. J. Eichler, G. M. A. Gad,** *Bis(Guanidinium) Zirconium bis(Nitrilotriacetate) hydrate, $[C(NH_2)_3]_2Zr[N(CH_2COO)_3]_2{\cdot}H_2O$ - a new crystal for Raman laser converters*, **Phys. Stat. Sol. (a) 193,** 167-178 (2002).

[4-12] **A. A. Kaminskii, J. Hulliger, H. J. Eichler,** *New nonlinear effects in $\chi^{(2)}$ – and $\chi^{(3)}$ - active organic crystals of 4′- nitrobenzylidene-3-acetamino-4-methoxyaniline (MNBA): high-order stimulated Raman scattering, self-frequency doubling, and self-sum frequency mixing*, **Phys. Stat. Sol. (a) 186,** R19-R21 (2001).

[4-13] **R. Burkhalter, B.Trusch, P. Franz, A.A. Kaminskii, H.J. Eichler, J. Hulliger,** *High-order stimulated Raman scattering in χ^3-active molecular glass: $Ca(NO_3)_2$: KNO_3 under picosecond excitation*, **J. Materials Chemistry 11,** 3211-3214 (2001).

[4-14] **R. Burkhalter, B. Trusch, A. A. Kaminskii, G. M. A. Gad, H. J. Eichler, J. Hulliger,** *Frequency conversion in $(NaPO_3)_x$ polyphosphate glass by stimulated Raman scattering*, **Adv. Materials 13,** (2001) 814-816.

[4-15] **G.M.A. Gad, H.J. Eichler, A.A. Kaminskii**, *Highly efficient 1.3 μm second-Stokes $PbWO_4$ Raman laser*, **Opt. Lett. 28,** 426-428 (2003).

[4-16] **W. Koechner,** *Solid-state-laser engineering*, **(Springer-Verlag, Berlin, 1976, 1980, 1991, 2000).**

[4-17] *Handbook of laser science and technology*, **Ed. by M. J. Weber (CRC Press. Boca Raton, 1982, 1991)**

[4-18] **T. Yanagitani, H. Yagi, Y. Hiro, Jpn. Patent No. 10-101411** (1998).

[4-19] **M. Sekita, H. Haneda, T. Yanagitani, S. Shiransaki,** *Induced emission cross section of Nd:$Y_3Al_5O_{12}$ ceramics*, **J. Appl. Phys. 67,** 453-458 (1990).

[4-20] **J. P. Hurrell, S. P. S. Porto, I. F. Chang, S.S. Mitra, R.P. Bauman,** *Optical phonons of Yttrium Aluminum Garnet* **Phys. Rev. 173,** 851 (1968).

[4-21] **D. L. Rousseau, R. P. Baumann, S. P. S. Porto,** *Normal mode determination in crystals*, **J. Raman Spectrosc. 10,** 253-290 (1981).

[4-22] **A. Ikesue, T. Kinoshita,** *Fabrication and optical-properties of high-performance polycrystalline Nd:YAG ceramics for solid-state laser*, **J. Am. Ceram. Soc. 78,** 1033-1040 (1995).

[4-23] **J. Lu, M. Prabhu, J. Song, C. Li, J. Xu, K. Ueda, A.A. Kaminskii, H. Yagi, T. Yanagitani,** *Optical properties and highly efficient laser oscillation of Nd:YAG ceramics*, **Appl. Phys. B 71,** 469-473 (2000).

[4-24] **S.P.S. Porto, J.F. Scott,** *Raman spectra of $CaWO_4$, $SrWO_4$, $CaMoO_4$, and $SrMoO_4$*, **Phys. Rev. 157,** 716 (1967).

[4-25] **M. Stencel, J. Springer, E. Silberman,** *Infrared and Raman multi-phonon spectra and structure of $PbWO_4$,* **J. Mol. Struct. 41,** 11 (1977).

[4-26] **J. Hanuza, M. Maczka, and J.H. van der Mass**, *Vibrational properties of double tungstates of the M^IM^{III} $(WO_4)_2$ family (M^I = Li, Na, K; M^{III} = BI, Cr)*, **J. Solid State Chem. 117,** 177 (1995).

[4-27] **T. Scheffen-Lauenroth, H. Klapper, R. A. Becker,** *Growth and perfection of organic crystals from undercooled melt*, **J. Cryst. Growth 55,** 557-570 (1981).

[4-28] **B. Wyncke, A. Hadni, D. Chanal, E. Decamps,** *Absorption of organic crystals in far IR and external vibrations of molecules*, **Ann. Phys. 2,** 123 (1967).

[4-29] **B. Wyncke, A. Hadni,** *Infrared absorption spectra 80°K of 5 organic crystals belonging to orthorhombic system*, **Spectrochim. Acta A 27,** 1929 (1971).

[4-30] **P. Ranson, P. Peretti, Y. Rousset, J. A. Koningstein,** *Low-frequency Raman spectrum of benzophenone at 300 and 30°K*, **Chem. Phys. Lett. 16,** 396-398 (1972).

[4-31] **H. Hellwig, J. Liebertz, L. Bohaty,** *Linear optical properties of the monoclinic bismuth borate BiB_3O_6,* **J. Appl. Phys. 88,** 240-244 (2000).

[4-32] **P. Becker, C. Wickleder,** *Crystal growth and spectroscopic characterization of $BiB_3O_6:RE^{3+}$ (RE^{3+} = Pr^{3+}, Nd^{3+}, Er^{3+}, Tm^{3+})*, **Cryst. Res. Technol. 36,** 27-37 (2001).

[4-33] **C. A. Morrison, R. P. Leavitt,** *Crystal field analyses of Nd^{3+} and Er^{3+} in $Bi_4Ge_3O_{12}$*, **J. Chem. Phyas. 74,** 25 (1981).

[4-34] **E. Dieguez, L. Arzimendi, J. M. Cabrera,** *X-ray induced luminescence, photoluminescence and thermoluminescence of $Bi_4Ge_3O_{12}$*, **J. Phys. C 18,** 4777-3783 (1985).

[4-35] **D. Bravo, F. J. Lopez,** *An electron paramagnetic resonance study of Er^{3+} in $Bi_4Ge_3O_{12}$ single crystals*, **J. Chem. Phys. 99,** 4952-4959 (1993).

[4-36] **K.S. Bagdasarov, A.A. Kaminskii, V.S. Krylov, V.I. Popov,** *Room-temperature induced emission of tetragonal YVO_4 crystals containing Nd^{3+}*, **Phys. Stat. Sol. 27,** K1 (1968).

[4-37] **J. E. Bernard, A. J. Alcock,** *High-efficiency diode-pumped Nd:YVO_4 slab laser*, **Opt.**

Lett. 18, 968-970 (1993)**.**

[4-38] **D. Shen, A. Liu, J. Song, K. Ueda,** Efficient Operation of an Intracavity-doubled Nd:YVO_4 KTP Laser End Pumped by a High-Brightness Laser Diode**, Appl. Opt. 37,** 7785-7788 (1998)**.**

[4-39] **C.P. Wyss, W. Luthy, H. P. Weber, V. I. Vlasov, Yu. D. Zavartsev, P. A. Studenkin, A. I. Zagumennyi, I. A. Shcherbakov,** *Performance of a Tm^{3+}:$GdVO_4$ microchip laser at 1.9 μm*, **Opt. Commun. 153,** 63-67 (1998)**.**

[4-40] **W. Chen, Y. Inagashige, T. Omatsu, M. Tateda, N. Takeuchi, Y. Usuki,** *Diode-pumped, self-stimulating, passively Q-switched Nd^{3+}:$PbWO_4$ Raman laser*, **Opt. Commun. 194,** 401-407 (2001)**.**

[4-41] **J. R. Lu, K. Ueda, H. Yagi, T. Yanagitani, Y. Akiyama, A. A. Kaminskii,** *Neodymium doped yttrium aluminum garnet ($Y_3Al_5O_{12}$) nanocrystalline ceramics-a new generation of solid state laser and optical materials*, **J. Alloys Compun. 341,** 220-225 (2002)**.**

[4-42] **S. K. Kurz, T. T. Perry,** *A powder technique for evaluation of nonlinear optical materials*, **J. Appl. Phys. 39,** 3798 (1968)**.**

[4-43] **P. A. Williams, A. H. Rose, K. S. Lee, D.C. Conrad, G.W. Day, P.D. Hale,** *Optical, thermo-optic, electro-optic and photo-elastic properties of bismuth germanate $Bi_4Ge_3O_{12}$*, **Appl. Opt. 35,** 3562-3569 (1996)**.**

[4-44] **P. Lecoq, I. Dafinei, E. Auffray, M. Schneegans, M.V. Korzhik, O.W. Missevitch, U.B. Polenko, A.A. Fdorov, A.N. Annanenkov, V.L. Kostylev, V.D. Lingun**, *Lead tungstate ($PbWO_4$) scintillators for LHC EM calorimetry*, **Nucl. Instrum. Methods Phys. Res. A 365,** 291 (1995)**.**

[4-45] **R. H. Stolen, C. Lin,** *in Handbook of Laser Science and Technology*, **Suppl. 1: Lasers (Ed: M. J. Weber), CRC Press, Boca Raton, FL** (1991)**,** 101-125**.**

[4-46] *Handbook of Laser Science and Technology*, **Suppl. 2: (Ed: M. J. Weber), CRC Press, Boca Raton, FL** (2001)**.**

[4-47] **C. Bosshard, K. Sutter, P. Pretre, J. Hulliger, M. Florsheimer, P. Kaatz, P. Günter,** *Organic nonlinear optical materials*, **Gordon and Breach, Reading, UK** (1995)**.**

[4-48] *Nonlinear optical properties of organic molecules and crystals*, **Vols. 1 and 2 (Eds: D. S. Chemla, J. Zyss) Academic, San Diego, CA** (1987)**.**

[4-49] *Nonlinear optics of organic molecules and polymers* **(Eds: H. S. Nalwa, S. Miyat),**

CRC Press. Boca Raton, FL (1996)**.**

[4-50] **G. Eckhard, R. W. Hellwarth, F. J. McClung, S. E. Schwarz, D. Weiner, E. J. Woodbury,** *Stimulated Raman scattering from organic liquids*, **Phys. Rev. Lett. 9,** 455-457 (1962)**.**

[4-51] **A. A. Kaminskii, H. J. Eichler, J. Hulliger, S. Haussühl, T. Chyba, D. Temple, J. C. Barnes, V. N. Dolbinina, J. Findeisen, Wang Jiyang, Lü Menkai,** *Multiple Stokes and anti-Stokes generation in triclinic γ-KIO_3 and hexagonal α-$LiIO_3$ nonlinear crystals*, **Laser Phys. 10,** 627-632 (2000)**.**

[4-52] **J. Hulliger, A. A. Kaminskii, H. J. Eichler,** *Molecular inorganic, organic crystalline, and glassy materials for Raman laser converters*, **Adv. Functional Materials 11,** 243-250 (2001)**.**

[4-53] **A.A. Kaminskii, S. N. Bagaev, K. Ueda, K. Takichi, H.J. Eichler,** *High-order picosecond SRS and self-SRS generation in Nd3+-doped $CaMoO_4$, $SrMoO_4$, and $SrWO_4$, laser crystals*, **Crystallography Reports 47,** 653-657 (2002)**.**

[4-54] **H. J. Eichler, G.M.A. Gad, A.A. Kaminskii, H. Rhee,** *Raman crystal lasers in the visible and near-infrared*, **J. Zhe. Uni. Scien. 4,** 241-253 (2003)**.**

Chapter 5-:

[5-1] **J.T. Murray, R.C. Powell, N. Peyghambarian, D. Smith, W. Austin, R.A. Stolzenberger,** *Generation of 1.5-μ m radiation through intracavity solid-state Raman shifting in $Ba(NO_3)_2$ nonlinear crystals*, **Opt. Lett. 20,** 1017 (1995)**.**

[5-2] **J.T. Murray, W. Austin, R.C. Powell, G.J. Quarles,** *Frequency doubled solid state laser for marine imaging lidar applications*, **Proc. ASSL.** 11-13 (1997)**.**

[5-3] **E.V. Browell, A.F. Carter, S.T. Shipley, R.J. Allen, C.F. Butler, M.N. Mayo, J.H. Siviter, W.M. Hall,** *NASA multipurpose airborne dial system and measurements of ozone and aerosol profiles*, **Appl. Opt. 22,** 522-534 (1983)**.**

[5-4] **C. Guntermann, V. Schulz-von der Gathen, H.F. Döbele,** *Raman shifting of Nd:YAG laser radiation in method: an efficient method to generate 3-μm radiation for medical uses*, **Appl. Opt. 28,** 135-138 (1983)**.**

[5-5] **P. G. Zverev, T. T. Basiev, A. M. Prokhorov,** *Stimulated Raman scattering of laser radiation in Raman crystals*, **Opt. Mater. 11,** 335-352 (1999)**.**

[5-6] **J. Findeisen, H.J. Eichler, A.A. Kaminskii,** *Efficient picosecond $PbWO_4$ and two-wavelength $KGd(WO_4)_2$ Raman lasers in the IR and visible*, **IEEE J. Quant.**

Electron. 35, 173-178 (1999)**.**

[5-7] **P. Cerny, H. Jelinkova, T.T. Basiev, P.G. Zverev,** *Highly efficient picosecond Raman generators based on the $BaWO_4$ crystal in the near infrared, visible, and ultraviolet*, **IEEE J. Ouant. Electron. 38,** 1471-1478 (2002)**.**

[5-8] **H. Kogelink, T. Li,** *Laser beams and resonators*, **Appl. Opt. 5,** 1550-1567 (1966)**.**

[5-9] **Y.B. Band, J.R. Ackerhalt, J.S. Krasinski, D.F. Heller,** *Intracavity Raman lasers*, **IEEE J. Quant. Electron. 25,** 208-213 (1989)**.**

[5-10] **J. F. Reintjes, Opt. Mat.,** 346 (1986)**.**

[5-11] **J. C. van den Heuvel, F. J. M. van Putten, R. J. L. Lerou,** *Quality of the Stokes beam in stimulated Raman scattering*, **IEEE J. Quant. Electron. 30,** 2211-2219 (1994)**.**

[5-12] **J.C. van den Heuvel, F.J.M. van Putten, R.J.L. Lerou,** *The stimulated Raman scattering threshold for a nondiffraction-limited pump beam*, **IEEE J. Quant. Electron. 28,** 1930-1936 (1992)**.**

Chapter 6-:

[6-1] **V. Wilke, W. Schmidt,** *Tunable coherent radiation sources covering a spectral range from 185 to 880 nm*, **Appl. Phys. 18,** 177 (1979)**.**

[6-2] **D.J. Brink, D. Proch,** *Efficient tunable ultraviolet source based on stimulated Raman scattering of an excimer pumped dye laser*, **Opt. Lett. 7,** 494 (1982)**.**

[6-3] **N. Morita, L.H. Lin, T. Yajima,** *Generation of picosecond UV pulses by stimulated anti-Stokes Raman scattering*, **Appl. Phys. B 31,** 63-67 (1983)**.**

[6-4] **P.R. Peterson, D.A. Cardimona, A. Gavrieledes,** *Anti-Stokes generation in focused geomeztries*, **J. Opt. Soc. Am. B. 4,** 1970 (1987)**.**

[6-5] **V. Wilke, W. Schmidt,** *Tunable UV radiation by stimulated Raman scattering in hydrogen*, **Appl. Phys. 16,** 151 (1978)**.**

[6-6] **C. Reiser, T.D. Raymond, R.B. Michie, A.P. Hickman,** *Efficient anti-Stokes Raman conversion in collimated beams*, **J. Opt. Soc. Am. B 6,** 1859-1869 (1989)**.**

[6-7] **J.J. Ottusch, M.S. Mangir, D.A. Rockwell,** *Efficient anti-Stokes Raman conversion by four-wave mixing in gases*, **J. Opt. Soc. Am. B 8,** 68-77 (1991)**.**

Acknowledgement

The present work has been carried out at the optical institute of the Technical University of Berlin (TU-Berlin) in collaboration with the Egyptian High-Education Ministry. I would like to thank sincerely the scientific and academic support of many co-workers and Professors, specially the following persons:

- Prof. Dr. H. J. Eichler, leader of the laser-group at the Optical Institute (TU-Berlin) for his valuable supervision, for the kindly disposition of scientific equipments required in the SRS and Raman lasers experiments, the creative discussion and kind guidance throughout the preparation of the thesis.
- Prof. Dr. A. A. Kaminskii, leader of the Crystallography Institute, Russian Academy of Sciences, Moscow, for the assistance in the SRS experiments and the provision of most Raman crystals investigated in this work.
- Department of Physics, Faculty of Science, Helwan University, Cairo, Egypt.
- Dipl. Phys. Hanjo Rhee, for his valuable help in the laboratory, interest and encourage to perform and develop new experiments in this amazing scientific field.
- A. Hermerschmidt, C. Scharfenorth, T. Riesbeck, J. Huyer, C. Theiss, F. Kentischer, Y. Abdel Hadi, for their collaboration in the laboratory and a friendly working atmosphere.

Financial support of different scientific organizations is also gratefully acknowledged, specially to:

- Egyptian High-Education Ministry, for the scholarship and academic support obtained during the realization of this Ph.D.-work.
- Astrium GmbH, Ottobrunn.

Last but not less, I would like to thank the unconditional support of my relatives and the infinite patient of my wife after all these years. I would like to thank my children Mohamed, Omar and Karim.

List of publications

Publications in different journals

1. **H. J. Eichler, G.M.A. Gad, A.A. Kaminskii, H. Rhee,** *Raman crystal lasers in the visible and near-infrared*, **J. Zhe. Uni. Scien. 4,** 241-253 (2003).
2. **G.M.A. Gad, H.J. Eichler, A.A. Kaminskii**, *Highly efficient 1.3 μm second-Stokes $PbWO_4$ Raman laser*, **Opt. Lett. 28,** 426-428 (2003).
3. **G.M.A. Gad, A.A.Kaminskii, H.J. Eichler, J. Pickardt,** *Double sulfate $KAl(SO_4)_2 \cdot 12H_2O$ single crystals (α-alum)-a new material for Raman laser converters*, **Phys. Stat. Sold. (a) 193,** R10-R12 (2002).
4. **A.A. Kaminskii, P. Becker, L. Bohaty, K. Ueda, K. Takichi, J. Hanuza, M. Moczka, H.J. Eichler, G.M.A. Gad,** *Monoclinic bismuth triborate BiB_3O_6 – a new efficient $\chi^{(2)}+\chi^{(3)}$ –nonlinear crystal: multiple stimulated Raman scattering and self-sum-frequency lasing effects*, **Opt. Commun. 206,** 179-191 (2002).
5. **A. A. Kaminskii, H. Klapper, J. Hulliger, H.J. Eichler, J. Hanuza, K. Ueda, K. Takichi, C. Wickleder, G.M.A. Gad, M. Moczka,** *High-order many-phonon stimulated Raman scattering in orthorhombic benzophenone ($C_{13}H_{10}O$) and monoclinic α-4-methylbenzophenone (α-$C_{14}H_{12}O$) crystals*, **Laser Phys. 12,** 1041-1053 (2002).
6. **A.A. Kaminskii, T. Kaino, T. Taima, A. Yokoo, K. Ueda, K. Takichi, J. Hulliger, H.J. Eichler, J. Hanuza, J. Fernandez, R. Balada, M. Moczka, G.M.A. Gad,** *Monocrystalline 2-Adamantylamino-5-Nitropyridine (AANP)- a novel organic material for laser Raman converters in the visible and near-IR*, **Jpn. J. Appl. Phys. 41,** 1041-1053 (2002).
7. **A.A. Kaminskii, E. Haussühl, J. Hulliger, K. Ueda, K. Takichi, J. Hanuza, M. Moczka, H.J. Eichler, G.M.A. Gad,** *Bis(Guanidinium) Zirconium bis(Nitrilotriacetate) hydrate, $[C(NH_2)_3]_2Zr[N(CH_2COO)_3]_2.H_2O$ - a new crystal for Raman laser converters*, **Phys. Stat. Sol. (a) 193,** 167-178 (2002).
8. **A. A. Kaminskii, J. Hulliger, H. J. Eichler,** *New nonlinear effects in $\chi^{(2)}$ – and $\chi^{(3)}$ - active organic crystals of 4′- nitrobenzylidene-3-acetamino-4-methoxyaniline (MNBA): high-order stimulated Raman scattering, self-frequency doubling, and self-sum frequency mixing*, **Phys. Stat. Sol. (a) 186,** R19-R21 (2001).
9. **A.A. Kaminskii**, **S.N. Bagayev, N.V. Kravtsov, S.N. Chekina, Ya.V. Vasiliev, N.I.**

Ivannikova, K. Ueda, J. Lu, H.J. Eichler, G.M.A. Gad, J. Hanuza, J. Fernandez, P. Reiche, *Spectroscopy and cw laser action, magnetooptics and nonlinear optical frequency conversion in Ln^{3+}doped and undoped $Bi_4Ge_3O_{12}$ and $Bi_4Si_3O_{12}$ crystals*, **Laser Spectroscopy 11,** 897-918 (2001).

10. **A.A. Kaminskii**, **K. Ueda, J. Lu, H.J. Eichler, Y. Kuwano, H. Kouta, S.N. Bagaev, T.H. Chyba, J.C. Branes, G.M.A. Gad, T. Murai, J. Lu,** *Tetragonal vanadates YVO_4 and $GdVO_4$-new efficient $\chi^{(3)}$-materials for Raman lasers*, **Opt. Comm. 194,** 201-206 (2001).
11. **R. Burkhalter, B.Trusch, P. Franz, A.A. Kaminskii, H.J. Eichler, J. Hulliger,** *High-order stimulated Raman scattering in χ^3-active molecular glass: $Ca(NO_3)_2$: KNO_3 under picosecond excitation*, **J. Materials Chemistry 11,** 3211-3214 (2001).
12. **R. Burkhalter, B. Trusch, A.A. Kaminskii, G.M.A. Gad, H.J. Eichler, J. Hulliger,** *Frequency conversion in $(NaPO_3)_x$ polyphosphate glass by stimulated Raman scattering*, **Adv. Materials 13,** (2001) 814-816.
13. **A.A. Kaminskii, H.J. Eichler, K. Ueda, P. Reiche, G.M.A. Gad,** *The first observation of SRS in a trigonal $LiCaAlF_6$ crystal*, **Quant. Electron. 30,** 1035-1036 (2000).
14. **A.A. Kaminskii, H.J. Eichler, K. Ueda, S.N. Bagaev, G.M.A. Gad, J. Lu, T. Murai, H. Yagi, T. Yanagitani,** *Observation of stimulated Raman scattering in $Y_3Al_5O_{12}$ single crystals and nanocrystalline ceramics and in these materials activated with laser ions Nd^{3+} and Yb^{3+}*, **JETP Lett. 72,** 499-502 (2000).
15. **A.A. Kaminskii, H.J. Eichler, K. Ueda, S.N. Bagaev, G.M.A. Gad, J. Lu, T. Murai, H. Yagi, T. Yanagitani,** *Stimulated Raman scattering in $Y_3Al_5O_{12}$ single crystal*, **Phys. Stat. Sol. (a) 181** R19-R21 (2000).
16. **A.A. Kaminskii, C.L. McCray, H.R. Lee, S.W. Lee, D.A. Temple, T.H. Chyba, W.D. Marsh, J.C. Barnes, A.N. Annanenkov, V.D. Legun, H.J. Eichler, G.M.A. Gad, K. Ueda,** *High efficiency nanosecond Raman lasers based on tetragonal $PbWO_4$ crystals*, **Opt. Commun. 183,** 277-287 (2000).

Publications in conferences

1. **G.M.A. Gad, H. J. Eichler, A.A. Kaminskii, H. Rhee,** *Second-Stokes Raman lasers*

with large wavelength shift from 1064 to 1316 nm wavelength in $PbWO_4$ crystas, **CLEO/Europe-EQEC, laser 2003, Munich** (2003).

2. **H. J. Eichler, G.M.A. Gad, A.A. Kaminskii,** *Raman crystal lasers in the visible and near-infrared*, **SPIE, San Jose, California,** (2003).
3. **G.M.A. Gad, H. J. Eichler, H. Kneipp, A.A. Kaminskii,** *Picosecond Raman scattering and lasers in $PbWO_4$*, **Lasers 2001, Tucson, Arizona,** (2001).
4. **G.M.A. Gad, H. J. Eichler,** *Stimulated Raman scattering and Raman lasers*, **Optical Institute, TU-Berlin,** (2001).
5. **G.M.A. Gad H. J. Eichler, , A.A. Kaminskii, T.H. Cyba, H. Kneipp,** *Efficient nano- and picosecond Raman scattering and lasers in $PbWO_4$*, **Poster in DGaO, Göttingen** (2001).
6. **G.M.A. Gad, H. J. Eichler, A.A. Kaminskii,** *Stimulated Raman scattering in undoped and doped YAG*, **DPG, Berlin,** (2001).

CURRICULUM VITAE

Name: ***Gad Mansour Ahmed Gad***

Permanent address: Gaafar Street No. 23, Helwan, Cairo, Egypt.

Birth date: 03.06.1966.

Nationality: Egyptian

e-mail: gad0432@moebius.physik.tu-berlin.de, gad100@hotmail.com

---

ACADEMIC QUALIFICATIONS

PhD. (Dr. rer. nat), Optical Institute, **Technical University-Berlin**, thesis work: "***Stimulated scattering in solids and new Raman lasers in near-infrared and visible regions***". (Experimental work). Date of grade: **25. July 2003**.
Supervisor: **Prof. Dr. H. J. Eichler.**

Diplom Physiker, **TU-Berlin.** *Diplom Hauptprüfung (Äquivalenz und Anerkennung)* in experimental, theoretical physics and master thesis. Date of grades: 26.03.99, 22.07.99 & 06.08.99.

Master degree in optical science (MSc. Optics), Faculty of Sciences, Helwan University, Cairo, Egypt. Period 1991-1994. Thesis work: "***Interferometric studies of two correlated diffusers***". (Theoretical and experimental work). Date of grade: 11.04.1994.
Supervisors: **Prof. Dr. M. M. EL-Niklawy,**
Prof. Dr. T. A. EL-Dessouki,
Ass. Prof. Dr. A. F. Hassan.

Bachelor of science in physics (B.Sc.), Physics Department, Faculty of sciences, Helwan University, Cairo, Egypt. Period 1984-1988.

WORK EXPERIENCE

- 10.02-today: , "***Scientific assistant"***, laser group of the Optical Institute, Technical University, Berlin.

- 1994-1998: "***Assistant Lecturer***", in Physics Department, Faculty of Sciences, Helwan University, Cairo, Egypt.
- 1998-1994: "***Demonstrator***", in Physics Department, Faculty of Sciences, Helwan University, Cairo, Egypt.

LANGUAGES

Arabic (100%), English (70%), German (50%).